UILU-WRC-86-200

RESEARCH REPORT 200   SECONDARY CIRCULATION IN NATURAL STREAMS

WRC

UNIVERSITY OF ILLINOIS
AT URBANA-CHAMPAIGN
WATER RESOURCES
CENTER

JULY 1986

BY MISGANAW DEMISSIE
     TA-WEI SOONG
     NANI G. BHOWMIK
     WILLIAM P. FITZPATRICK
      ILLINOIS STATE WATER SURVEY

     W. HALL C. MAXWELL
     DEPARTMENT OF CIVIL ENGINEERING

     UNIVERSITY OF ILLINOIS AT
     URBANA-CHAMPAIGN

WRC RESEARCH REPORT NO. 200

SECONDARY CIRCULATION IN NATURAL STREAMS

by
Misganaw Demissie, Ta-Wei Soong,
Nani G. Bhowmik, and William P. Fitzpatrick
Surface Water Section
Illinois State Water Survey
Champaign, Illinois 61820

and
W. Hall C. Maxwell
Department of Civil Engineering
University of Illinois at Urbana-Champaign
Urbana, Illinois 61801

July 1986

University of Illinois
Water Resources Center
Urbana, Illinois 61801

SECONDARY CIRCULATION IN NATURAL STREAMS

ABSTRACT

Secondary circulation which is sometimes referred to as secondary flow, secondary current or transverse current is an important phenomenon in natural streams and plays an important role in many natural processes in streams such as stream channel meander, bank erosion, bed scour, resuspension, and movement of sediment. Secondary circulation is that component of flow which is not in the main flow direction and is small as compared to the main flow velocity. A computerized data collection system for secondary circulation data acquisition in natural streams was developed and utilized in the field. The system includes an electromagnetic current meter, a micro-computer, an interface between the computer and the current meter, and a specially designed supporting structure. Secondary circulation data was collected in the Sangamon River near Mahomet, Illinois, utilizing the data collection system. A mathematical model for secondary circulation based on an existing model has been developed and tested against the data collected in the field. Model results generally reproduce similar secondary circulation patterns as observed from the field data but over-estimate the magnitudes of the velocities.

Demissie, M., Soong, T.W., Bhowmik, N.G., Fitzpatrick, W.P., and Maxwell, W. Hall C.

CONTENTS

INTRODUCTION

The main component of flow in any stream, river, or canal might be expected to be parallel to the channel bed in the downstream direction. However, because of a variety of reasons including the resistance flow due to stream banks, a rotational or cellular movement of flow will occur in the main channel. This persistent flow component that is not in the main flow direction has been termed secondary circulation, secondary flow, secondary current, or transverse current. This type of flow, which is always present in any open channel flow, is completely different from induced flow circulations in some pockets found on the side of open channels.

The direction of secondary flow is strongly associated with the primary velocity distribution. Areas of high velocities near the bed or bank are associated with outward secondary flow, while areas of low velocities are associated with inward secondary flow. This phenomenon has significant implications with respect to bank erosion and bed scour, since areas of high velocities are much more susceptible to erosion and scour.

Considerable agreement exists among researchers that secondary circulation is an important phenomenon in natural rivers and is partially responsible for the development of meander patterns, bank erosion, bed scour, resuspension and movement of sediment, and an increase in boundary shear and flow resistance (24, 26, 29, 37, 38, 39, 41, 44, 45, 47, 53, 54). For example, the existence of strong secondary circulation near a certain region close to the bank with a component of velocity directed toward the bank will indicate the location of potential bank erosion areas.

Objectives

The main objectives of this proposed research were:
1) To determine the magnitude and nature of secondary circulation in natural streams by direct measurement in the field.
2) To develop and verify a mathematical model for predicting secondary circulation in natural streams.
3) To determine the effects of secondary circulation on bank erosion by quantifying its effects on velocity and shear stress distribution, and on dispersion and transport of sediment in natural streams.

REVIEW OF LITERATURE

        It is important to have a clear understanding of what the term secondary
circulation means before proceeding further. When researchers talk about
secondary flow, they are actually describing the three-dimensional nature of
open channel flow. Ciray (18) defined the secondary velocity as follows:

> When the magnitude of the vector composed by any two
> components of the local velocity vector in a three
> dimensional flow is small compared with the magnitude of the
> third component, the latter forms the main flow whereas the
> remaining two form the secondary.

        Although this definition appears to be adequate to some extent, it lacks
completeness. Perhaps more attention should be paid to the individual
components of velocity than to the resultant of two vector quantities. In
this line of thought, Chiu et al. (13) defined the secondary flow as the two
components of flow which are in the transverse direction not coincident with
the primary flow. Because of the presence of snags, obstructions, trees,
etc., on the bed of a river, the velocity vector in a direction other than the

2

primary direction of the flow may be of greater magnitude than the primary velocity vector. Considering all these factors, Bhowmik (7) proposed the following definition:

> In an open channel flow, any persistent component of velocity which is not parallel to or tangent to the center line of the channel and also not parallel to and in the same general downstream direction of the overall bed slope should be termed as secondary velocity.

Secondary current will be taken as the flow which is parallel to and also in the same direction as the secondary velocity. The definition stated above will ensure that the primary flow velocity is interpreted as the velocity in the downstream direction that coincides with the general direction of flow.

Historical Background

Historically, late nineteenth century hydraulic engineers, noting that the maximum velocity is below the water surface rather than at the water surface, offered the explanation that the frictional resistance at the air-water interface is responsible for this phenomenon. However, many researchers working at the time did not accept this idea, and they tried and were successful in correctly identifying the mechanisms of secondary circulation. They also indicated that these mechanisms might be responsible for the lower flow velocity at the air-water interface. These researchers did not identify secondary circulation by name, but they recognized its presence in concept. They include Bazin and Barcy in 1865, Gerrard in 1878, Francis in 1878, Wood in 1879, Stearns in 1883, and Cunningham in 1882 (7, 19).

In 1909 Gibson (30) analyzed the then-existing literature and offered his thoughts on why the filament of maximum velocity is below the water surface. He said that this phenomenon is "... due to the action of the sides of the channel in producing transverse currents inwards along the surface and outwards along the bed of the stream, thus distributing a layer of slowly moving water over the central part of the stream." He also indicated that the presence of curves in the stream's alignment can and will modify this phenomenon. He showed that the secondary flow velocity is about 5 percent of the main stream velocity.

It is noteworthy that almost 100 years after the initial postulations about the effect of wall roughness on the transverse flow phenomenon that were

3

made by Wood (59), Stearns (55), Francis (25), and others, Perkins (49) showed
that the mean streamwise vorticity in turbulent flow arises both from mean
flow skewing and from the inhomogeneity of anisotropic wall turbulence.

In the early twentieth century many others also worked on the transverse
flow phenomenon. In 1917, Helstrom estimated the secondary flow velocity to
be about 11 percent of the main stream velocity (32). In 1930 Nikuradse
published results showing that secondary flow exists in noncircular conduits
(27).

Laboratory Measurements

Once the concept of secondary flow was recognized, researchers tried to
measure the secondary circulation, especially in laboratory channels under
ideal flow conditions. The simplest method is of course to use dye or
neutrally buoyant particles to measure qualitatively the existence and the
direction of secondary currents (3, 58). Another fairly sophisticated
instrument used to measure secondary current in laboratory experiments is the
hot-wire anemometer. Researchers such as Brundrett and Baines (8), Gessner
and Jones (28), Hoagland (33), Tracy (57), and Liggett et al. (42) utilized
hot wire anemometry systems to measure components of secondary currents.
Launder and Ying (40) collected turbulence-induced secondary current data by
using a DISA hot-wire probe. Muller (43) reported the results of laboratory
experiments where a Laser Doppler Anemometer was used to measure the vertical
and axial component of flow velocity. The presence and absence of secondary
flow were interpolated on the basis of the increase or decrease of the
turbulence and momentum exchange. All of Muller's experiments were conducted
for supercritical flow ranges, i.e., the Froude number was more than unity.
However, all these research projects were confined to laboratory
experimentations.

Field Measurements

While various researchers have measured secondary circulation in
laboratory experiments, field instrumentations and measurements are rare.
Only a very limited number of attempts have been made to measure secondary
circulation in the field.

Kanwisher and Lawson (36) have described an electromagnetic flow sensor
for measuring flow in natural open channels, which can be modified to measure

both the main stream and lateral flow velocities. This electromagnetic flow sensor has the potential of being used in the field to measure secondary flow velocities.

One of the most serious and comprehensive attempts that was made by any group of researchers to measure secondary currents in gravel bed rivers was that made by Bathurst et al. (4, 5). Their measurements were made at four bends on the River Severn in Wales, United Kingdom. Direct measurements of secondary velocities were made with an electromagnetic flow meter that had the capability of measuring two mutually perpendicular components of velocity simultaneously. The measuring head was 2 inches (50 mm) in diameter, and the instrument was accurate to within 0.33 fps (10 mm/s). All the measurements were confined to bends. The instrument worked out fairly well. The primary velocity data were collected with an Ott C-31 current meter. Isovels were developed, and their shapes were compared with the shape and pattern of secondary cells that could be sketched on the basis of the shape of the primary isovels. The data indicated that the peak values of shear stress were associated with the core of the maximum velocity.

Thome et al. (56) conducted other detailed bend-flow hydraulics measurements on the Fall River, Rocky Mountain National Park, Wyoming. Primary and lateral velocity components were measured using a Marsh-McBirney Model 511 two-component electromagnetic current meter. The current meter simultaneously measures two mutually perpendicular velocity components with an accuracy of 0.01 ft/sec (3 mm/s). Much more accurate data were recorded, and secondary cells were often found to exist at outer and inner banks. The device used by Thorne et al. could not record the orientation of the sensor probe, which remained a difficulty in the data reduction. Demissie et al. (20, 21) developed a measuring system in which the current meter is supported by a self-standing system and data are transmitted to a computer on the stream bank for processing and storage. The flow velocity components are measured by a Marsh-McBirney current meter, Model 527, which can also measure the bearing of the sensor from the magnetic north in a clockwise direction.

Indirect Techniques

Field data collected by Bathurst et al. (4, 5) indicated that it is possible to draw secondary flow cells on the basis of the primary velocity isovels. Such an attempt was made by Bhowmik (7) for the field data collected

from the Kaskaskia River in Illinois. Fig. 1 shows the isovels at a section
where the secondary flow cells were sketched. Data shown are from the same
cross section but for two flow conditions: low and high flows. If it is
assumed that the isovels are a set of flexible membranes held in place by
fluids in between them, then a bulging or deformity in their shape indicates
the presence of some force acting normal to the face of the membranes. Thus,
if the membranes bulge inward, it indicates the presence of a force from the
outside to the inside and vice versa. The approximate locations of the
secondary cells in Fig. 1 were drawn on the basis of this technique. Data
from any other isovels can similarly be used to draw the patterns of secondary
cells. Brundrett and Baines (8) and Liggett et al. (42) expressed some doubt
as to the validity of sketching secondary flow cells on the basis of primary
velocity isovels. Their conclusions were based on laboratory experiments.
However, even though it is not a precise technique, it provides a good
qualitative picture of secondary circulation in natural channels.

Recently Ikeda (35) indicated a technique of sketching the patterns of
secondary current cells in sand bed laboratory channels on the basis of the
nature and existence of bed undulations or topography. In a deformable
channel such as a sand bed channel, the bed profile in the lateral direction
may partially reflect the magnitude and direction of the secondary current
cells near the bed. Only qualitative information is obtained by using isovels
or bed topography.

Mathematical Modeling

A few researchers have worked on the development of mathematical models
related to secondary circulation in open channels. However, most of their
work has been confined to cases with flow around bends. A strong secondary
current is generated in a bend because of the imbalance of horizontal fluid
forces; thus it is easier to quantify this current for flow around bends than
for straight reaches.

Einstein and Li (23) have shown theoretically that uniform flow in
straight channels can exist only in the case of laminar flow. For turbulent
flow, they have shown that secondary currents will be generated and that the
nonexistence of parallel isovels results from the presence of secondary flows,
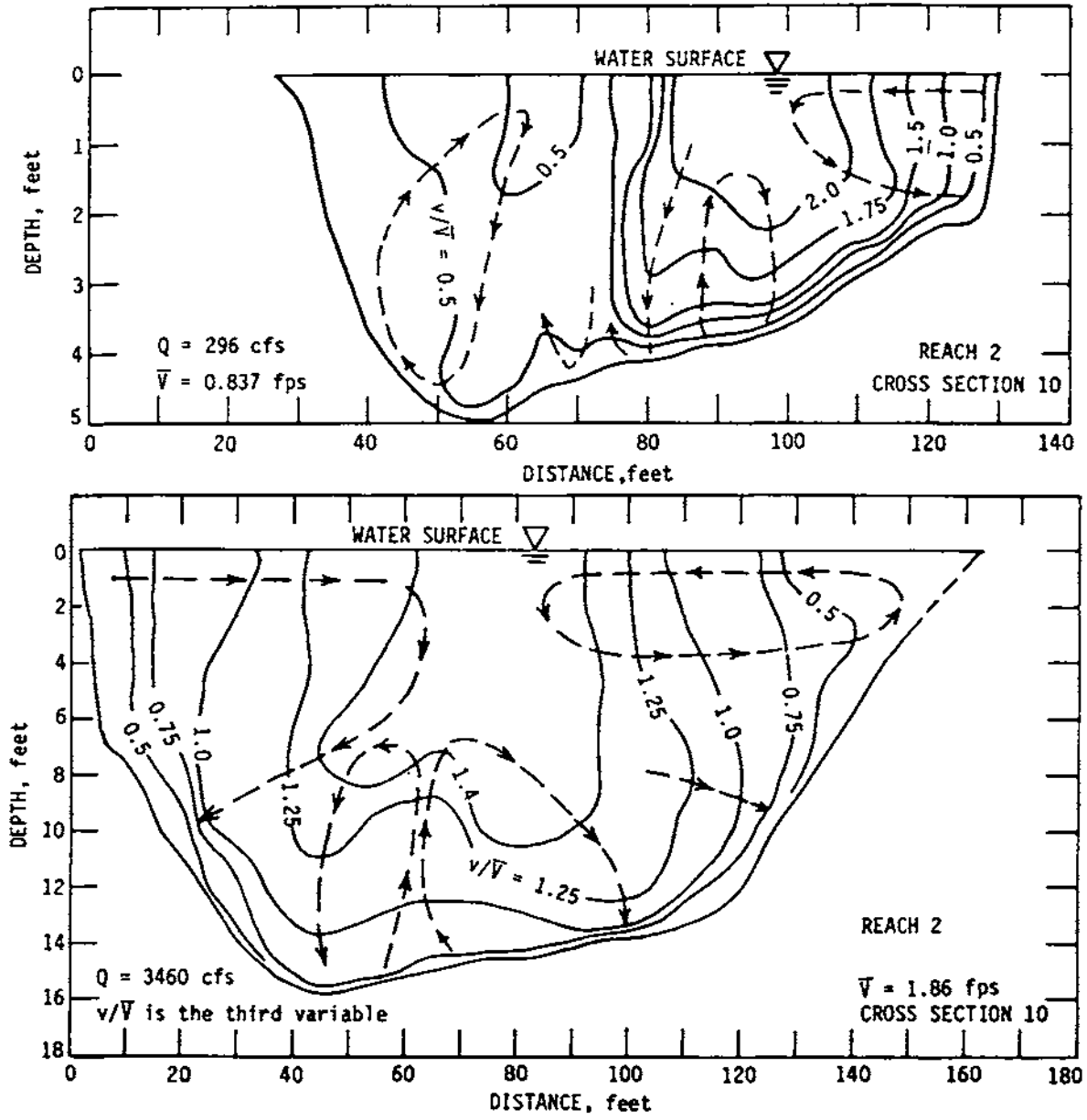especially near the frictional boundary. Some other researchers who have

6

Figure 1. Isovels and secondary flow cells in a natural river (7)

worked on the mathematical formulation of secondary currents are Ibragimov et al. (34), Ananian (2), Ciray (18), Prasad (50), Tracy (57), Liggett et al. (42), and Odgaard (46).

One of the most significant contributions to the mathematical modeling of secondary circulation was made by Chiu and his associates (10-17). Much of Chiu's work related to secondary circulation around channel bends. He also worked in the analyses of secondary currents in straight open channels, and has indicated that whenever the three components of shearing force are not in equilibrium everywhere in a channel, the presence of secondary current is inevitable.

By introducing a coordinate transformation function, Chiu et al. (12) developed a model which appears to have considerable potential for application to natural open channel flow problems. A curvilinear orthogonal coordinate system which is constructed by computed isovels and their orthogonal trajectories forms the basis for the model. The model was used to compute secondary flows on the basis of some hydraulic data collected from the Rio Grande Canal (12, 13). Later, different functions for approximating isovels and shear stresses were used to improve the model (14-17). Comparisons of model results with measured data on the East Fork River (Wyoming) showed reasonable agreement. Field data such as cross-sectional area, discharge, depth, water surface profile, and primary velocity distribution patterns are needed to use the model.

MATHEMATICAL MODEL

Mathematical Derivations

This part of the report discusses the derivation of equations used in a new mathematical model for calculating secondary velocity components. The model is based primarily on Chiu's work (10-17). Detailed derivations for some functions are presented here so the mathematical model can be clearly understood.

In general, the model consists of the momentum and the continuity equations. Once the isovels for a cross section are approximated by mathematical functions, the momentum and the continuity equations are then transformed into a curvilinear coordinate system, which is based on the simulated isovels and their orthogonal trajectories. After the transformation

of these equations, one of the secondary velocity components is computed directly from the momentum equation, and the other component is derived by solving the continuity equation. Shear stresses are assumed to vary quadratically from the boundary line to the point of maximum velocity in the new coordinate system. Finally the secondary velocity components are transformed back to the cartesian coordinate system by following inverse transformation rules.

Coordinate Transformation

Coordinate   System

The curvilinear coordinate system consists of two components   and   as shown in Fig. 2, where a constant value **of**   is an equal velocity line (isovel) and   is the coordinate perpendicular to the   lines. Assuming that the primary velocity distribution follows the logarithmic rule, which is reasonable for most natural channels, the velocity distribution can be represented by:

$$u = \frac{u*}{k} \ln \frac{\xi}{\xi o} \tag{1}$$

in which

   u = the primary velocity

   k = universal constant

     = transformed coordinate

   o = coefficient characterizing the velocity distribution of the primary
       flow

   u* = $\sqrt{g R S_e}$ = mean shear velocity, where

       g = gravitational acceleration

       R = hydraulic radius

       S_e = energy slope

 Eq. 1 defines the primary velocity distribution in a direction vertical to   curves in the channel cross section. Since u* and k are constant at a given cross section, Eq. 1 states that for a given   all the velocities on this curve will have the same magnitude, i.e., a constant   is an isovel curve. The curve   = o is the line where primary velocities vanish. The coordinates of f and   in terms of Y and Z coordinates are given as (15):

9
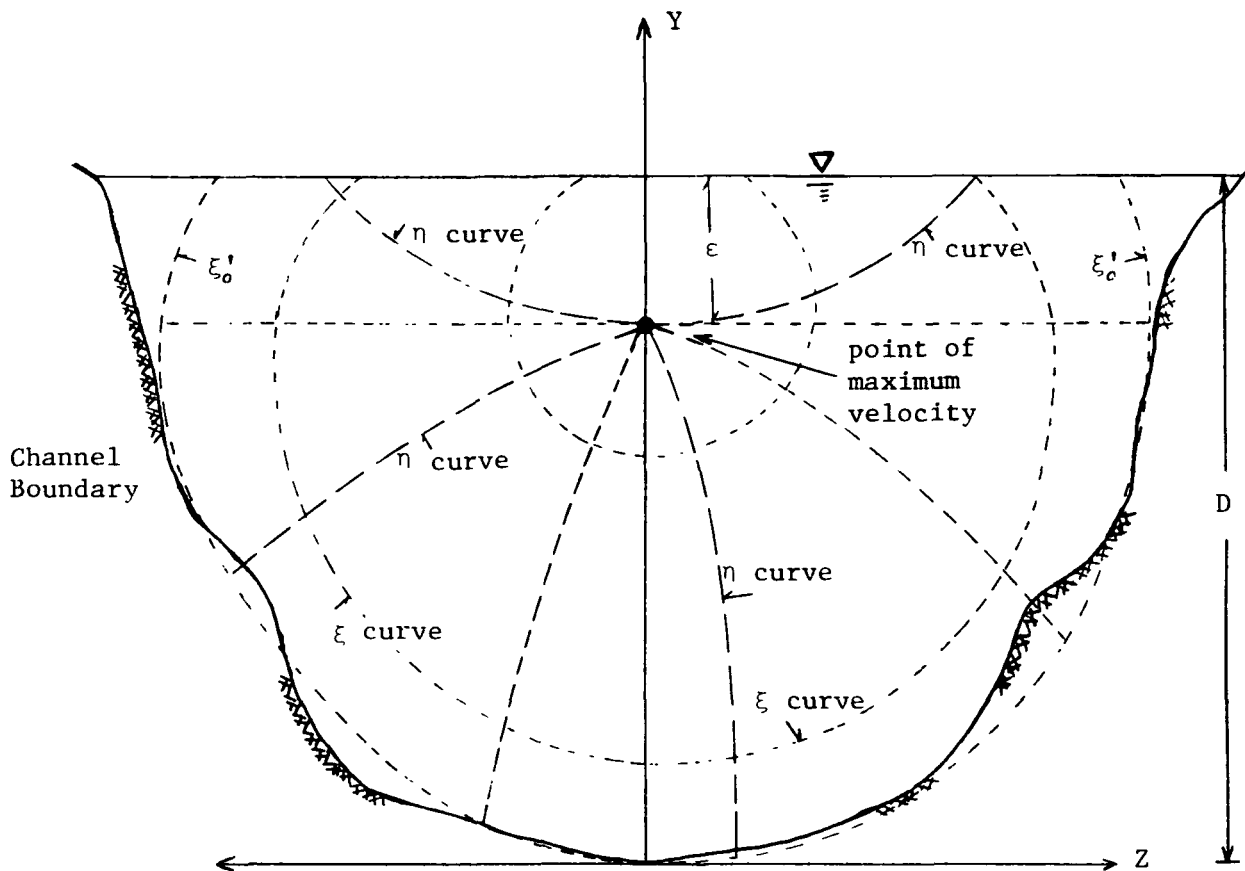
Figure 2. Curvilinear coordinate system

10

$$\xi = Y(1-Z)^{\beta_i} \exp(\beta_i Z - Y + 1) \tag{2}$$

$$\eta = \pm \frac{1}{Z} \ (|1-Y|)^{\beta_i \left[\frac{D+\delta_y+\varepsilon}{B_i+\delta_i}\right]^2} \exp\ [Z+\beta_i(\frac{D+\delta_y+\varepsilon}{B_i+\delta_i})Y]^2 \tag{3}$$

in which

$$Y = \frac{y+\delta_y}{D+\delta_y+\varepsilon} \tag{4}$$

$$Z = \frac{|z|}{B_i+\delta_i} \tag{5}$$

i, i. and y are parameters determined from the distribution of the primary velocity; i = 1 or 2 for either the left or right half of a cross section; = the distance from the water surface to the point of maximum velocity; Bi = the width of either the left or right half of a cross section; and D is the water depth (Fig. 2). The point of maximum velocity is assumed to be either below the water surface (as shown in Fig. 2 when > o), at the water surface (when = o), or above the water surface (when < o).

Scaling   Factors

Eqs. 2 and 3 define a transformation relation between the new curvilinear coordinate system and the (Y, Z) coordinate system. The scaling factors are derived by referring to Fig. 3 and assuming that $\vec{j}$ and $\vec{k}$ are unit vectors in the Y and Z directions and tangent to   and   at point p; the directions of $\vec{j}$ and $\vec{k}$ are in the increasing direction of , ; S and S are the incremental distances along the positive   and   directions; and $\vec{r}$ is the position vector to p from a fixed origin.
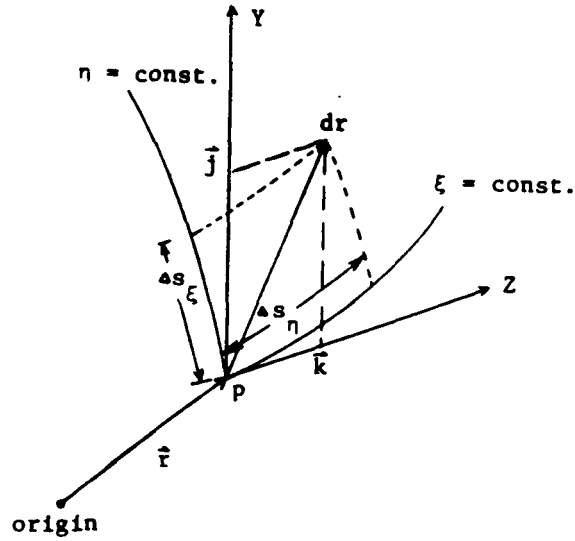
Figure 3. Relationship between the (Y-Z) coordinate system and the
curvilinear coordinate system (-17).

The derivatives of $\vec{r}$ with respect to   and   are derived as follows:

$$\frac{\partial \vec{r}}{\Delta \xi} = \lim_{\Delta \xi \to 0} \left(\frac{\Delta \vec{r}}{\Delta \xi}\right)_{\eta = c}$$

$$= \lim_{\Delta \xi \to 0} \left(\frac{\Delta \vec{r}}{\Delta s_\eta} \cdot \frac{\Delta s_\eta}{\Delta \xi}\right)_{\eta = c}$$

$$= \left(\frac{\partial s_\eta}{\partial \xi}\right)_p \cdot \left(\frac{\partial \vec{r}}{\partial s_\eta}\right)_p$$

$$= \left(\frac{\partial s_\eta}{\partial \xi}\right)_p \cdot \vec{k}$$

Set $h_\xi = \dfrac{\partial s_\eta}{\partial \xi}$

Then

$$h_\xi \cdot \vec{k} = \frac{\partial \vec{r}}{\partial \xi}$$

Similarly

$$h_\eta \cdot \vec{j} = \frac{\partial \vec{r}}{\partial \eta}$$

12

On the other hand, the derivations of $\vec{r}$ with respect to   and   can be written in terms of Y and Z as:

$$\frac{\partial \vec{r}}{\partial \xi} + \frac{\partial \vec{r}}{\partial \eta} = (\frac{\partial Y}{\partial \xi} + \frac{\partial Y}{\partial \eta})\vec{j} + (\frac{\partial Z}{\partial \xi} + \frac{\partial Z}{\partial \eta})\vec{k}$$

By using the above relations the following equations are derived:

$$h_{\xi}^{2} = (\frac{\partial Y}{\partial \xi})^{2} + (\frac{\partial Z}{\partial \xi})^{2} \tag{6}$$

and

$$h_{\eta}^{2} = (\frac{\partial Y}{\partial \eta})^{2} + (\frac{\partial Z}{\partial \eta})^{2} \tag{7}$$

The differentials of   and   with respect to Y and Z can be obtained from Eqs. 2 and 3 directly. They are:

$$\frac{\partial \xi}{\partial Y} = (1-Y)(1-Z)^{\beta i} \exp (\beta_{i} Z - Y + 1) \tag{8}$$

$$\frac{\partial \xi}{\partial Z} = \beta_{i}(1-Z)^{\beta i} Y \exp (\beta_{i} Z - Y + 1)(- \frac{Z}{1-Z}) \tag{9}$$

For Y < 1 $\frac{\partial \eta}{\partial Y} = \frac{1}{Z} C_{i} (1-Y)^{C i} \exp (Z + C_{i} Y)(\frac{-Y}{1-Y})$ (10)

$$\frac{\partial \eta}{\partial Z} = \frac{1}{Z} (1-Y)^{C i} \exp (Z + C_{i} Y)(1 - \frac{1}{Z}) \tag{11}$$

For Y > 1 $\frac{\partial \eta}{\partial Y} = \frac{1}{Z} C_{i} (Y-1)^{C i} \exp (Z + C_{i} Y)(\frac{-Y}{Y-1})$ (12)

$$\frac{\partial \eta}{\partial Z} = \frac{1}{Z} (Y-1)^{C i} \exp (Z + C_{i} Y)(\frac{1-Z}{Z}) \tag{13}$$

where

$$C_{i} = \beta_{i} \left[\frac{D + \delta_{y} + \varepsilon}{B_{i} + \delta_{i}}\right]^{2} \tag{14}$$

The differentials of Y and Z with respect to   and   can be obtained from equations 8 to 13 as follows:

$$\frac{\partial Y}{\partial \xi} = \frac{Y(1-Z)^{2}(1-Y)}{[(1-Y)^{2}(1-Z)^{2} + \beta_{i} C_{i} Y^{2} Z^{2}]} \cdot \frac{1}{\xi} \tag{15}$$

13

$$\frac{\partial Z}{\partial \xi} = \frac{- C_i \ Y^2 Z \ (1-Z)}{[(1-Y)^2(1-Z)^2 + \beta_i \ C_i \ Y^2 \ Z^2]} \cdot \frac{1}{\xi} \tag{16}$$

$$\frac{\partial Y}{\partial \eta} = \frac{-\beta_i \ Y \ Z^2 \ (1-Y)}{[(1-Y)^2(1-Z)^2 + \beta_i \ C_i \ Y^2 \ Z^2]} \cdot \frac{1}{\eta} \tag{17}$$

$$\frac{\partial Z}{\partial \eta} = \frac{-Z \ (1-Y)^2 \ (1-Z)}{[(1-Y)^2 \ (1-Z)^2 + \beta_i \ C_i \ Y^2 \ Z^2]} \cdot \frac{1}{\eta} \tag{18}$$

The scaling factors can now be derived from Eqs. 6 and 7, and Eqs. 15 to 18. As given by Chiu and Lin (16) the relations for h and h are:

$$h_\xi = \frac{(D + \delta_y + \varepsilon)(1-Z) \ Y}{\xi \ \sqrt{(1-Y)^2(1-Z)^2 + C_i^2 \ Y^2 \ Z^2}} \tag{19}$$

$$h_\eta = \frac{(B_i + \delta_i)}{(D + \delta_y + \varepsilon)} \cdot \frac{\xi}{\eta} \cdot \frac{Z \ (1-Y)}{Y \ (1-Z)} \ h_\xi \tag{20}$$

Derivation of the Equation for the V Velocity Component

The momentum equation in the curvilinear coordinate system is derived on the assumption that the control volume in Fig. 4 represents a volume of water in the curvilinear coordinate system.
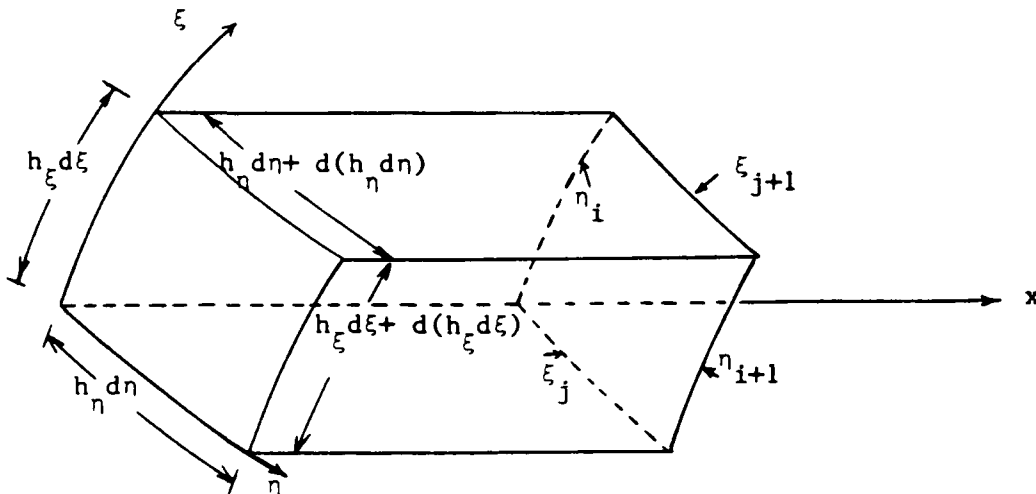
Figure 4. A control volume in the curvilinear coordinate system

14

Since each   = j line in Fig. 4 represents an equal primary velocity line, there is no change of primary velocity along this   line, i.e.,

$$\left.\frac{\partial u_j}{\partial \eta}\right|_{\xi=\xi_j} = 0$$

where u_j is the primary velocity on the jth isovel. The longitudinal component of the momentum equation in cartesian coordinates is given as :

$$\frac{\partial u}{\partial t} + u\frac{\partial u}{\partial x} + v\frac{\partial u}{\partial y} + w\frac{\partial u}{\partial z} = -\frac{1}{\rho} \left[\frac{\partial}{\partial x}(p+\rho gH)-\left(\frac{\partial \tau_{xx}}{\partial x} + \frac{\partial \tau_{yx}}{\partial y} + \frac{\partial \tau_{zx}}{\partial z}\right)\right] \qquad (21)$$

in which

x, y, z are the coordinates

t — the time

u = the primary velocity in x direction

v = the velocity components in y direction

w = the velocity component in z direction

  = the water density

p — the hydrostatic pressure

g = gravitational acceleration

H = distance from the channel bottom to a datum

$_{ix}$ = is the shear stress on the i^{tn} face acting in the x direction in which i = x, y, or z.

This equation can be written in x, Y, Z coordinates directly using the transformation equations given in Eqs. 4 and 5. Since the partial derivatives are as shown in the following equation:

$$\partial Y = \partial y$$

$$\partial Z = \begin{cases} \partial z & \text{if } z > 0 \\ -\partial z & \text{if } z < 0 \end{cases} \qquad (22)$$

Eq. 22 will change in sign only for z < 0.

The transformation relationship between Y, Z coordinates and   , coordinates can be written in a general form as follows:

$$\vec{e_\xi} = h_\xi \frac{\partial \xi}{\partial Y} \vec{j} + h_\xi\frac{\partial \xi}{\partial Z} \vec{k}$$

$$\qquad (23)$$

$$\vec{e_\eta} = h_\eta \frac{\partial \eta}{\partial Y} \vec{j} + h_\eta\frac{\partial \eta}{\partial Z} \vec{k}$$

in which $\vec{e}_\xi$ and $\vec{e}_\eta$ are unit vectors in the   and   directions, respectively, and $\vec{j}$ and $\vec{k}$ are unit vectors in the Y and Z directions, respectively.

Using Eq. 23, the transformation relationships for the velocity components between the two coordinate systems can be written as:

$$V_\xi = h_\xi \frac{\partial \xi}{\partial Y} v + h_\xi \frac{\partial \xi}{\partial Z} w$$

$$\text{(24)}$$

$$V_\eta = h_\eta \frac{\partial \eta}{\partial Y} v + h_\eta \frac{\partial \eta}{\partial Z} w$$

where V and V are velocity components in the   and   directions, respectively. Since   and   are orthogonal to each other as are the Y and Z coordinates, the following relations exist:

$$h_\eta \frac{\partial \eta}{\partial Y} = - h_\xi \frac{\partial \xi}{\partial Z}$$

$$\text{(25)}$$

$$h_\xi \frac{\partial \xi}{\partial Y} = h_\eta \frac{\partial \eta}{\partial Z}$$

These can be proved by referring to Fig. 5.

$$h_\eta \frac{\partial \eta}{\partial Y} = \cos(\eta, Y) = \sin(Y, \xi)$$

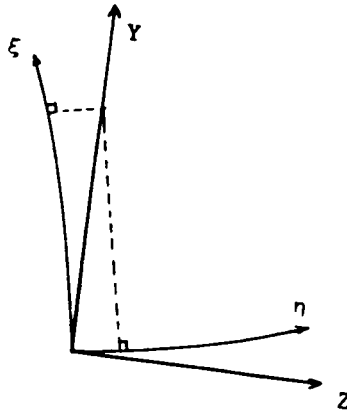$$h_\xi \frac{\partial \xi}{\partial Z} = \cos(\xi, Z) = \cos(Z, \eta) = - \sin(Y, \xi)$$

Figure 5. Definition sketch for derivatives between Y, Z and ξ ,

Therefore,

$$h_\eta \frac{\partial \eta}{\partial Y} = - h_\xi \frac{\partial \xi}{\partial Z}$$

By definition,

angle(Z,) + angle(, Y) = angle(, Y) + angle(Y,)

Thus,

angle (Z,) = angle(Y,).

Similarly,

$$h_\xi \frac{\partial \xi}{\partial Y} = \cos \ (\xi, Y)$$

$$h_\eta \frac{\partial \eta}{\partial Z} = \cos \ (\eta, Z)$$

Therefore

$$h_\xi \frac{\partial \xi}{\partial Y} = h_\eta \frac{\partial \eta}{\partial Z}$$

Now the left hand side (LHS) of the momentum equation (Eg. 21) can be rewritten as:

$$\frac{\partial u}{\partial t} + u \frac{\partial u}{\partial x} + v \frac{\partial u}{\partial y} + w \frac{\partial u}{\partial z} = \frac{\partial u}{\partial t} + u \frac{\partial u}{\partial x} + [v(\frac{\partial u}{\partial \xi} \frac{\partial \xi}{\partial Y} + \frac{\partial u}{\partial \eta} \frac{\partial \eta}{\partial Y}) + w(\frac{\partial u}{\partial \xi} \frac{\partial \xi}{\partial Z} + \frac{\partial u}{\partial \eta} \frac{\partial \eta}{\partial Z})]$$

$$= \frac{\partial u}{\partial t} + u \frac{\partial u}{\partial x} + [v(\frac{\partial u}{\partial \xi} \frac{\partial \xi}{\partial Y}) + w(\frac{\partial u}{\partial \xi} \frac{\partial \xi}{\partial Z})]$$

$$= \frac{\partial u}{\partial t} + u \frac{\partial u}{\partial x} + (v\frac{\partial \xi}{\partial Y} + w\frac{\partial \xi}{\partial Z}) \frac{\partial u}{\partial \xi}$$

$$= \frac{\partial u}{\partial t} + u \frac{\partial u}{\partial x} + \frac{V_\xi}{h_\xi} \frac{\partial u}{\partial \xi} \qquad (26)$$

where only one velocity component, V , is retained.

The transformation of the right hand side (RHS) of the momentum equation into   and   coordinates can also proceed as follows:

The shear stresses in the x direction can be written as

$$\tau_{Yx} = (\tau_{\xi x}.\vec{e}_\xi + \tau_{\eta x}.\vec{e}_\eta) \cdot \vec{j}$$

$$\qquad (27)$$

$$\tau_{Zx} = (\tau_{\xi x}.\vec{e}_\xi + \tau_{\eta x}.\vec{e}_\eta) \cdot \vec{k}$$

Since there is no velocity change in the direction on each curve,

$$\tau_{\eta x} = 0 \qquad (28)$$

Substituting this equation, as well as Eq. 23, into Eq. 27 results in the following equations:

$$\tau_{Yx} = \tau_{\xi x} \cdot h_\xi \frac{\partial \xi}{\partial Y}$$

$$\qquad (29)$$

$$\tau_{Zx} = \tau_{\xi x} \cdot h_\xi \frac{\partial \xi}{\partial Z}$$

Using the chain rule for derivatives, the following relations can be derived.

$$\frac{\partial \tau_{Yx}}{\partial Y} = \frac{\partial \tau_{Yx}}{\partial \xi} \frac{\partial \xi}{\partial Y} + \frac{\partial \tau_{Yx}}{\partial \eta} \frac{\partial \eta}{\partial Y}$$

$$\qquad (30)$$

$$\frac{\partial \tau_{Zx}}{\partial Z} = \frac{\partial \tau_{Zx}}{\partial \xi} \frac{\partial \xi}{\partial Z} + \frac{\partial \tau_{Zx}}{\partial \eta} \frac{\partial \eta}{\partial Z}$$

Substituting Eq. 29 into Eq. 30 gives:

$$\frac{\partial \tau_{Yx}}{\partial Y} = \frac{\partial}{\partial \xi}(\tau_{\xi x} \cdot h_\xi)(\frac{\partial \xi}{\partial Y})^2 + \frac{\partial}{\partial \eta}(\tau_{\xi x} \cdot h_\xi)(\frac{\partial \xi}{\partial Y} \cdot \frac{\partial \eta}{\partial Y})$$

$$\qquad (31)$$

$$\frac{\partial \tau_{Zx}}{\partial Z} = \frac{\partial}{\partial \xi}(\tau_{\xi x} \ h_\xi) \cdot (\frac{\partial \xi}{\partial Z})^2 + \frac{\partial}{\partial \eta}(\tau_{\xi x} \cdot h_\xi)(\frac{\partial \xi}{\partial Z} \cdot \frac{\partial \eta}{\partial Z})$$

Summation of the two terms results in the following:

$$\frac{\partial \tau_{Zx}}{\partial Z} + \frac{\partial \tau_{Yx}}{\partial Y} = \frac{\partial}{\partial \xi}(\tau_{\xi x} \cdot h_\xi)[(\frac{\partial \xi}{\partial Y})^2 + (\frac{\partial \xi}{\partial Z})^2] + \frac{\partial}{\partial \eta}(\tau_{\xi x} \cdot h_\xi)[(\frac{\partial \xi}{\partial Y} \frac{\partial \eta}{\partial Y} + \frac{\partial \xi}{\partial Z} \cdot \frac{\partial \eta}{\partial Z})] \quad (32)$$

From Eq. 25 and the equations derived from Fig. 5, the following relations can be derived:

$$(\frac{\partial \xi}{\partial Y})^2 + (\frac{\partial \xi}{\partial Z})^2 = (\frac{1}{h_\xi})^2$$

$$\frac{\partial \xi}{\partial Y} \frac{\partial \eta}{\partial Y} + \frac{\partial \xi}{\partial Z} \frac{\partial \eta}{\partial Z} = -\frac{1}{h_\xi} \frac{1}{h_\eta} \cos(\xi, Y) \sin(\xi, Y) + \frac{1}{h_\xi} \frac{1}{h_\eta} \cos(\eta, Z) \sin(\xi, Y) = 0$$

Substituting the above relations into Eq. 32 results in the following equation:

$$\frac{\partial \tau_{Yx}}{\partial Y} + \frac{\partial \tau_{Zx}}{\partial Z} = \frac{1}{h_\xi 2} \frac{\partial}{\partial \xi} (\tau_{\xi x} h_\xi)$$

$$= \frac{\tau_{\xi x}}{h_\xi 2} \frac{\partial}{\partial \xi} (h_\xi) + \frac{1}{h_\xi} \frac{\partial}{\partial \xi} (\tau_{\xi x})$$

The RHS of the momentum equation can now be rewritten as:

$$- \frac{1}{\rho} [\frac{\partial}{\partial x} (p + \rho g H) - (\frac{\partial \tau_{xx}}{\partial x} + \frac{\partial \tau_{Yx}}{\partial Y} + \frac{\partial \tau_{Zx}}{\partial Z})]$$

$$= - \frac{1}{\rho} [\frac{\partial}{\partial x} (p + \rho g H) - \frac{\partial}{\partial x} (\tau_{xx}) - \frac{\tau_{\xi x}}{h_\xi 2} \frac{\partial}{\partial \xi} h_\xi - \frac{1}{h_\xi} \frac{\partial}{\partial \xi} (\tau_{\xi x})]$$

An equation to further simplify the term involving h_ξ^2 is derived as follows.

Since $h_\xi \frac{\partial \xi}{\partial Y} = h_\eta \frac{\partial \eta}{\partial Z}$, differentiating both sides by ξ and using the same relationship again results in

$$\frac{1}{h_\xi} \frac{\partial h_\xi}{\partial \xi} = \frac{1}{h_\eta} \frac{\partial h_\eta}{\partial \xi}$$

This equation is substituted into the transformed RHS equation above; then

$$RHS = - \frac{1}{\rho} [\frac{\partial}{\partial x} (p+\rho g H) - \frac{\partial}{\partial x} (\tau_{xx}) - \frac{\tau_{\xi x}}{h_\xi h_\eta} \frac{h_\eta}{\partial \xi} - \frac{1}{h_\xi} \frac{\partial}{\partial \xi} (\tau_{\xi x})]$$

Equating the transformed LHS and RHS equations results in the following momentum equation.

$$\frac{\partial u}{\partial t} + u\frac{\partial u}{\partial x} + \frac{V_\xi}{h_\xi} \frac{\partial u}{\partial \xi} = - \frac{1}{\rho}[\frac{\partial}{\partial x} (p+\rho g H) - \frac{\partial}{\partial x} (\tau_{xx}) - \frac{\tau_{\xi X}}{h_\xi h_\eta} \frac{\partial h_\eta}{\partial \xi} - \frac{1}{h_\xi} \frac{\partial}{\partial \xi} (\tau_{\xi x})]$$

or

$$V_\xi (\frac{\rho}{h_\xi} \frac{\partial u}{\partial \xi}) = - \rho\frac{\partial u}{\partial t} - \rho u\frac{\partial u}{\partial x} - \frac{\partial}{\partial x} (p+\rho g H) + \frac{\partial}{\partial x} (\tau_{xx}) + \frac{\tau_{\xi x}}{h_\xi h_\eta} \frac{\partial h_\eta}{\partial \xi} + \frac{1}{h_\xi} \frac{\partial}{\partial \xi} \tau_{\xi x})]$$

or

$$V_\xi = (\frac{\rho}{h_\xi} \frac{\partial u}{\partial \xi})^{-1} [-\rho\frac{\partial u}{\partial t} - \rho u\frac{\partial u}{\partial x} - \frac{\partial}{\partial x} (p+\rho g H) + \frac{\partial}{\partial x}(\tau_{xx}) + \frac{\tau_{\xi x}}{h_\xi h_\eta} \frac{\partial h_\eta}{\partial \xi} + \frac{1}{h_\xi} \frac{\partial}{\partial \xi}(\tau_{\xi x})] \quad (33)$$

where the velocity component in the   direction is isolated from the velocity component in the   direction.

Derivation of the Equation for the V Velocity Component

The continuity equation in the x, Y, Z coordinate system is

$$\frac{\partial u}{\partial x} + \frac{\partial v}{\partial Y} + \frac{\partial w}{\partial Z} = 0$$

Applying the transformation rule between the two coordinate systems on v/Y and $\partial w/\partial z$ results in the following relation:

$$\frac{\partial v}{\partial Y} + \frac{\partial w}{\partial Z} = \frac{1}{h_\xi \ h_\eta} \ [\frac{\partial}{\partial \xi} \ (h_\eta V_\xi) + \frac{\partial}{\partial \eta} \ (h_\xi V_\eta)]$$

The continuity equation in the curvilinear coordinate system is therefore:

$$\frac{\partial u}{\partial x} + \frac{1}{h_\xi \ h_\eta} \ [\frac{\partial}{\partial \xi} \ (h_\eta V_\xi) + \frac{\partial}{\partial \eta} \ (h_\xi V_\eta)] = 0$$

or

$$\frac{\partial}{\partial \eta} \ (h_\xi V_\eta) = - \ h_\xi h_\eta \ \frac{\partial u}{\partial x} - \frac{\partial}{\partial \xi} \ (h_\eta V_\xi)$$

Integrating both sides of this equation results in:

$$h_\xi \ V_\eta = -\int_{\eta*}^{\eta} [(h_\xi \ h_\eta \ \frac{\partial u}{\partial x} + \frac{\partial}{\partial \xi} \ (h_\eta \ V_\xi)]d\eta + C$$

in which

77* = the value on the water surface

C = an integration constant

The integration constant can be determined by using the boundary condition on the water surface. The continuity equation in the x, ξ, coordinate system can finally be written as:

$$V_\eta = - \ \frac{1}{h_\xi}\int_{\eta*}^{\eta} [(h_\xi h_\eta \ \frac{\partial u}{\partial x} + \frac{\partial}{\partial \xi} \ (h_\xi V_\xi)] \ d\eta + V_\eta* \tag{34}$$

where V77* is the velocity V at point (, *). The velocity component in the 77 direction is therefore computed from Eq. 34.

Approximation of Shear Stresses

To compute the velocity component v from Eq. 33, the shear stresses are needed. However, the shear stresses are also dependent on the velocity components. Therefore an additional equation is needed to solve the shear stresses and velocities. The additional equation is provided from the

distribution of shear stress in the new coordinate system. Chiu and Hsiung (14) assumed that the shear stress varies quadratically in the   direction as follows:

$$\tau_{\xi x}(\xi,\eta) = \alpha_o + \alpha_1[\xi_{max}(\eta)-\xi] + \alpha_2[\xi_{max}(\eta)-\xi]^2 \tag{35}$$

in which $_o$, a_1, and $_2$ are coefficients and $\xi_{max}(\eta)$ is the maximum ξ value on an   curve. The coefficients $_1$, and α_2 are determined from boundary conditions. As developed by Chiu, these are:

a) ε < 0 (the point of maximum velocity is below the water surface)

$$\alpha_o = o \tag{36}$$

$$\alpha_1 = f_1(\xi_o', \eta) \tag{37}$$

in which

$_o' = $ curve that approximates the channel boundary and

$$f_1(\xi,\eta) = \frac{-h_\xi F_o - \alpha_2 \{2 - \dfrac{1}{h\eta}\dfrac{\partial h\eta}{\partial \xi}[\xi_{max}(\eta) - \xi]\}(\xi_{max}(\eta) - \xi)}{1 - \dfrac{1}{h_\eta}\dfrac{\partial h\eta}{\partial \xi}[\xi_{max}(\eta) - \xi]}$$

where

$$F_o = \rho(\frac{\partial u}{\partial t} + u\frac{\partial u}{\partial x}) + \frac{\partial}{\partial x}(p + \rho gH) - \frac{\partial \tau_{xx}}{\partial x} \tag{38}$$

$\xi_{max}(77) = 1$ for   curves that intersect with the stream banks or bed For   curves that intersect with the water surface, it can be reasonably assumed that $\tau_{\xi\eta} = o$ if the wind effects are ignored; then

$$\alpha_1 = - \alpha_2[1 - \xi_D(\eta)] \tag{39}$$

where $\xi_{D(\eta)}$ is the ξ value of this   curve at the water surface.

$$\alpha_2 = [\frac{-1}{\overline{\xi_{max}(\eta) - \xi_o'}\, f_2(\eta)}]\,[\overline{\rho g S_f + h_\xi\, F_o\, f_2(\eta)}] \tag{40}$$

in which

$$f_2(\eta) = \frac{\xi_{max}(\eta) - \xi_o'}{1 - \dfrac{1}{h_\eta}\dfrac{\partial h\eta}{\partial \xi}[\xi_{max}(\eta) - \xi_o']} \tag{41}$$

and the overbar means the average value over the wetted perimeter, which is computed as

$$\bar{A} = \frac{1}{W.P.} \int_{W.P.} A \; h_\eta \; (\xi_o',\eta) \; d\eta \tag{42}$$

and W.P. = total length of wetted perimeter.

b) = o (the point of maximum velocity is on the water surface). For this case, Eqs. 36, 37, and 40 can still be used.

c) > o (the point of maximum velocity is above the water surface). In this case the maximum value of ( ) at the water surface is

   max( ) = o( )

and Eqs. 36, 37, and 40 are still valid.

Computer Model

The mathematical equations for computing the secondary velocities were presented in the preceding section. The equations, which were established in cartesian (x, y, z) coordinates, were first translated into the cross-section-wise (x, Y, Z) coordinates, and were then transformed into the curvilinear (x, ,) coordinates. Several parameters were used in these translation and transformation processes. The functions of these parameters were to relate the channel geometry and primary velocity distribution pattern to the governing equations.

After the equations in the curvilinear coordinate system are established, the computations are carried out in a grid system constructed on the (,) coordinates. The secondary velocities in the (x, y, z) coordinate system are obtained by using inverse transformations.

The overall computational procedures are hence separated into two phases. Phase I determines the best fitted coefficients i, i, k, y, o', and o for approximating the primary velocity distribution and the channel geometry. Phase II uses these parameters to construct a computational grid system and carries out the computations for secondary circulation. In order to make a clear presentation of the model, two flow charts, shown in Figs. 6 and 7, are used to illustrate the computational procedures.
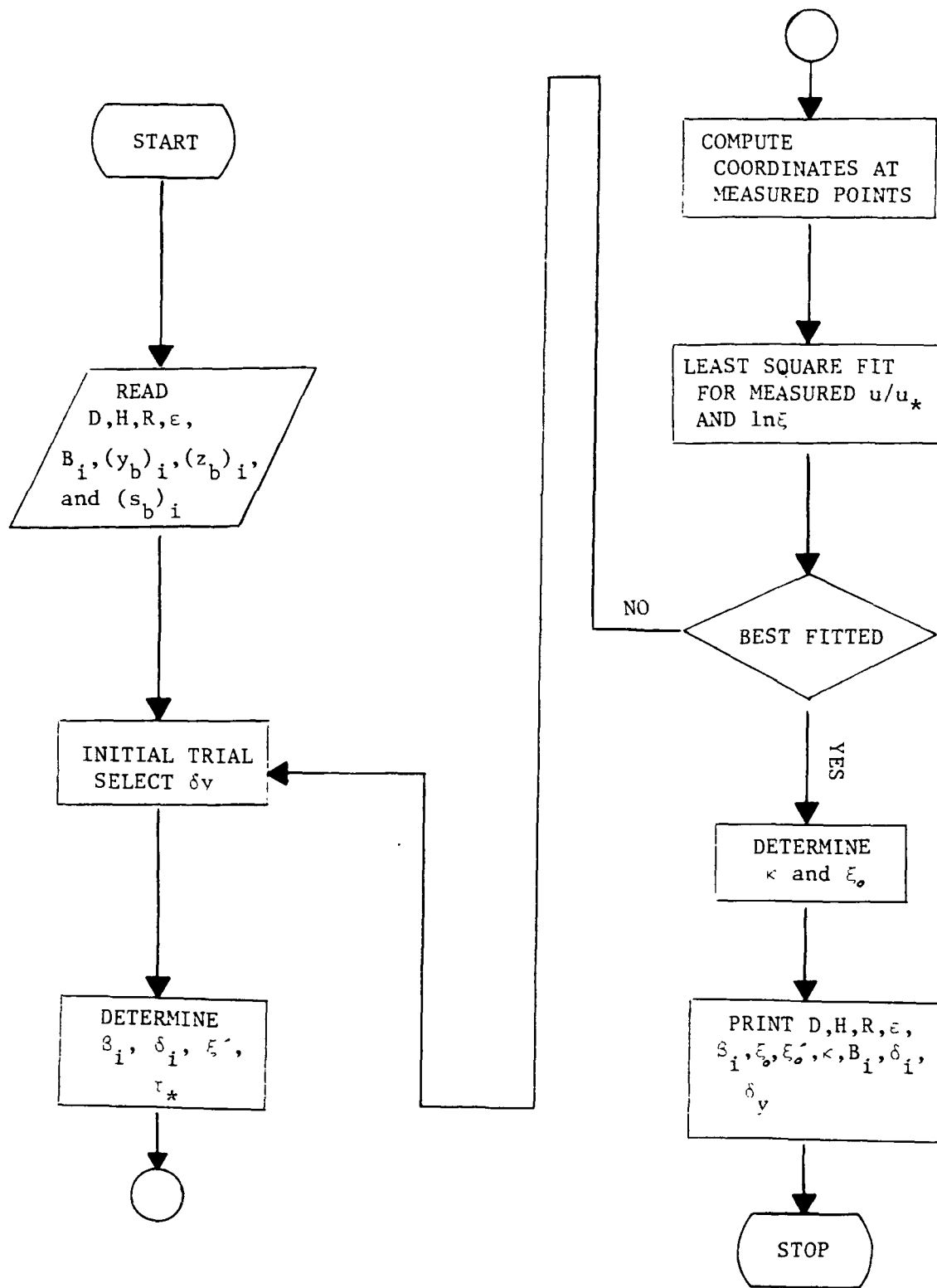
Figure 6. Flow chart of phase I analysis
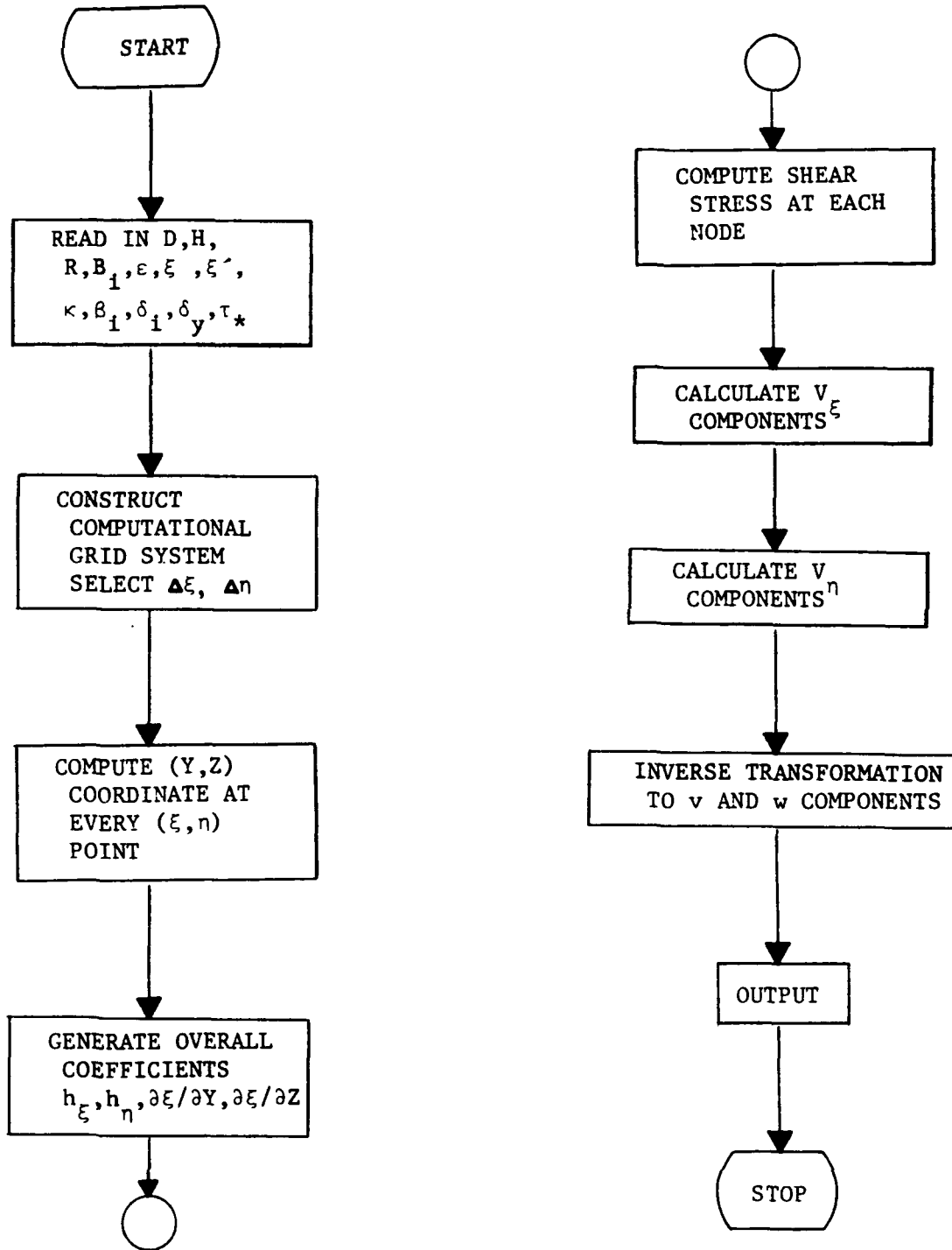
Figure 7. Flow chart of phase II analysis

Phase I Analysis

The Phase I analysis performs the following functions: 1) analyzes field data and determines parameters; 2) derives parameters for Phase II computations.

The channel cross section and isovels of the measured primary velocities are plotted first. Then determinations are made of the mean elevation of the channel bottom, H; the hydraulic radius, R; and the distance from the water surface to the point of maximum velocity, (Fig. 8). The axis which passes through the point of maximum velocity divides the channel cross section into two computational halves, as defined by subscripts i = 1 or 2 previously. The water surface width of each half, Bi, and the water depth D are then determined. Before proceeding to the steps described in Fig. 6, additional data need to be determined. These include (yb, zb)i. and the corresponding slopes Si for each bank. This information is needed for the following computations.

Figure. 8. Definition sketch for field parameters

On the assumption that the ξ_o' curve approximates the channel geometry, this curve should pass through (y_b, z_b). At such a point, the slope of the ξ_o' curve (i.e. boundary) is

$$S_\xi = \frac{\partial y}{\partial \xi} = \frac{\partial \xi}{\partial \xi / \partial y} \cdot \frac{\partial z}{\partial y} = \frac{(\partial \xi / \partial z)(\partial z / \partial \xi)}{(\partial \xi / \partial Y)(\partial Y / \partial y)}$$

$$= \beta_i \frac{D+\delta_y+\varepsilon}{B_i+\delta_i} \frac{Y \cdot Z}{(1-Z)(1-Y)} \tag{43}$$

Equation 43 can be rewritten as

$$\beta_i = (S_\xi) \frac{B_i+\delta_i}{D+\delta_y+\varepsilon} \frac{(B_i+\delta_i-z_b)(D+\varepsilon-y_b)}{z_b(Y_b+\delta_y)} \tag{44}$$
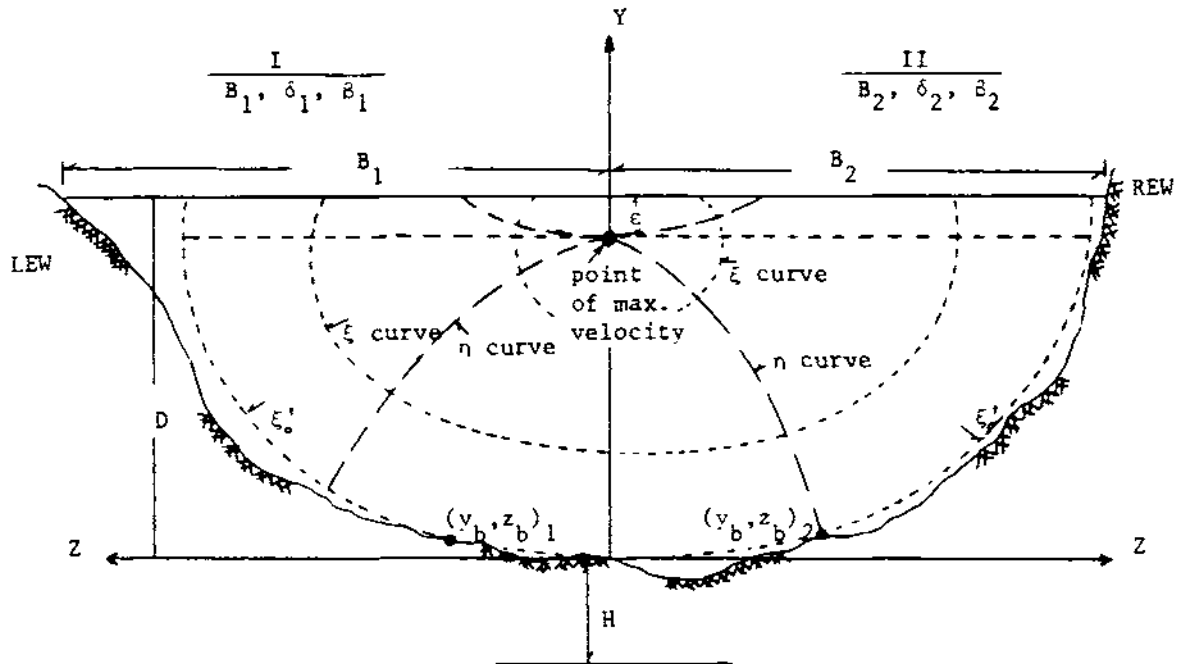
On the other hand, the ξ_o' curve can also be described, by using Eq. 2, as

$$\xi_o' = \frac{y_b+\delta_y}{D+\delta_y+\varepsilon}(1-\frac{|z_b|}{B_i+\delta_i})^{\beta_i} \exp\left(\frac{\beta_i|z_b|}{B_i+\delta_i} - \frac{y_b+\delta_y}{D+\delta_y+\varepsilon} + 1\right) \tag{45}$$

or as

$$\beta_i = \frac{\ln(\delta_y) - \ln(y_b+\delta_y) + y_b/(D+\delta_y+\varepsilon)}{z_b/(B_i+\delta_i) + \ln(B_i+\delta_i-|z_b|) - \ln(B_i+\delta_i)} \tag{46}$$

This β_i value is the same β_i value described by Eq. 44. Moreover, the boundary condition at the origin gives the ξ_o' value as

$$\xi_o' = \frac{\delta_y}{D+\delta_y+\varepsilon} \exp\left(-\frac{\delta_y}{D+\delta_y+\varepsilon} + 1\right) \tag{47}$$

which is derived from Eq. 45 by setting $y_b = z_b = o$. Equating Eqs. 44 and 46 gives an equation which contains two unknowns: δ_i and δ_y. By assuming a δ_y value, β_i and δ_i values can be computed. Therefore an iterative procedure to determine the β_i and δ_i values is used to generate the closest computed velocity distribution to the measured primary velocities in a given channel.

Since the boundary curve ξ_o' and all the other ξ curves have to fit a logarithmic velocity distribution as described in Eq. 1, the following iterative steps depicted in Fig. 6 are used to determine the coefficients needed for Phase II.

(1) assume trial δ_y values

(2) calculate β_i from Eq. 44 and Eq. 46

(3) compute δ_i

26

(4) compute   values at every data point where u is measured

(5) perform linear regression on u/u* and In

(6) determine k and $_{o}$ from intercept and slopes of step (5)

(7) repeat step (1) to step (6)

The $_{o}$ value obtained in step 6 is the line which defines zero velocity, while the $_{o}$' line is the line which approximates the boundary. The best fitted coefficients are those coefficients which generate a primary velocity distribution that has the least standard deviation in comparison with the measured velocities.

The measured hydraulics parameters, i.e., D, Bi, ε, H, R, and the derived parameters δ_{i}, β_{i}, k, $_{o}$, $_{o}$'i and *, are then transmitted to Phase II for velocity and shear stress computations.

Phase II Analysis

The Phase II analysis involves solving the equations discussed in the last section for field variables. The parameters, determined from field data in Phase I, relate these equations to local hydraulic conditions. The characteristics of these equations require building the computations on a grid system, similar to that of a finite difference method. Using the   and curves to form the grid, field data parameters are calculated at the grid nodal points. Also many variables (e.g., h and h) require the corresponding Y, Z coordinate values in their calculations. Consequently the Y, Z coordinates at each grid point have to be retrieved.

Grid   System   Construction

The grid system is constructed by drawing   curves and   curves with predetermined   and   intervals, between the maximum   and   values and the minimum   and   values. These maximum and minimum   and   values can be derived from Eqs. 2 and 3 once the parameters which depend on field data are determined through Phase I analysis, but the   and   values have to be determined by trial and error. The   and   values, once determined, are used in the numerical evaluation of the velocity components   and V , and significantly affect the accuracy and cost of computations. From Eq. 34 it can be seen that a smaller   value will give greater accuracy in the numerical integration. On the other hand, a larger   value will result in a shorter computation time. It is therefore desirable to have the   value as

27

large as possible and to keep the computational error within an allowable range.

The   values, however, depend on   (Eq. 34) values. The   value becomes available in the numerical evaluation of derivatives with respect to
. Finer   values are needed near the channel boundary areas, since the primary velocity gradient is the highest at this location. The derivatives with respect to , when evaluated by a numerical method, produce error. This error is the sum of two errors, truncation and rounding off. The round-off error is negligible on a large machine such as the CDC-6400 that carries numbers to 5 digits beyond the decimal point; therefore the   value is selected to minimize the truncation error. The computation of h /h   (in Eq. 33) is used for checking this   selection. Two examples of a grid system generated using the procedures above are illustrated in Fig. 9.

Solving for   (Y,Z)   Given (, η)

The values of   and   can be computed directly from given Y, Z coordinates by using Eqs. 2 and 3. However, obtaining the values of Y and Z for given   and   coordinates requires solution of the two nonlinear equations. The "modified Regula Falsi" iteration method (51) is used to solve these non-linear equations. Since the variations of   and   curves are different in various regions, the following four algorithms are used to solve the equations:

    (1) Solve Y for fixed Z from   curve
    (2) Solve Z for fixed Y from   curve
    (3) Solve Y for fixed Z from   curve
    (4) Solve Z for fixed Y from   curve

The algorithms are illustrated in Fig. 10. With these four algorithms, one can solve for Y (or Z) for an assumed value of Z (or Y) on a selected curve of
  or 77. The choice of the   (or 77) curve for solutions depends on the tangent values at two consecutive points on that curve. If the tangent values are very close to each other on one curve, then the other curve is selected. The algorithm converges quickly after the first (Y, Z) coordinate point is found, which then becomes the initial trial value for the next (Y, Z) point.

28
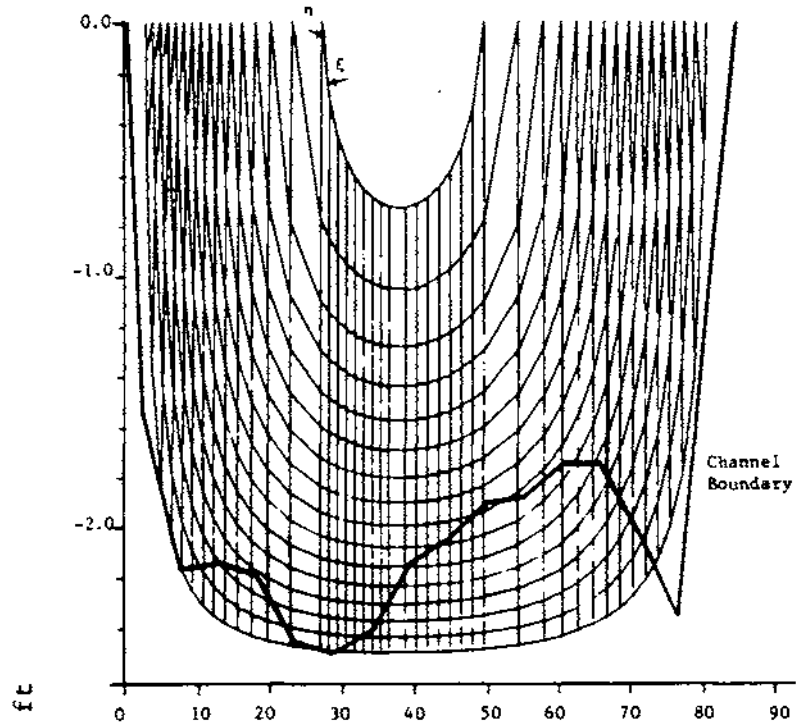
(a) Cross section 6, August 6, 1985
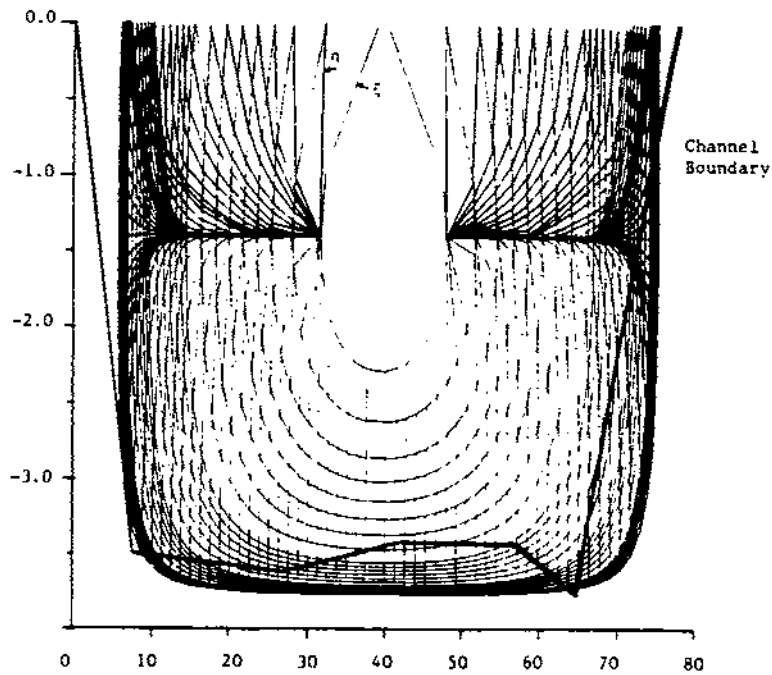
(b) Cross section 8, August 8, 1985

DISTANCE, ft

Figure 9. Grid systems for computational model
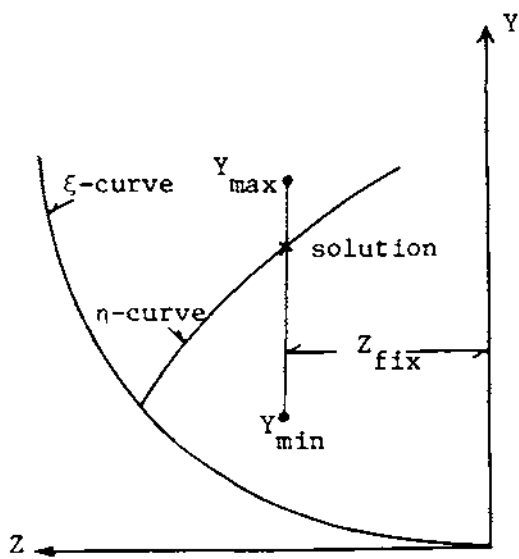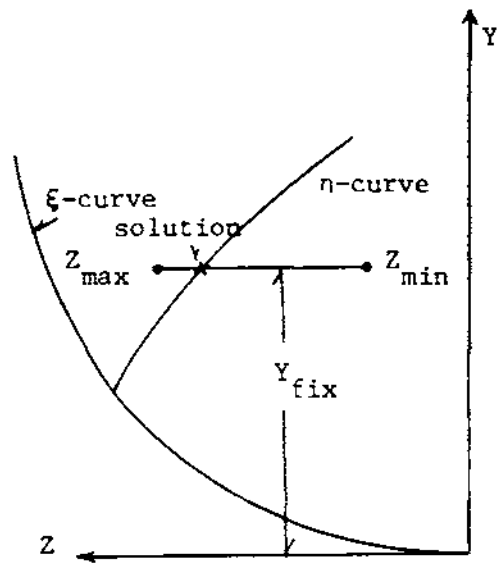
Figure 10. Algorithms for solving Y or Z from ξ and η

Computation for V

The V component is computed from Eq. 33 on every grid point. In general, the normal stress term $\tau_{xx}/\partial x$ is small and is included in the hydrostatic pressure variation term. If the flow is steady and uniform, then
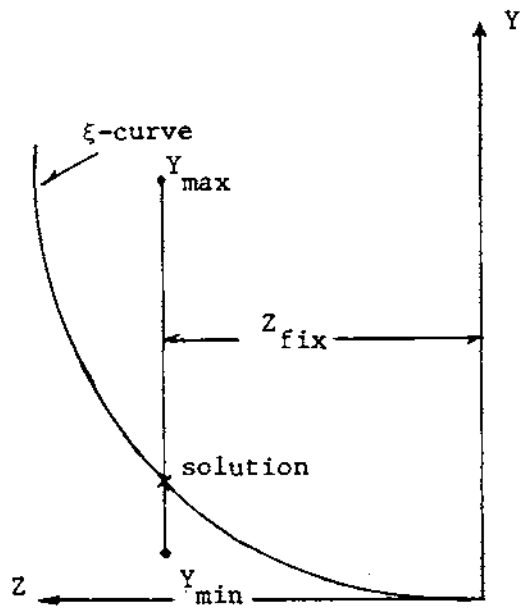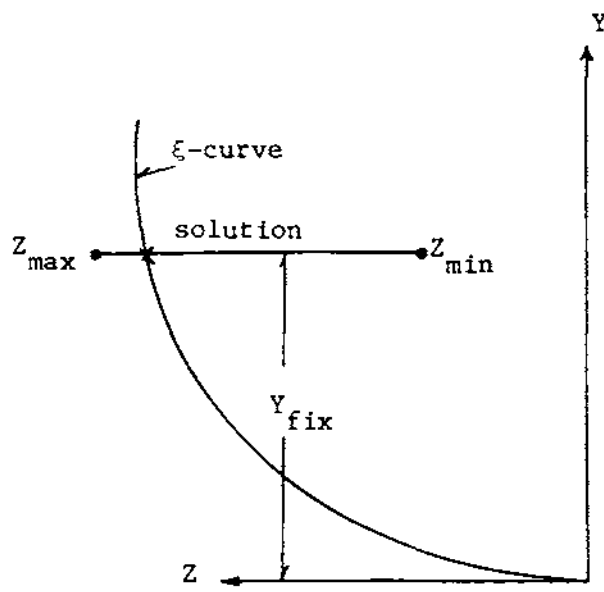
$$\frac{\partial}{\partial x} (\rho g H) = \rho g S \tag{48}$$

where S is the slope of the channel bottom. Since the primary velocity is assumed to have a logarithmic distribution, and the shear stress a quadratic distribution, the velocity and shear stress derivatives can be written as:

$$\frac{\partial u}{\partial \xi} = \frac{\partial}{\partial \xi} \left(\frac{u_*}{k} \ln \frac{\xi}{\xi_o} \right) = \frac{u_*}{\xi k} \tag{49}$$

and

$$\frac{\partial \tau_{\xi x}}{\partial \xi} = - \alpha_1 - 2\alpha_2 (\xi_{max} - \xi) \tag{50}$$

The derivative of h with respect to can be computed in Y and Z coordinates by using this relationship:

$$\frac{1}{h_\eta} \frac{\partial h_\eta}{\partial \xi} = \frac{\partial}{\partial \xi} (ln \; h_\eta)$$

Therefore

$$\frac{1}{h_\eta} \frac{\partial h_\eta}{\partial \xi} = - \frac{\beta_i c_i \; Y^2 Z^2 (1-Z)^2 + c_i \; Y^2 (1-Y)^2 (1-Z)^2}{\xi [(1-Y)^2 (1-Z)^2 + \beta_i c_i \; Y^2 Z^2]^2} \tag{51}$$

With these terms known and $\partial u / \partial x$ determined from field measurement, the V component at each node is computed in a straightforward manner.

Computation for $V\eta$

Eq. 34 can be rewritten as:

$$V_\eta = - \frac{1}{h_\xi} \int_{\eta^*}^{\eta} [h_\xi h_\eta \frac{\partial u}{\partial x} + \frac{\partial}{\partial \xi} (h_\xi V_\xi)] + V_{\eta^*} \tag{52}$$

The following steps are needed to solve Eq. 52.

31

(1) Determine the boundary value V *

$$V_Z = V_\xi (h_\xi \frac{\partial \xi}{\partial Z})^{-1} \quad \text{or } V_Z \text{ from field data}$$

$$V_{\eta *} = h_\eta \quad V_\xi \frac{\partial \eta}{\partial \xi} \tag{53}$$

(2) By using Leibnitz's rule, transform Eq. 52 as follows:

$$V_\eta = -\frac{1}{h_\xi} \int_{\eta *}^{\eta} h_\xi h_\eta \frac{\partial u}{\partial x} d\eta - \frac{1}{h_\xi} \frac{\partial}{\partial \xi} \int_{\eta *}^{\eta} (h_\eta V_\xi) \, d\eta + V_{\eta *} \tag{54}$$

$$\text{or} = \Sigma \frac{-1}{h_\xi} \int_{\eta_i}^{\eta_{i+1}} h_\xi h_\eta \frac{\partial u}{\partial x} \, d\eta - \Sigma \frac{1}{h_\xi} \frac{\partial}{\partial \xi} \Psi + V_{\eta *} \tag{55}$$

where $\Psi = \int_{\eta *}^{\eta} (h_\eta V_\xi) d\eta$

(3) The numerical integration for each integral on the right-hand side is evaluated as:

$$\int_{\eta_i}^{\eta_{i+1}} A \, h_\eta d\eta = \int_{-1}^{+1} (N_1 A_1 + N_2 A_2)(N_1 h \eta_1 + N_2 h \eta_2) [\frac{dN}{dr}1 \, \eta_1 + \frac{dN}{dr}2 \, \eta_2] \, dr$$

$$= \frac{1}{2} (\eta_2 - \eta_1) \sum_{m=1}^{M} (N_1 A_1 + N_2 A_2)(N_i h_{\eta 1} + N_2 h_{\eta 2}) \, W_m \tag{56}$$

where $N_1 = \frac{1-r}{2}$, $N_2 = \frac{1+r}{2}$, r is the reference parameter ranging from -1 to +1,

M is the Gaussian point, and W_m is the weight coefficient.

(4) The derivative of Ψ with respect to   is calculated by:

$$\frac{\partial}{\partial \xi} \Psi_n = \frac{[\Psi_n]_{i+1} - [\Psi_n]_{i-1}}{2 \Delta \xi} \tag{57}$$

which is the central difference approximation.

The whole computation is carried out on an   curve, and the values of Ψ on neighboring   curves are also required.

A complete listing of the computer program for the model is provided in Appendix A.

FIELD DATA COLLECTION

The field data collection component of the project consists of development of the instrumentation needed to measure secondary circulation in natural channels, and the actual data collection. A computerized field data collection system was developed for the project and used successfully in the field. In addition to the acquisition of secondary circulation data, other measurements and sampling for flow discharges, suspended sediment concentrations, bed loads, and bed material were performed during the field data collection periods. This section of the report describes the instruments used to collect the data and the data collection procedures, and presents a summary of the data collected.

Field Data Collection Site

Three sets of field data were collected for the project. Data were collected in May and June 1984 and in August 1985. All the data were collected in the Sangamon River near Mahomet (near the junction of Sections 19, 20, 29, and 30, Township 20N., Range 7E.; river mile 180.6 above the Illinois River; and about 3.8 miles downstream of the Highway 47 bridge, Mahomet, IL). The Sangamon River near Mahomet, among other sites considered, was found to be the best site in terms of water depth requirements and site accessibility. The location of the study site is shown in Fig. 11. The stream channel at the study site is nearly a straight reach for about 500 feet, and then follows a gradual bend. At the upstream end of the site there is a bridge. The bridge piers did not obstruct the flow during the field trips; thus there were no eddies from the bridge piers. This was felt to be an important consideration in all secondary circulation measurements.

The channel width at this reach is almost constant (approximately 75 feet) and the cross section geometry is almost trapezoidal, which is an ideal case for the application of the mathematical model. Water depth at the study site varied from 2 to 4 feet, which made the data collection program relatively easy. The site is easily accessible by car, which facilitated the transport of equipment to the study site.
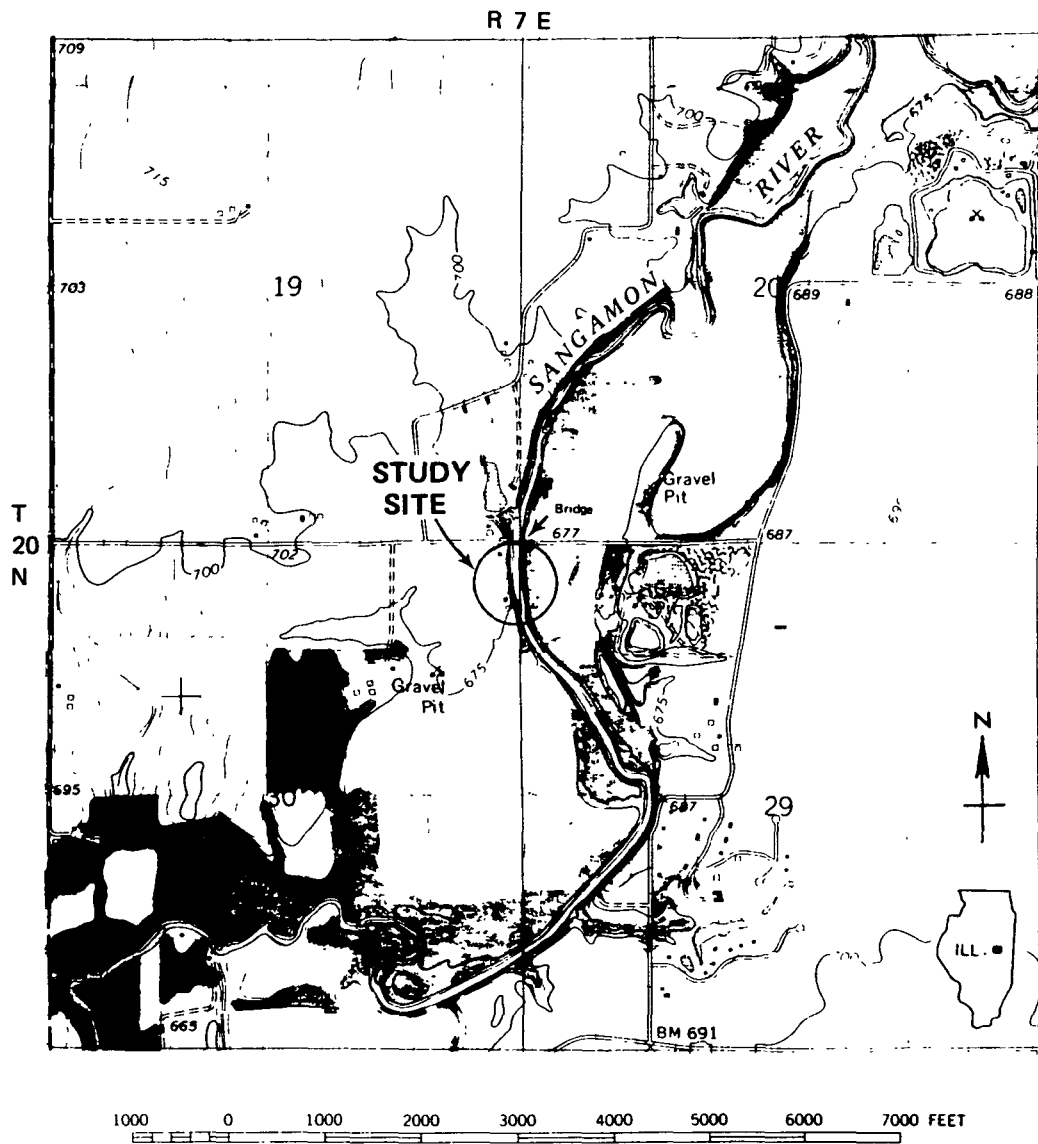
Figure 11. Location of study site

<u>Instrumentation</u>

Three-Dimensional Flow Measurement Setup

The instrumentation for measuring secondary circulation includes a
Marsh-McBirney (Model 527) electromagnetic current meter, a Commodore (Model
8032) micro-computer with tape drive, an interface between the current meter
and the computer, and a rigid support system for the current meter (Fig. 12).
The support system includes a yoke which allows the current meter to be
rotated 90 degrees so that both the lateral and vertical components of the
secondary velocities may be measured.

Using the setup shown in Fig. 12, a continuous velocity reading from the
current meter can be digitized and transmitted to the computer. Either the
time history or an average and standard deviation of the velocity for a given
period can be calculated and stored on cassette tapes.

Marsh-McBirney   527   Electromagnetic   Current   Meter

The Marsh-McBirney 527 Electromagnetic Water Current Meter consists of a
transducer probe with a geomagnetic compass, a cable, and a signal processor.
The probe is a 4-inch-diameter sphere on a 1-inch-diameter rod. The current
meter measures the flow of water in a plane normal to the longitudinal axis of
the probe. The current meter operates on the Faraday Principle of
Electromagnetic Induction, which, simply stated, says: "a conductor moving in
a magnetic field (generated from within the probe) produces a voltage that is
proportional to its velocity." The electrodes placed on the wall of the probe
detect the voltages caused by water flowing past the probe in a plane normal
to the probe's axes. The flow sensing volume around the probe is a sphere 12
inches in diameter (3 probe diameters).

The two components of velocity together with the compass reading can be
directly monitored on the three panel meters on the signal processor. The
panel meter has three selectable full-scale ranges of ±2, ±5, and ±10 ft/sec.
The outputs are within 2% of full scale over the velocity range of the
instrument, and the compass accuracy is ±10° at tilt angles of up to 25°.
Also provided on the signal processor is a voltage output jack, which makes
the velocity and the compass readings available to external data logging
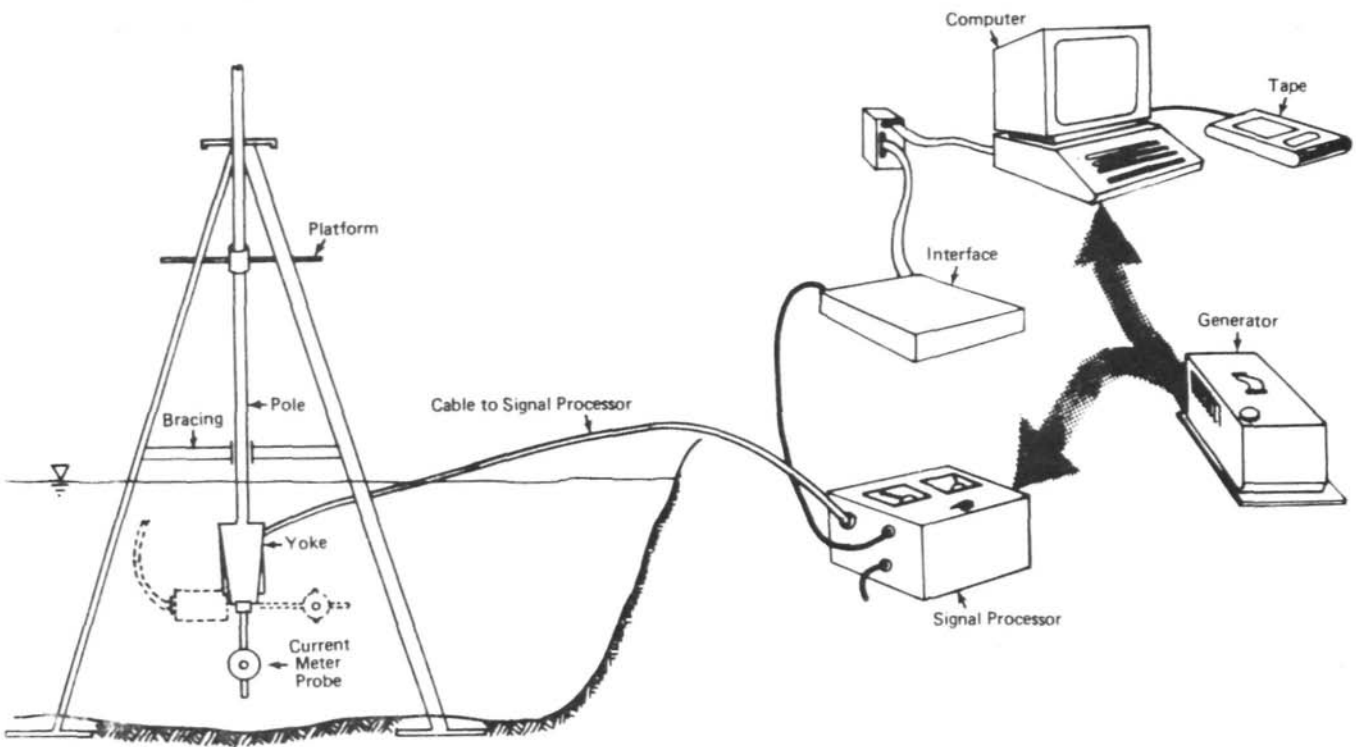equipment; i.e., computers or any other data logging devices.

Figure 12. Field instrumentation setup

36

Interface   and   Computer

Since the Marsh-McBirney electromagnetic current meter output is in an analog signal, and it is almost impossible to visually average the velocity readings from the panel meters, it was decided to construct a data logger system based on a micro-computer. The initial step is to build an interface between the current meter and the computer. An interface which can receive the current meter output at selected frequencies and average the values for specified time periods was built at the Illinois State Water Survey Electronic Shop. The interface transfers the voltage outputs to the computer as digital signals.

The computer used for this system is a Commodore micro-computer (Model 8032) with a cassette tape drive. A computer program was developed to control the sampling procedure; to calculate the means, standard deviations of the velocity components, and the angle; and to store the data on cassette tapes. Additional information such as on site descriptions, coordinates and rotation of the current meter, time, and the gain selected for amplification of the signal is entered into the computer before sampling is initiated. The data stored on the tapes include the descriptive information and the actual data.

Once in the office, the data stored in the tapes is transmitted from the micro-computer to a main-frame computer (CYBER) by using a communication program and a modem. Further analysis of the data is carried out on the CYBER computer.

Support   System   for   the   Current   Meter

The support system for the current meter was an important consideration in the development of the data acquisition system. The current meter has to be placed at a known depth in the stream, and the orientation of the current meter has to remain the same during the sampling period to obtain consistent data. To achieve these objectives, a rigid support system which could be moved from place to place had to be built. This was accomplished by modifying an aluminum stepladder and building a supporting platform, pole, and yoke as shown in Fig. 12. The yoke was designed to allow a 90° rotation of the current meter so that secondary currents both in the transverse and vertical directions could be measured. The yoke is supported by a pole which can be raised or lowered at regular intervals to change the depth of the measuring point. The pole is supported by the platform, which is attached to the

ladder. Additional bracings were used to reduce the vibration of the current meter generated by the stream current. A complete cross-sectional velocity distribution is measured by moving the whole support system along the channel width, lowering and raising the pole, and rotating the current meter.

Rotating Bucket Current Meter

This instrument, a standard Price-type meter, has a rotor with six cone-shaped cups mounted on a vertical stainless steel shaft. The meter has been calibrated by the manufacturer to a standard rating table where the number of rotations of the rotor over a specified time corresponds to a specific velocity.

The current meter is attached to a 30-lb weight to keep it from drifting in the current and is suspended into the stream from a bridge deck with a cable/winch/crane assembly. This meter was used to measure flow velocity in the Sangamon River at the bridge site shown in Fig. 11. These velocity data were used to determine the discharge at the test reach.

Suspended Sediment Samplers

Two types of suspended sediment samplers were used for this investigation: the US DH-59 and DH-48, which are standard samplers designed for the United States Geological Survey. These samplers are designed to accumulate a water-sediment sample from a stream vertical at such a rate that the velocity in the nozzle at the point of intake is as close as possible to the stream velocity. These types of samplers, properly used, will withdraw a sample of the sediment water mixture that represents an average of the sediment concentration through a stream vertical weighted for velocity so that proper sediment load calculations can be made.

Both samplers use standard 1-pint glass milk bottles to collect the sediment-water samples. The DH-59 sampler was designed to be suspended by a hand-held rope or a cable/winch/crane assembly. This sampler was used to determine sediment concentrations of the stream at the bridge site (Fig. 11). The DH-48 sampler was used to sample for sediment concentration at sites away from the bridge. It was designed to be suspended from a wading rod and lowered into the stream by hand.

Bed Load Sampler

A Helley-Smith bed load sampler was used to measure the component of the total sediment load that moves in close proximity to the streambed. This sampler was designed for sampling coarse material where the diameter of the bed load material is above 0.25 mm. The sampler was designed to be lowered to the streambed, left in contact with the bed for a certain period of time, and then retrieved from the water. Samples are retained by a mesh bag (0.25-mm mesh openings) open to the flow through a 3-inch-square opening. The quantity of material trapped by the sampler over a certain period of time indicates the amount of bed load moving through the 3-inch-square area, and by extrapolation (to the total bed width of the stream) the total quantity of bed load carried by the stream can be calculated.

Sonar Stage Meter

An electronic sonar distance meter was used to measure the stage or height of the stream. Readings were made throughout the data collection period in order to assess the changes over time in stage. The sonar meter is placed at a known datum on the bridge and transmits the sonar signal downward to the stream water surface. The water surface reflects the signal back to the meter and the distance is calculated on the basis of the lag time between transmission and return. The meter is calibrated for the effect of air temperature on the speed of sound. The instrument used was an Exact Technologies Corporation Dimensional Measurement Computer. It has a resolution of 1 inch over a range of up to 50 feet.

Data Collection Procedures

Secondary Circulation

Secondary circulation data were collected from cross section to cross section within the study reach. Measurements are taken at several depths for each vertical. Normally ten or more verticals per cross section were selected for data collection. Generally data collection at one cross section lasted one full day.

The data collection procedure for secondary circulation is as follows: First the support platform and pole are moved into the stream and firmly set at the data collection site. Then the yoke with the current meter is securely attached to the pole on the platform. The cable from the current meter is

then connected to the signal processor, which is located on the stream bank. The output from the signal processor is first transferred to the interface and then to the computer by cables between the devices. After all the connections between the devices are completed, power is turned on to activate the system. The computer program which controls the data collection and storage is then loaded into the computer and run. The computer prompts with header lines for inputting general information such as location, date, and time. It then asks for coordinates and gain (or amplification) being used. Once the above procedures are completed,.sampling is initiated and terminated by pressing designated keys on the computer keyboard. Finally, the data are displayed on the screen for inspection and then transferred to cassette tapes for further analysis.

Data   Reduction

All the cross sections where measurements were taken were aligned to be normal to the stream banks. However, this selection does not guarantee that the cross sections are normal to the main flow direction. Furthermore, it is very difficult to keep the orientation of the current meter consistent for all measurements. Thus the measured values of secondary flows might not represent the true values. The measured velocities were adjusted to reflect the true longitudinal and secondary currents by using the orientation of the current meter with respect to the magnetic north, which is measured simultaneously with the velocities, and by using one of the following two criteria: 1) The discharges measured by the two current meters, the electromagnetic and the rotating bucket mechanical current meter, should be equal; and 2) the continuity of secondary flows must be satisfied between downstream and upstream cross sections.

The method employed to check the continuity of secondary discharge is that proposed by Dietrich and Smith (22), and also used by Thorne et al. (56). In this method, the net secondary discharge is determined by integrating the secondary velocity over the depth. The continuity of discharge requires that the net secondary discharge at a cross section be equal to that of the section immediately upstream or downstream. If the two differ, the section is reoriented to change the secondary velocities until an agreement is reached.

The measured velocity components V_x and V_y, shown in Fig. 13, are first converted to resultant velocities from which the downstream and cross-stream velocities are computed.

The magnitude of the resultant velocity = $\sqrt{V_x{}^2 + V_y{}^2}$

The angle of the resultant velocity with respect to magnetic north (0) is determined as:

$$\theta = \left\{ \begin{array}{ll} \tan^{-1}(V_x/V_y) & \text{if } V_y > o \\[8pt] \tan^{-1}(V_x/V_y) + \pi & \text{if } V_y < o \end{array} \right. \tag{58}$$

The angle of the main downstream velocity with respect to the magnetic north (θ_N) is given by:

$$\theta_N = \theta + \theta_c \tag{59}$$

in which

V_y , V_x = measured velocity

θ_c = bearing of sensor with respect to magnetic north

θ_N = bearing of left bank with respect to magnetic north

θ = bearing of resultant flow with respect to magnetic north

The downstream and cross stream components of the velocity are then given by:

downstream velocity = (resultant) (cos θ)

cross stream velocity = (resultant) (sin θ) $\hspace{2cm}$ (60)

Sampling   Period

Two major factors are considered before selecting the sampling period: 1) the sampling period should be long enough that the velocity fluctuations will average out and a true mean velocity will be obtained; and 2) the sampling duration should be short enough that the measurements for at least one cross section can be completed within a day.

Theoretically the true mean velocity is the average of the velocity measurements for an infinite time period. In practice, however, a period of averaging time is determined which gives a mean velocity very close to the long-time average with specified tolerance limits.

One method of estimating the averaging period is to determine the mean velocities for several averaging periods and then select the averaging period which gives a mean within a specified range from the true mean. This will require taking long period samples for each of the sampling periods. However,
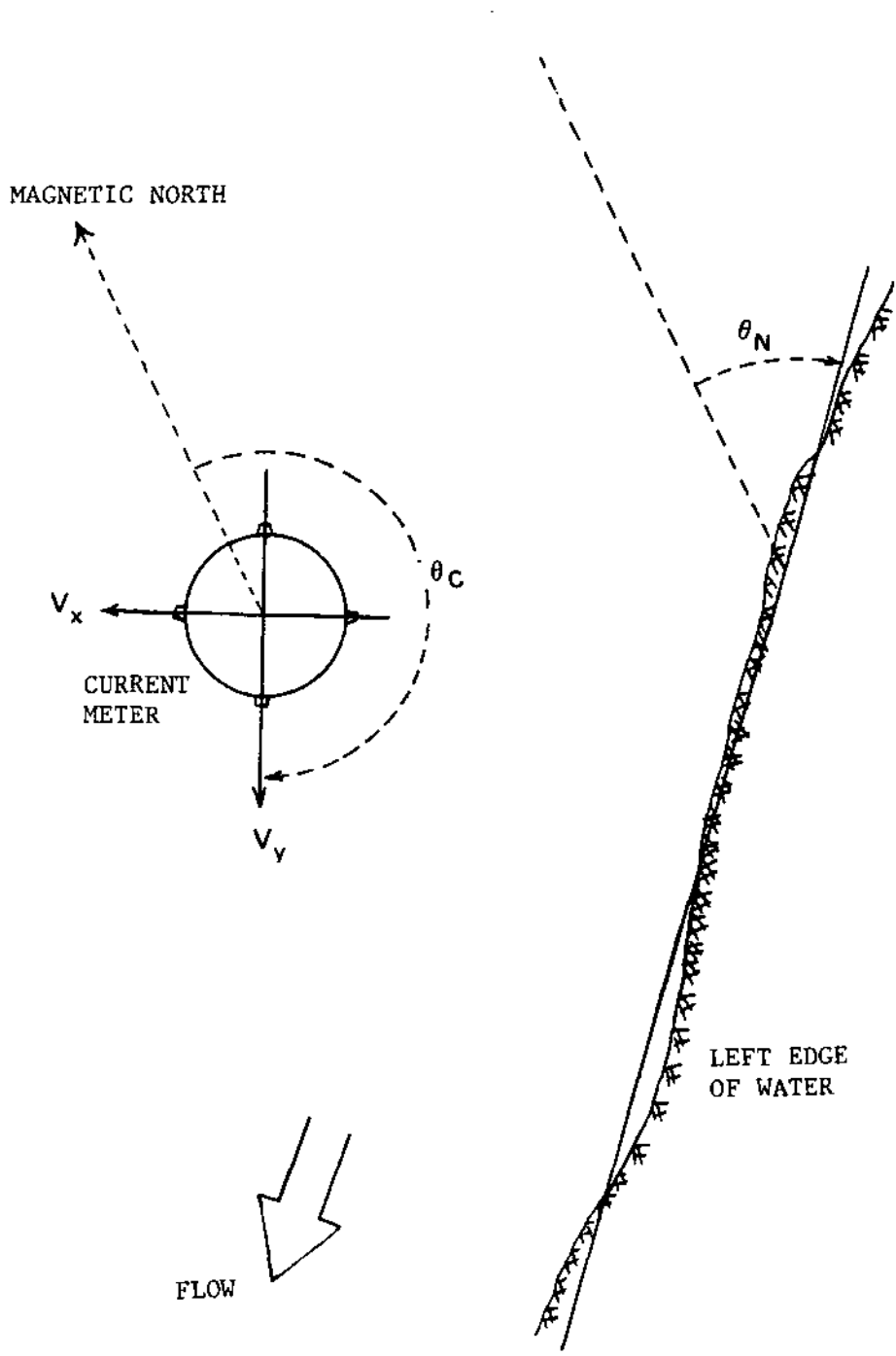
MAGNETIC NORTH

θ_C

V_x

V_y

CURRENT
METER

θ_N

LEFT EDGE
OF WATER

FLOW

Figure 13. Orientation of measured velocities with respect to the main
flow direction

42

an equivalent result is obtained from one long period sample as follows. A
set of sampling periods τ_i, i = 1,2,3 ...M are first selected. Then the
sample is subdivided into blocks of N_i samples for each τ_i. The mean, $\bar{u}$, and
the standard error, S_m, which is the standard deviation in the mean, for each
averaging period are then computed by the following equations (48)

$$\bar{u} = \frac{1}{T_m} \int_o^{T_m} u \, dt \tag{61}$$

$$S_{m_i} = \frac{\left[\sum_{j=i}^{N_i} (v_j - \bar{u})^2 \right]^{1/2}}{N_i} \tag{62}$$

where $v_j = \frac{1}{\tau_i} \int_o^{\tau_i} u_i \, dt$ = time average velocity for the period of τ_i

   N_i = the number of averages with an average period of τ_i

   T_m = the sampling period of the whole sample

   $\bar{u}$ = the long-term average or the true mean

   u = velocity at time t

To generalize the standard error for variable magnitudes of velocity, it is
convenient to non-dimensionalize the standard error by the mean velocity. The
normalized error, S_{mi}, is therefore given by:

$$\bar{S}_{m_i} = \frac{S_{m_i}}{\bar{u}} \tag{63}$$

Two sets of velocity measurements are shown in Fig. 14 to illustrate how
the sampling periods were selected. The first measurement was taken near the
center of the channel (42 feet from the left bank) and 1.25 feet from the
water surface, while the second sample was taken close to the stream bank (26
feet from the left bank) and 1 foot from the water surface.

The total sampling time, Tm, for both samples was 5 minutes. The
sampling periods, τ_i, were 14, 27, 50, 99, and 150 seconds. The relationship
between the sampling period and the normalized standard error for both samples
is shown in Fig. 15. As shown in the figure the normalized standard error
near the bank is greater than at the center of the channel. This is probably
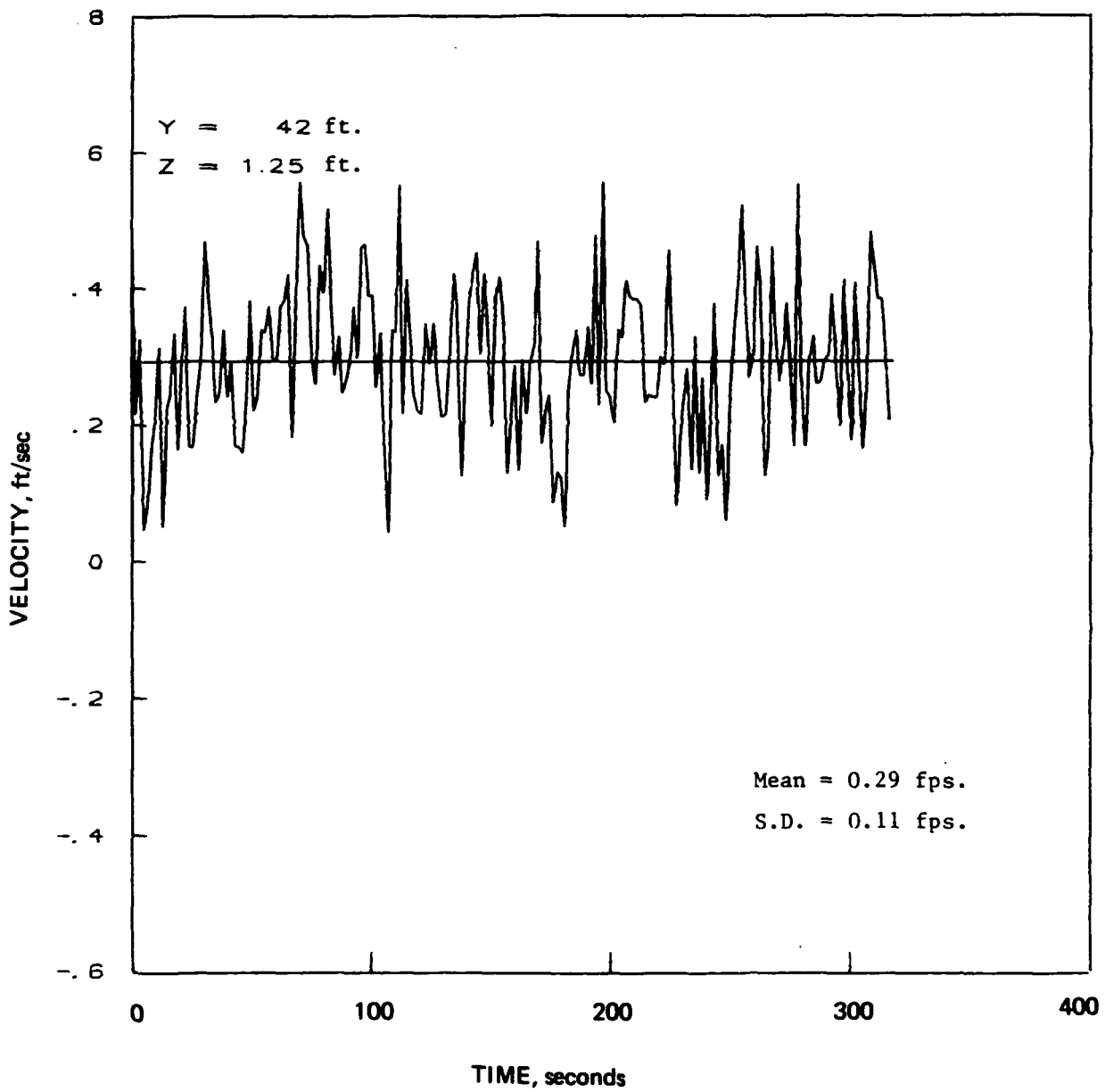because of greater secondary currents and turbulence intensity near the banks

43

Figure 14a. Velocity fluctuations at a point (distance - 4 2 ft, depth = 1.25 ft), cross section 9, August 9, 1985
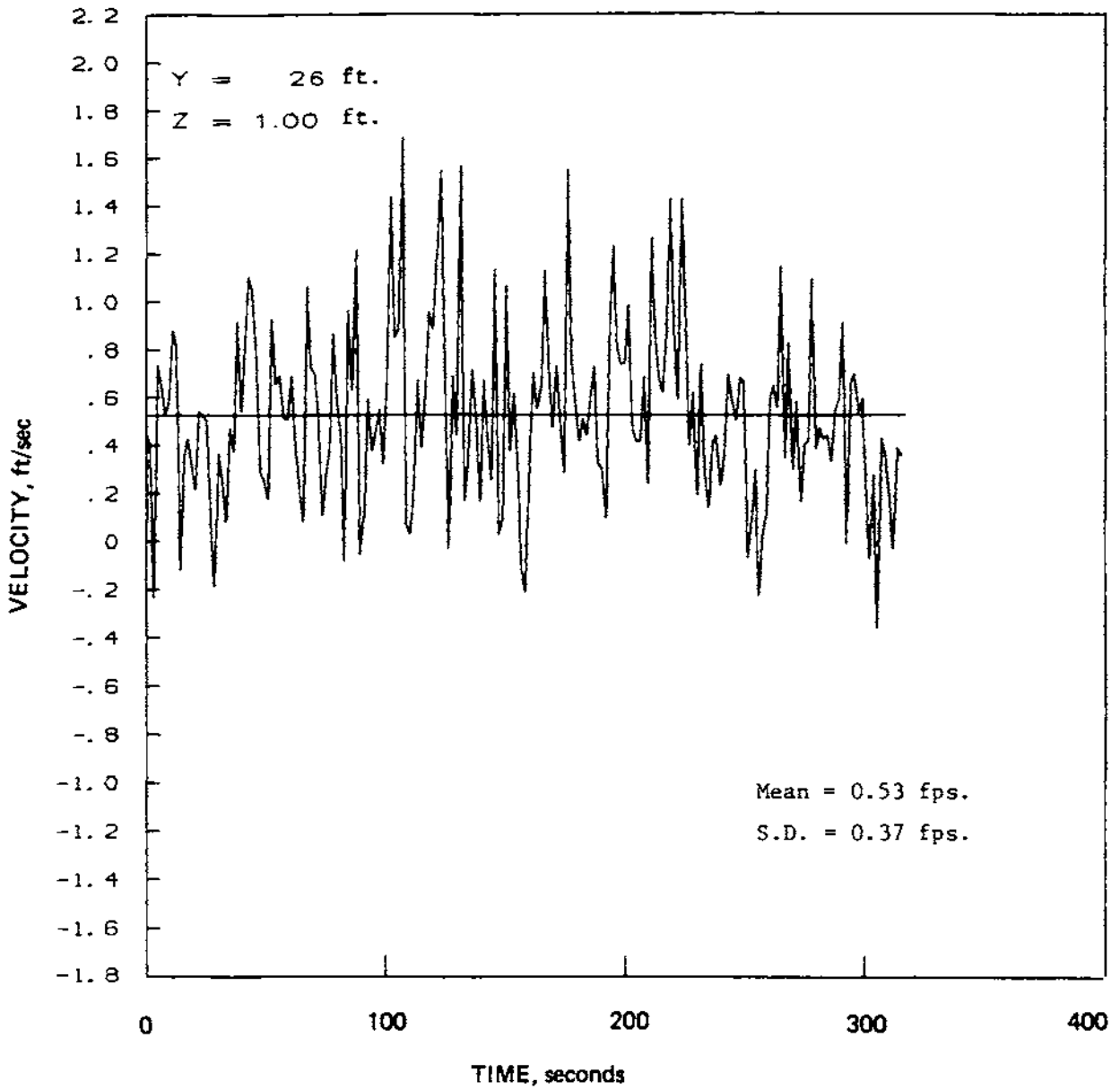
Figure 14b. Velocity fluctuations at a point (distance - 26 ft, depth = 1.00 ft), cross section 7, August 7, 1985
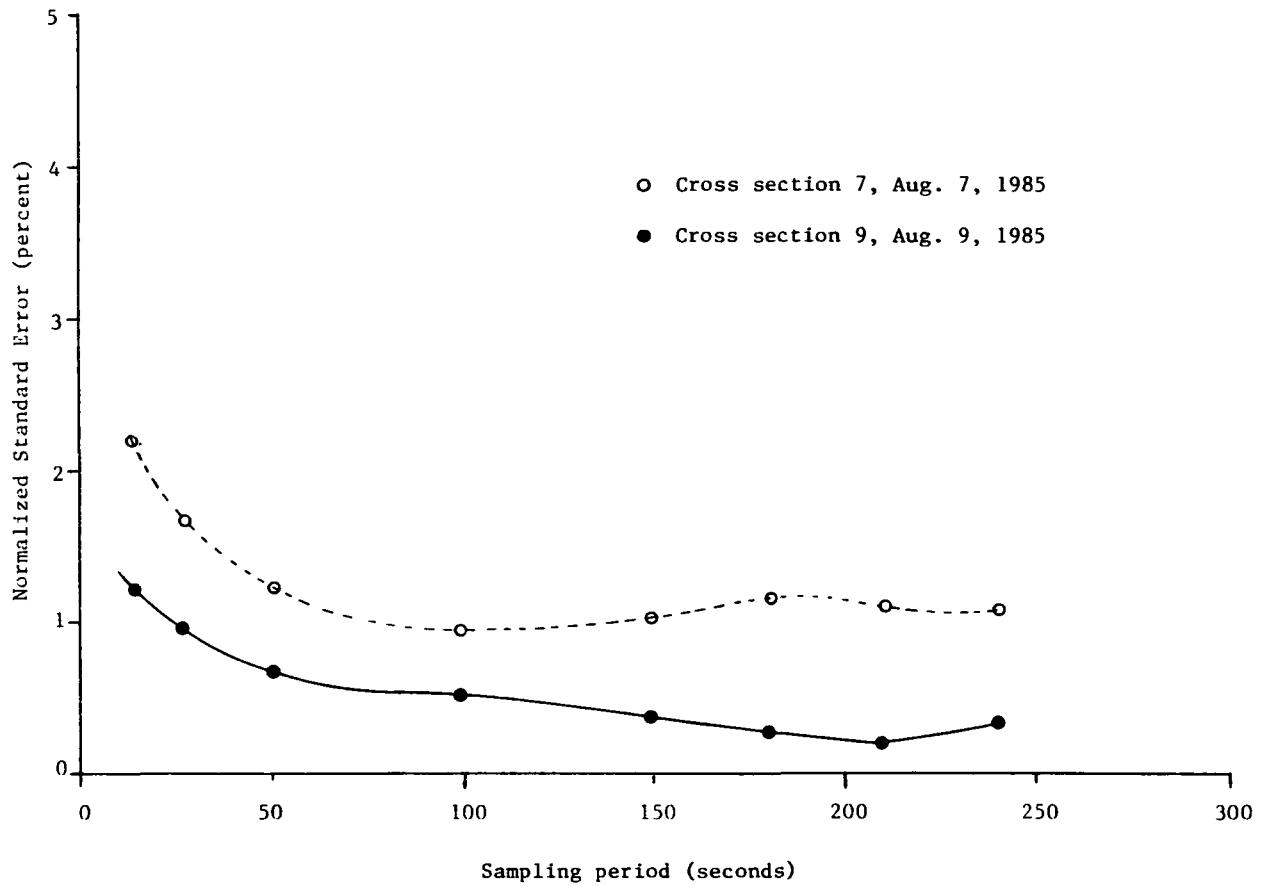
Figure 15. Relationship between sampling period and the normalized standard error for two sets of velocity measurements

than at the center of the channel. However, the normalized error for both
samples decreases with increasing sampling period. The error decreases
sharply for sampling periods more than 60 seconds and gradually thereafter.
It was decided to use 60 seconds as the sampling period for an efficient and
reliable data collection procedure.

Stream Discharge Measurement

The discharges of the Sangamon River at the study site were measured
several times during each field trip. Two types of instrumentation were used
to measure discharge of the Sangamon River: 1) the electromagnetic two-
dimensional current meter, and 2) the rotating bucket mechanical current
meter. The electromagnetic meter was employed primarily to measure secondary
circulation. However, since the meter also measures the flow in the
downstream direction, the data generated were used to compute the stream
discharge. The rotating bucket mechanical meter was used to measure stream
velocity and to compute stream discharge for a comparative analysis between
results of the two methods.

The stream discharge measurement techniques used for the rotating bucket
current meter were those recommended by the United States Geological Survey
(9) and the American Society for Testing and Materials, Standard Practice for
Open-Channel Flow Measurement of Water by Velocity-Area Method, Designation:
D 3858-79 (1). Stream discharges are determined by subdividing a cross
section of the stream into partial sections; the average velocity of the flow
at each partial section is measured and multiplied by the flow area of the
partial section. The sum of the individual partial section discharges equals
the total stream discharge.

Discharge measurements performed at the bridge site used the rotating
bucket current meter. The stream cross section under the bridge was divided
into 7 partial sections, each approximately 10 feet wide. The velocity meter,
suspended by a cable/winch/crane assembly, was lowered into the stream at the
midpoint of each partial section. A depth gage built into the winch read the
total depth of the stream at the midpoint of the partial section. This depth
was recorded and later used to calculate the flow area of the partial section.
Velocity measurements were then made at the vertical in the midpoint of the
partial section. The meter was positioned below the water surface at 0.2 and
0.8 of the total depth (for total depths greater than 2.0 ft) or at 0.6 of the

total depth (for total depths less than 2.0 ft). The velocity of the stream
at the measured points was recorded and used to calculate the average velocity
of the partial section. Stream discharges were then calculated by multiplying
the mean velocity for each partial section by the respective cross-sectional
area. Total discharge for the section was obtained by summing all the
individual partial discharges.

Suspended Sediment Concentrations and Particle Size Sampling

Sediment sampling was performed using the US DH-59 and US DH-48 samplers
as described in "Instrumentation." The sediment sampling was performed to
determine the concentration of suspended sediment and the total sediment load
in the stream. The methods used were developed by the USGS (31) and are
proposed practices of the American Society for Testing and Materials Committee
D-19 (water) and Subcommittee D-19.07 (sediment) (1).

The sampling methodology employed the equal width increment method where
the stream cross section is divided into three or four partial sections and
the midpoint of each partial section is sampled. At each midpoint a clean
sample bottle is inserted into the sampler and the sampler is carefully
lowered from the stream surface to the bottom and raised back to the surface
at a constant rate of 1 foot per second. The sample bottle is then capped,
identified, and noted in the field book. This procedure is repeated at each
partial section midpoint until the entire width is sampled. The purpose of
using equal width increment and depth integrated techniques is to quantify the
total amount of sediment carried in suspension by a stream where the
concentration of sediment varies across the width and depth.

Suspended sediment concentration sampling was performed at the study
site on most of the days of data collection. The sample bottles were
identified and labeled in the field and then brought into the office for
logging and preparation for delivery to the Inter-Survey Geotechnical
Laboratory for analysis.

Suspended sediment particle size analysis was performed on three samples
obtained by dip sampling. Dip sampling was used instead of the methods
outlined above for suspended sediment concentration because of the low
concentration of suspended sediment, which made it necessary to collect a
large quantity of samples for the laboratory analysis.

Bed Load Measurement

The coarse fraction of the sediment load (>0.25 mm) moving in contact with or within 3 inches of the streambed was sampled using a Helley-Smith bed load sampler. This sampler was lowered to the streambed at the thalweg and left there for a period of five minutes. The sampler allows the streamflow near the bed to pass through the intake opening and into a fine mesh. The sample in the mesh bag at the time of retrieval was then examined for quantity and types of sediment (inorganic, wood, leaves, etc.). Field observations of the sample were then entered into the field notebook. Only one bed load measurement was collected as part of this investigation because of low flow conditions during sampling periods, at which time no appreciable bed load movement was observed.

Bed Material Sampling

The streambed sediment was sampled in order to characterize the stream bed and to determine the distribution of sediment particle sizes that are available for transport as bed load and suspended load. The streambed was sampled across its width 100 ft downstream of the bridge sampling site. Three discrete samples were obtained from the bed at three locations: the midpoint, and the left and right quarter points. The bed samples were obtained using a shallow bucket 10 inches across and 3 inches deep. The bucket was lowered through the water column by hand and then tilted so that one edge could cut a sample from the top inch of the streambed. The bucket and sample were brought to the water surface carefully to avoid agitating or dispersing the material. The excess water was drained away from the sample and the sample was placed into whirl-pack sampling bags. The samples averaged approximately 500 grams each. All sample bags were labeled to identify date, time, and sampling location. The samples were then brought into the office for logging and preparation and delivered to the Inter-Survey Geotechnical Laboratory for analysis.

Stage Measurement

The relative change in the stream surface elevation was monitored daily at the bridge site using a sonar distance meter. At a minimum, readings were made at the beginning and end of the work day. The sonar readings were

adjusted to reflect possible temperature effects on the speed of sound.
Relevant data were recorded in the field notebook for later analysis.

Summary of Field Data Collected

A summary of all the field data collected for the project is presented
in this section. A complete list of all the data is included in Appendix B.
All the cross sections where data were collected are shown in Fig. 16. Table
1 shows the dates when the data were collected at each cross section.

Secondary Circulation

The velocity measurements used to construct secondary circulation were
first processed separately to illustrate the distribution of each component in
a cross section. Fig. 17 shows the distribution of the longitudinal,
transverse, and vertical components of the velocity at cross section 7. It
should be noted that different scales are used for the three components shown
in the figure, so that the distributions of the lateral and vertical
components, which are much smaller than the longitudinal component, can be
shown effectively. The distribution of the longitudinal component (Fig. 17a)
indicates that the higher velocities are located close to the center of the
channel and the lower velocities are near the banks, as should be the case.

Table 1. Dates of Field Data Collection

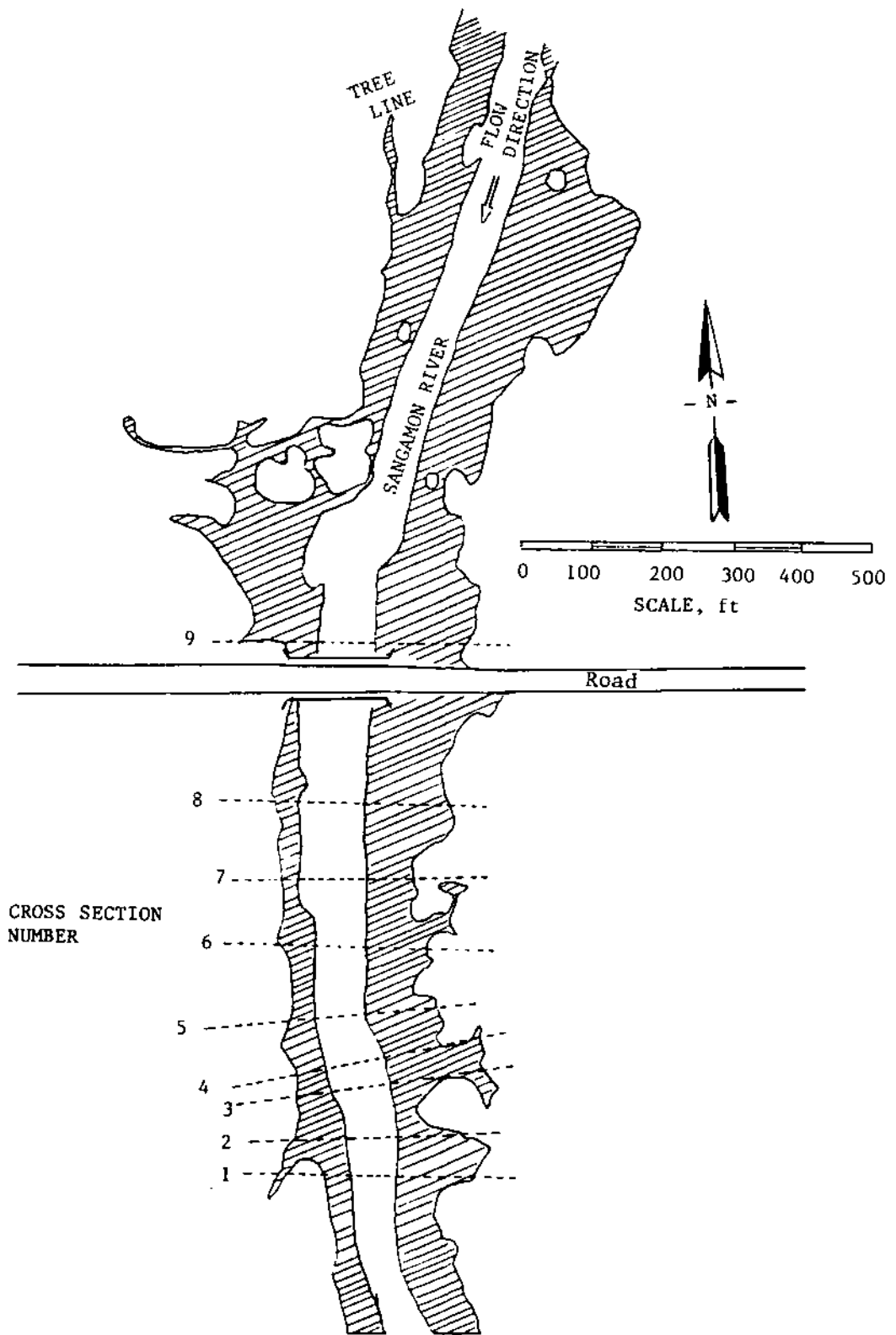| Date Month/day/year	Cross section number where data were collected
06/27/84	7
06/28/84	6
06/29/84	5
07/09/84	3
07/10/84	4
07/12/84	2
07/13/84	1
08/05/85	5
08/06/85	6
08/07/85	7
08/08/85	8
08/09/85	9

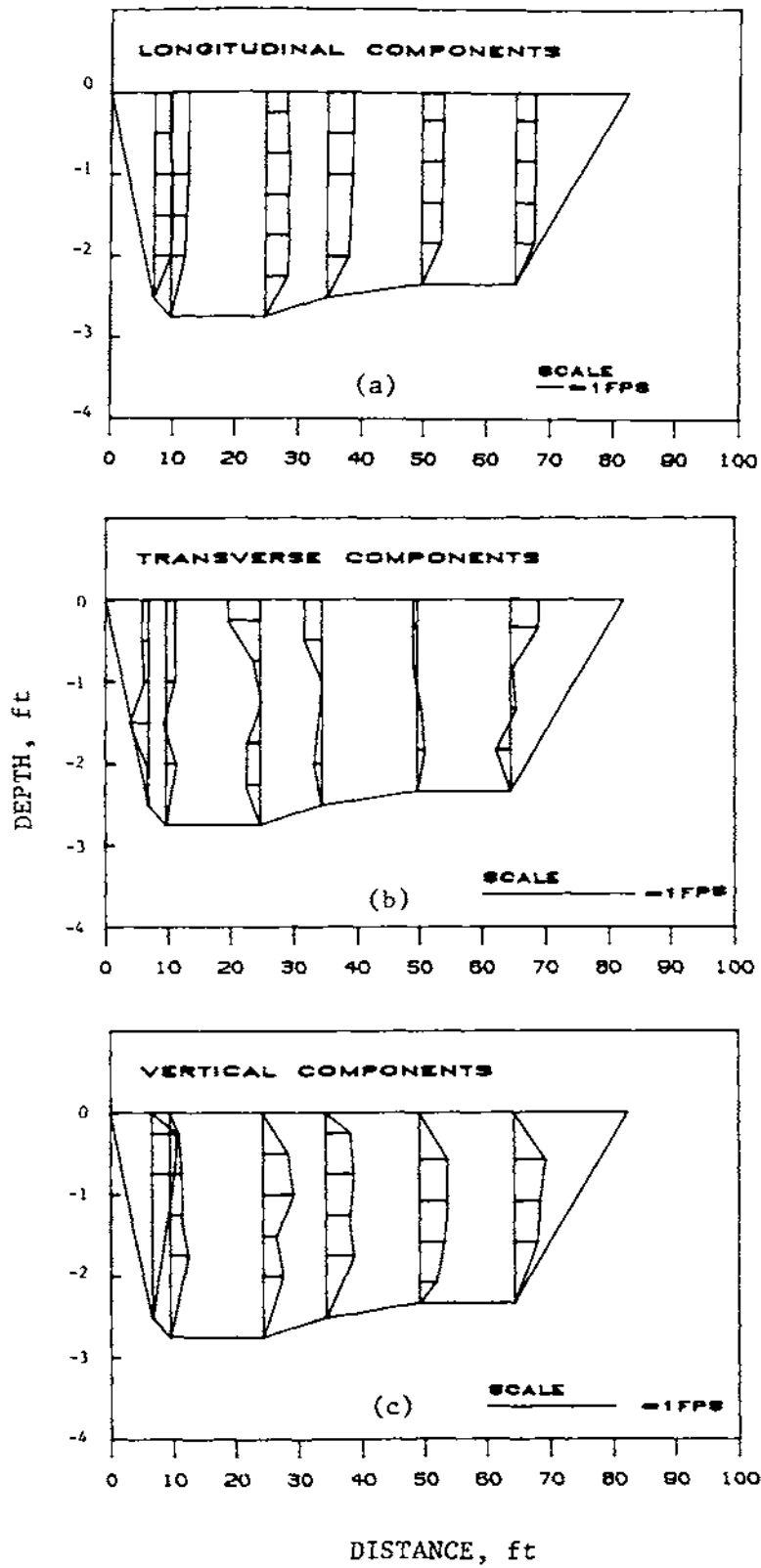Figure 16. Location of cross sections at the study site

51

Figure 17. Distribution of measured longitudinal, transverse and vertical components of velocity at cross section 7, June 27, 1984

52

The distribution of the transverse component shown in Fig. 17b is, however, highly variable in magnitude and direction. The vertical components for this particular cross section (Fig. 17c) show some variation in magnitude but not as much as the lateral components. Fig. 17 is just an example to illustrate the type of data collected and how they were analyzed. Similar plots for all the data collected in the field are given in Appendix B.

The longitudinal velocity was further processed to generate isovels as shown in Fig. 18. Since the model used for this project utilizes the isovels as the basis for coordinate transformation, it was felt important to generate the isovels for measured data so that they could be compared with the model. Isovel plots for all the measurements are also shown in Appendix B.

The transverse and vertical components of the velocity were combined to generate the secondary current vectors as shown in Fig. 19. For this particular case, the measured values indicate primarily upward and lateral movements of the secondary currents. The downward currents were either missed in the measuring process or are located close to the banks. As with the previous plots, the rest of the secondary current plots are included in Appendix **B.**

Stream Discharge

The discharge of the Sangamon River at the study site was measured at the bridge cross section using the rotating bucket current meter for the purposes of monitoring the changes in the daily streamflows. Stream discharges were also calculated on the basis of the secondary current measurements at the different cross sections. Table 2 presents a summary of the discharge measurements, as determined by both the rotating bucket and electromagnetic current meters. As shown in the table there are some differences in the stream discharges calculated from the two sets of measurements. Considering that the discharges were not measured at the same cross sections, and considering the errors in stream flow measurements, the agreement between the two sets of measurements was satisfactory for most cases.
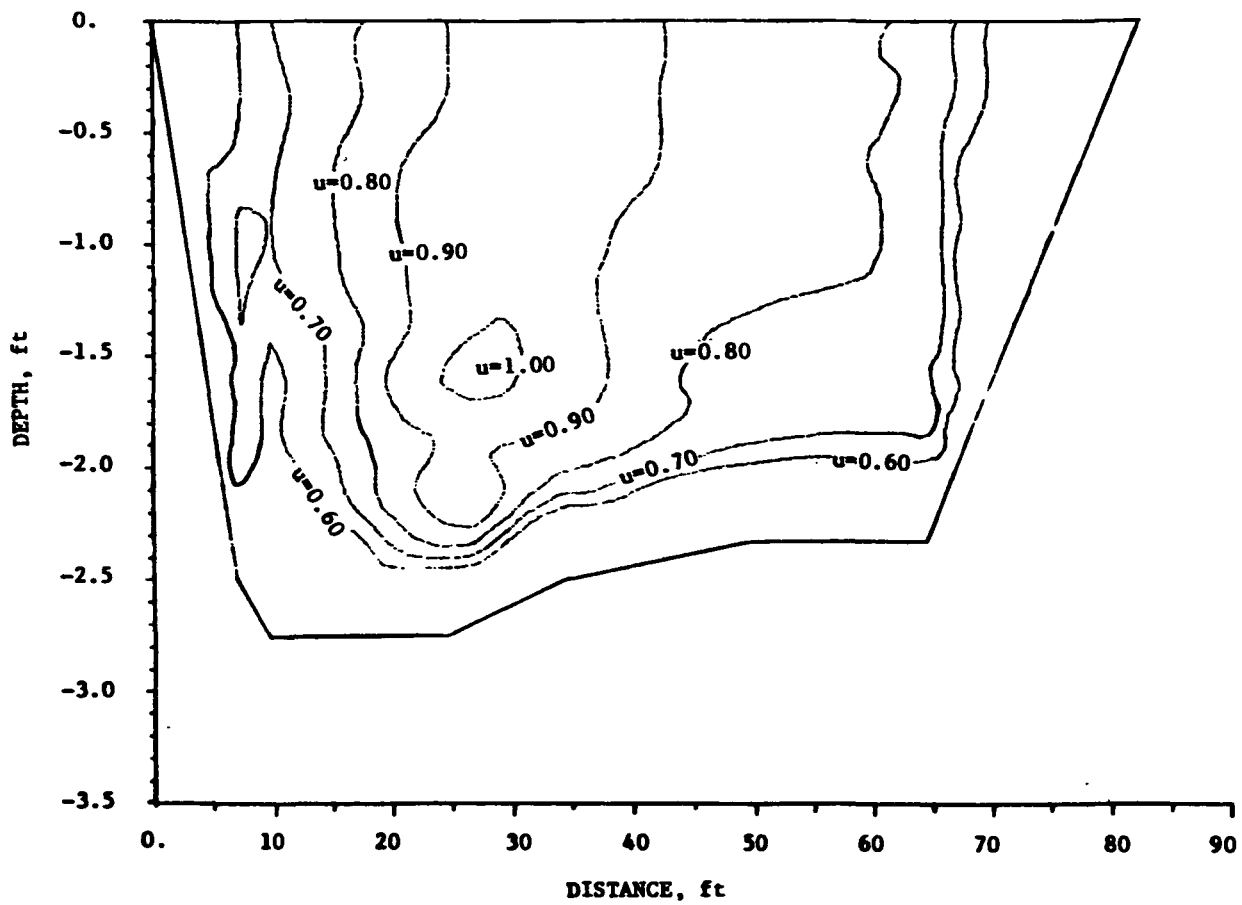
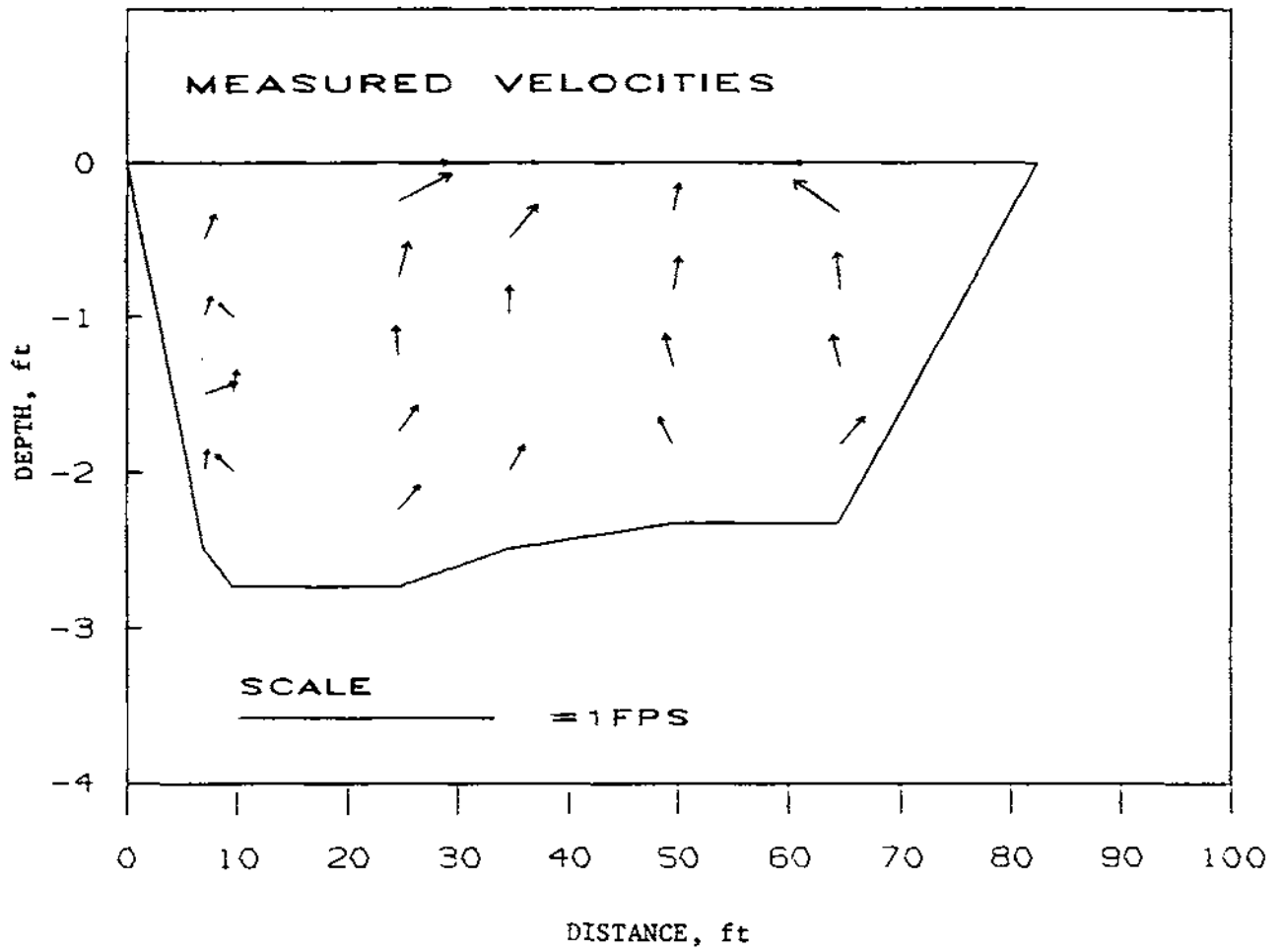Figure 18. Isovels of the longitudinal velocity at cross section 7, June 27, 1984

54

Figure 19. Measured secondary current vectors at cross section 7, June 27, 1984

Table 2. Water Discharge and Sediment Load Measurements During Data
Collection Period

| Date | Water discharge (cfs) | | Suspended sediment | |
	Rotating bucket	Electromagnetic	Concentration (ppm)	Load (tons/day)
6/27/84	--	139	--	--
6/28/84	--	140	205	77
6/29/84	--	119	--	--
7/09/84	71	48	--	--
7/10/84	65	58	114	20
7/12/84	36	--	--	--
8/05/85	126	75	85	29
8/06/85	100	115	94	25
8/07/85	73	66	48	10
8/08/85	--	115	--	--
8/09/85	80	59	52	11
8/14/85	70	--	103	20

The highest and lowest discharges measured in the 1984 data collection
period were 140 cfs on June 28, and 36 cfs on July 12, respectively. For the
1985 data the highest discharge was 126 cfs on August 5 and the lowest was 59
cfs on August 9. The discharges measured during the field data collection
periods are all below the mean streamflow and generally fall in the range of
flows exceeded from 40 to 70 percent of the time as indicated in the flow
duration curve shown in Fig. 20. The flow duration curve was developed from
historical streamflow records of the Sangamon River gaging station at Mahomet,
which is 4 miles upstream of the study site. Data collection was not
conducted during higher flows because of logistic requirements of deep water
measurements, which require using a boat to move the instrumentation from
station to station. For water depths less than 4 feet the instrumentation is
moved from station to station by wading in the stream channel and physically
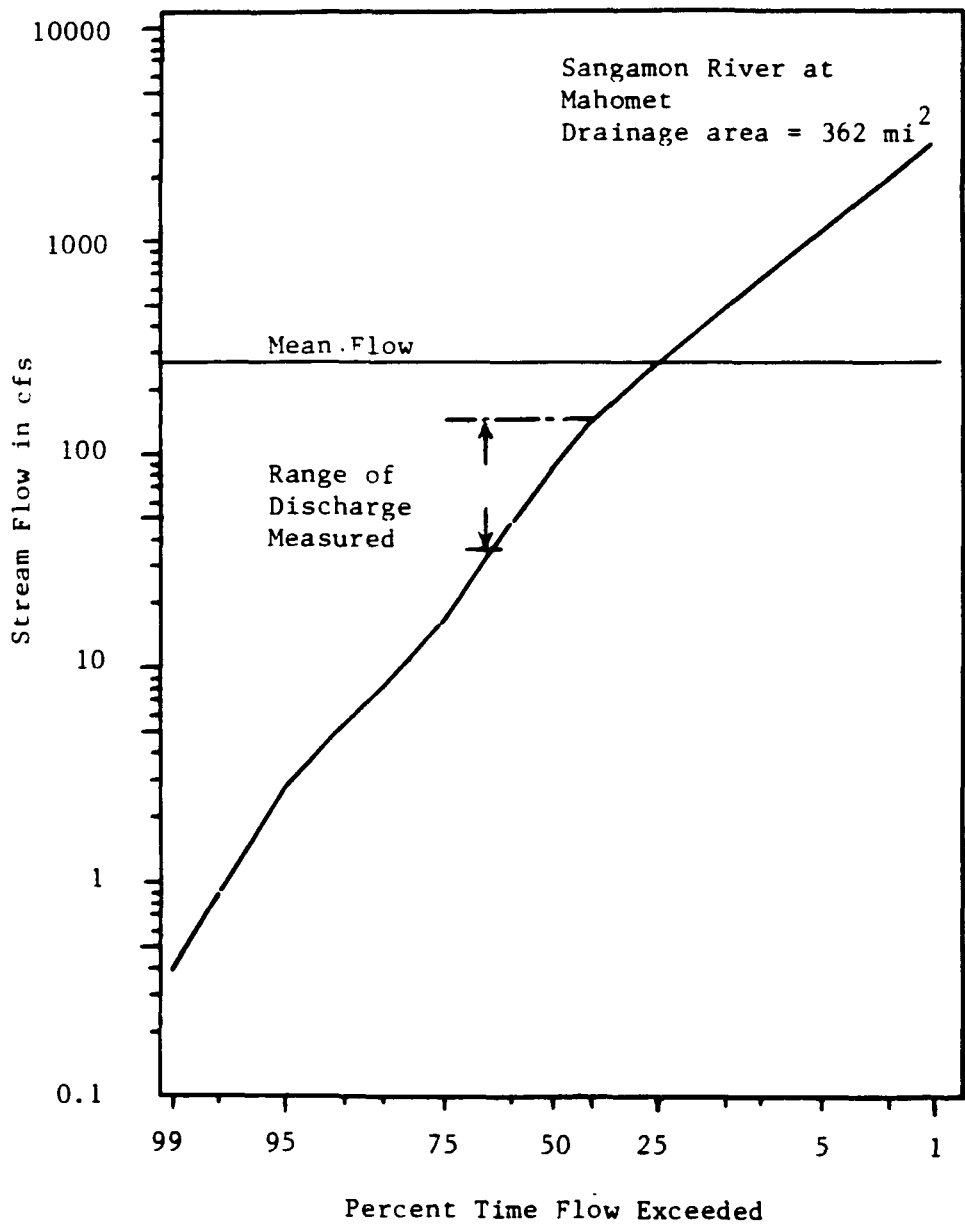carrying the platform.

Figure 20. Flow duration curve for the Sangamon River at Mahomet, Illinois

Suspended Sediment Concentration

A total of 48 suspended sediment concentration measurements were made during the data collection field trips. Several of the measurements were detailed cross-sectional measurements, while some were representative samples for calculating sediment load. The concentration measurements were averaged for the whole cross section and the suspended sediment loads were calculated from the average concentrations. These results are shown in Table 2. The suspended sediment concentrations during the 1984 data collection periods are generally higher than those in 1985. This is probably the influence of a major flood event in 1984 which preceded the data collection period. The suspended sediment load in the Sangamon River during the data collection period ranged from a low of 10 tons per day on August 7, 1985, to a high of 77 tons per day on June 28, 1984 (Table 2).

One detailed suspended sediment concentration measurement was performed on August 8, 1985, to investigate the distribution of sediment in the stream channel. A total of 21 point samples were collected at seven verticals. Fig. 21 shows the point concentration values and the equal concentration lines generated from the data. As can be seen in the figure, the suspended sediment concentration is higher towards the channel bottom and there are some regions of higher concentration which might be associated with secondary currents. However, there is no significant variation of concentration at that particular time of data collection, and more intensive data collection similar to that done here will be needed at different flows to conclusively associate concentration distribution with secondary currents.

Bed Load

Only one bed load measurement was made at the study site. This measurement, which was made on August 6, 1985, yielded a bed load sample of 4.5 grams for a sampling period of five minutes. The sample consisted of inorganic fine gravel and coarse sand. The bed load flow area was estimated to be the central 50 feet of the stream channel, which had a total width of 69 feet. Bed load was calculated by multiplying the sampler intake width by the bed load flow area width and then extending the rate per unit time to a 24-hour period to determine total load per day. The bed load was estimated to be 0.3 tons per day. In comparison, the suspended load was 25 tons per day.
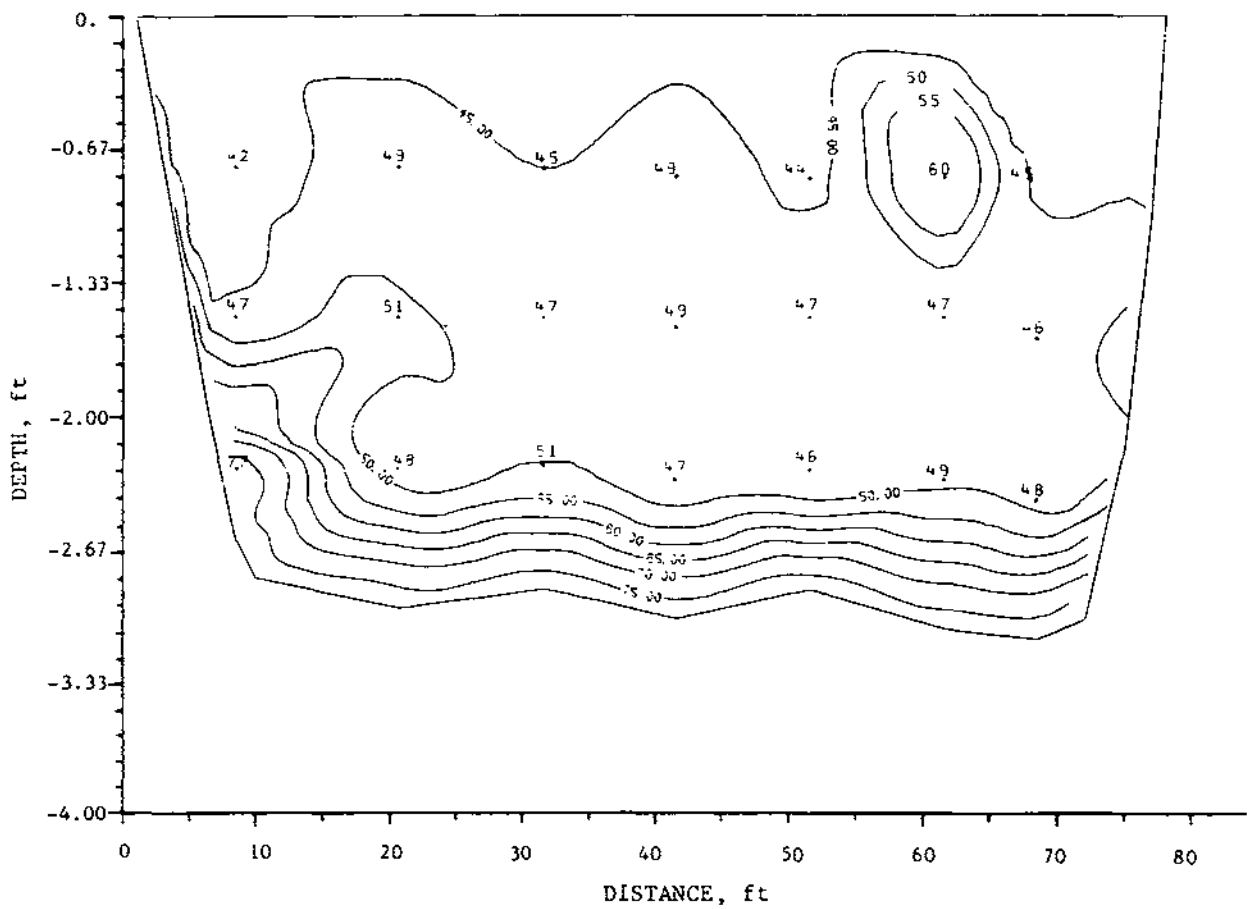
Figure 21. Distribution of suspended sediment concentration in parts per million, cross section 8, August 8, 1985

Therefore the bed load represents approximately 1.2 percent of the total sediment load (bed and suspended) on August 6, 1985, at this location.

Bed Material Characteristics

The Sangamon River's bed is composed primarily of sand and some gravel. Sand and gravel bars are common in the river. Riffles in the river are composed of gravels up to 3 inches in diameter and coarse sand. Pools in the river occur between the riffles and are underlaid by sand and silt.

Table 3 summarizes the laboratory and statistical analyses of bed material samples obtained at the study site in 1984 and 1985. In 1984 two composite samples obtained by mixing four discrete samples taken at equal distances across the stream were collected at cross sections 2 and 4. In 1985 three separate samples were collected at cross section 8, one at mid-channel and one each at the one-fourth point of the stream width from the stream bank. In table 3 the individual sample results of the 1985 samples are averaged in order to provide a composite average for comparison with the 1984 samples. Sand predominates in the composite samples, and gravel makes up the bulk of the remaining sample with less than 5 percent silt and clay. All the composite samples are descriptively classified as "gravelly sand with silt."

The bed material varies in composition with respect to particle size distribution across the width and length of the river. The individual samples obtained on August 14, 1985, show a trend of increasing average particle size from the west to the east as shown in table 3. The longitudinal variation of particle sizes can also be seen in table 3 by comparing the composite samples obtained at the two cross sections in 1984. The gravel concentration was higher at cross section 2 than at cross section 4, and the sand concentrations were lower at cross section 2 than at cross section 4 (Fig. 16). The data provided here are intended to provide a general description of the channel bed material characteristics at the study site for use in comparing and contrasting different study sites. This was not a detailed channel morphologic investigation.

Stage

The stage (height) of the river was measured during the 1985 data collection period to assess changes over time in the stage and water

60

Table 3. Characteristics of streambed material samples at the study site.

Date**	Location	Mean	Median	Standard deviation	%Gravel	%Sand	Silt and clay	Description
7/10/84	x-s #2*	1.41	1.02	.25	36.83	58.44	4.73	gravelly sand
7/12/84	x-s #4*	.86	.73	.41	16.95	81.19	1.86	gravelly sand
8/14/85	west 1/4	.50	.51	.53	2.99	93.40	3.61	silty sand
8/14/85	midpoint	.86	.68	.33	26.15	69.17	4.68	gravelly sand
8/14/85	east 1/4	2.06	2.85	.21	58.30	37.38	4.32	sandy gravel
8/14/85	composit	1.17	.31	.29	29.15	66.65	4.20	gravelly sand

* x-s = cross section

  west and east 1/4 refer to a point one-fourth of the stream width from the stream bank

**All 1985 samples obtained from a cross section 100' downstream of the bridge site.

  All 1984 samples were composited prior to laboratory analysis from 4 discrete samples obtained at equal distances across the stream width.

discharge. Figure 22 summarizes the stage measurements over the period August 5-14, 1985. The highest stage was recorded on August 5 and 8. The lowest stage occured on August 14. The general trend was a gradual decrease in the stage from August 5 to 7 and from August 8 to 14, with some rise in between from the 7th to the 8th. The change in the stage is similar to that exhibited by the discharge in table 2.

MODEL RESULTS

The mathematical model discussed earlier was used to generate secondary velocities corresponding to seven different measurements in the Sangamon River. In this section the results of the model are discussed and compared to the measured values. The comparisons between the computed and measured values are shown in two sets of figures for each cross section. In the first figure, computed and measured secondary velocity vectors generated from the lateral and vertical components are compared. In the second figure, the primary velocity isovels approximated by the model are compared to the actual isovels developed using the measured values. A table is also presented that summarizes the magnitudes of the computed and measured velocities for all the cases considered. Finally, a section on shear stress distribution is presented.

Comparison of Computed and Measured Velocities

The comparisons for cross section 6 as measured on June 28, 1984, are shown in Figs. 23 and 24. Fig. 23a shows the secondary velocity vectors generated by the model, while Fig. 23b shows the vectors from the measured velocities. It should be mentioned here that the vectors for the measured velocities were obtained by interpolating the vertical components around the points where transverse velocities were measured. This was necessary because it was not possible to measure the vertical and transverse components at the same point simultaneously.

As shown in Fig. 23 the general pattern of secondary circulation generated by the model is similar to the measured one; however, the downward circulation indicated near both the right and left banks by the model (Fig. 23a) are not present in the measured velocities (Fig. 23b). Velocity measurements were not taken very close to the stream banks and the channel
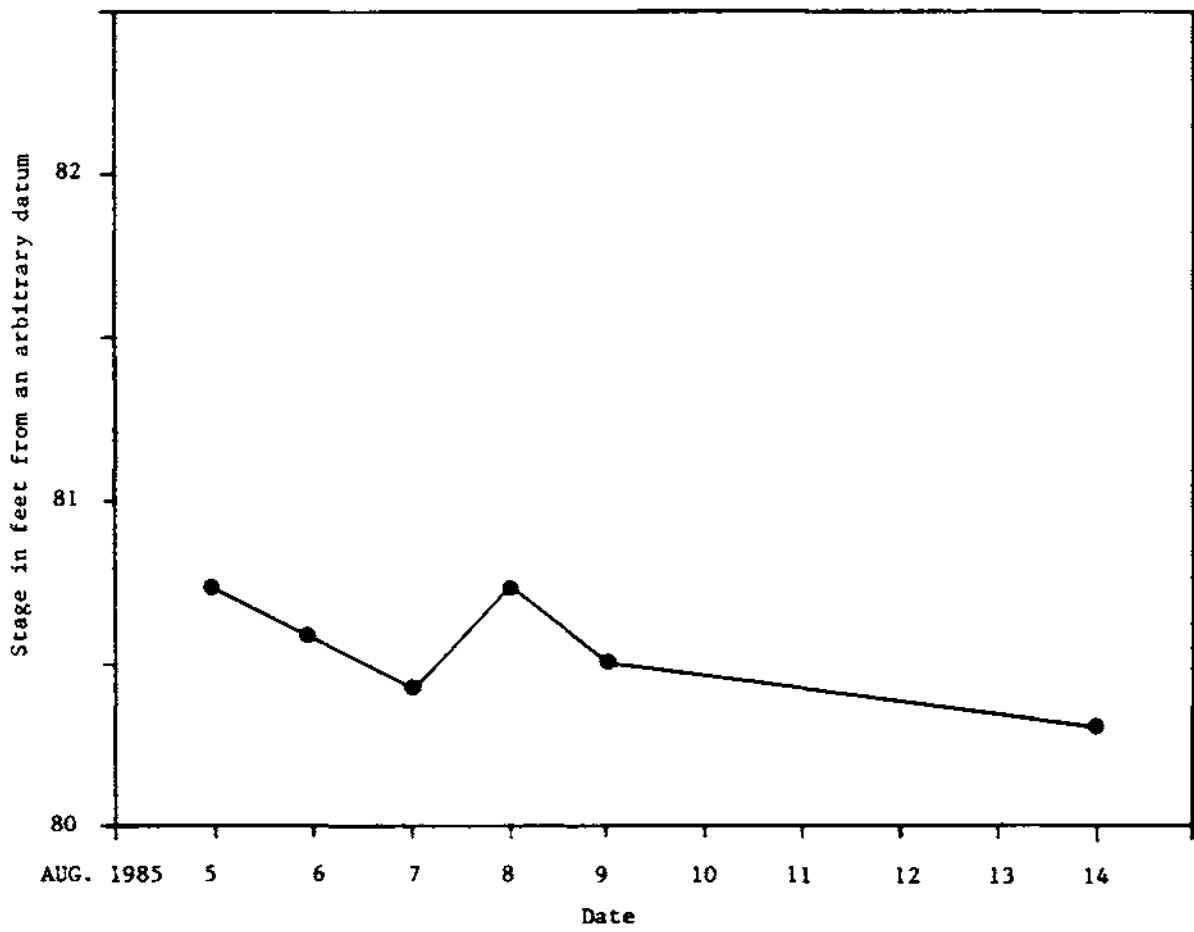
Figure 22. Variation of stream stages during field data collection
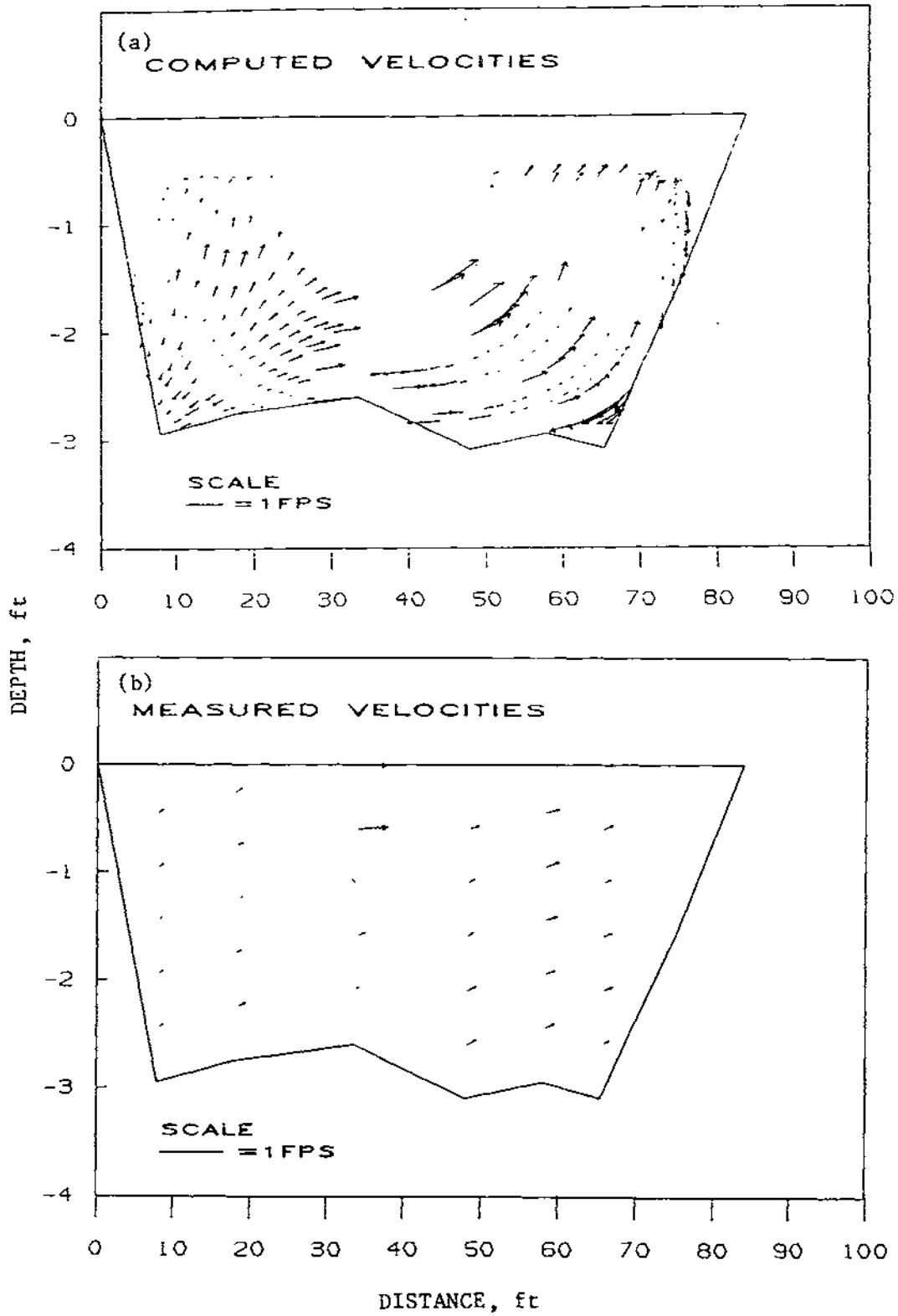
Figure 23. Comparison between computed and measured secondary velocities, cross section 6, June 28, 1984
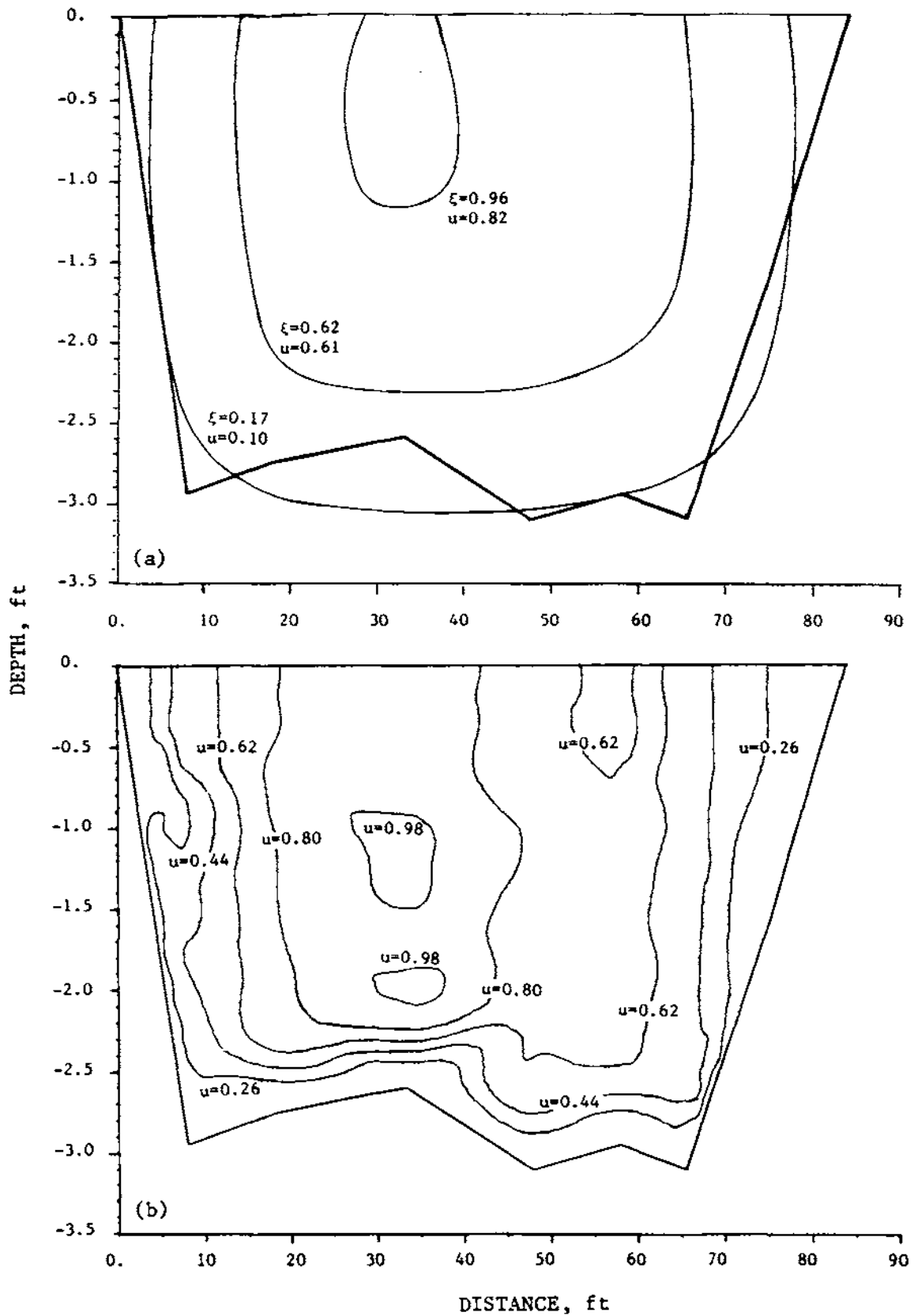
Figure 24.   Comparison between isovels derived from computed and measured
data, cross section 6, June 28, 1984

bottom because of the physical limitations of the equipment setup. The lack of these measurements makes it difficult to make conclusive remarks on the comparison of the model results with the measured values for areas close to the bank.

The measured secondary velocities are generally smaller than those generated by the model. This is true for all seven cross sections used for the model. The values of the primary, transverse, and vertical components of the velocity for all the cross sections are summarized in table 4. The percentages of the computed with respect to the measured transverse and vertical velocities are given in columns 9 and 11 in table 4. The percentages in both columns are all higher than 100 percent and in some cases extremely high. Because of the small magnitudes of the velocities, a very small error in velocity measurements or slight overestimation by the model results in very high percentages. However, further refinement of the model is needed and possible. Unfortunately this could not be accomplished within this project.

Table 4 also provides the relative magnitudes of the measured transverse and vertical velocity components with respect to the primary velocity component in columns 5 and 7, respectively. The transverse components range from 8 to 43.7 percent of the primary velocity, while the vertical components range from 4.1 to 40.4 percent. These values are in most cases higher than those reported in the literature, but might be because of the low flow conditions in the Sangamon River during data collection. Additional data during higher flows are required to more definitely define the relative magnitude of secondary velocity components as compared to the primary velocity.

Fig. 24 shows the primary velocity isovels generated by the model (Fig. 24a) and those developed from the measured velocities for cross section 6 discussed above. There is a clear similarity between these two plots; however, as can be seen in the figure, the isovels for the model are smooth curves, while the isovels from the measured velocities are irregular and show deformations at different places. This discrepancy was anticipated from the beginning since the model formulations assume smooth isovels which can be approximated by mathematical functions. The assumption of smooth isovels is the most limiting factor in secondary circulation models based on coordinate transformation.

Table 4. Mean Measured and Computed Velocities

Cross Section	Date	Measured longitudinal component (fps)	Measured transverse component (fps)	col (4) col (3) (%)	Measured vertical component (fps)	col (6) col (3) (%)	Component transverse component (fps)	col (8) col (4) (%)	Computed vertical component (fps)	col (10) col (6) (%)
7	6/27/84	.599	.048	8.0	.138	23.0	--	--	--	--
6	6/28/84	.535	.118	22.1	.022	4.1	.22	186	.27	1227
5	6/29/84	.465	.060	12.9	.137	29.5	.19	317	.15	109
3	7/09/84	.352	.054	15.3	.115	32.7	.16	296	.12	104
4	7/10/84	.302	.055	18.2	.122	40.4	.28	509	.38	311
2	7/12/84	1.0009	.064	6.3	.088	8.7	--	--	--	--
1	7/13/84	.744	.172	23.1	.067	9.0	--	--	--	--
5	8/05/85	.444	.081	18.2	.072	16.2	.13	160	.16	222
6	8/06/85	.627	.274	43.7	.211	33.6	.40	146	.51	242
7	8/07/85	.316	.068	21.5	.101	31.9	--	--	--	--
8	8/08/85	.373	.091	24.4	.073	19.6	.30	330	.39	534
9	8/09/85	.251	.105	41.8	.069	27.5	--	--	--	--

67

The comparisons of the model results with the measured values for the remaining six measurements are shown in Figs. 25 to 36. In general, the preceding discussion for cross section 6 (June 28, 1984) is applicable for all the comparisons. Some of the comparisons indicate a better correlation between measured and computed velocities and some are worse than the ones shown for cross section 6, as summarized in Table 4. A complete listing of the velocities generated by the model is included in Appendix C. Additional work both in data collection and in refinement of the model is definitely needed before the model adapted for this project can be applied to flow conditions in natural streams.

Shear Stress Distribution

As discussed in the section on approximation of shear stresses, the shear stresses were assumed to vary quadratically in the , direction according to Eq. 35. The coefficients for Eq. 35 are derived from boundary conditions, which depend on the flow conditions and the channel boundary. The shear stress distributions generated by the model for two sets of measurements at cross section 6 are shown in Figs. 37 and 38. $/_o$ is the ratio of the shear stress at any point ( ) to that at the channel bottom ($_o$). The figures clearly show higher shear stresses around the junctions of the stream bank with the stream bed, which might indicate areas of higher erosion rates as compared to the whole channel cross section.
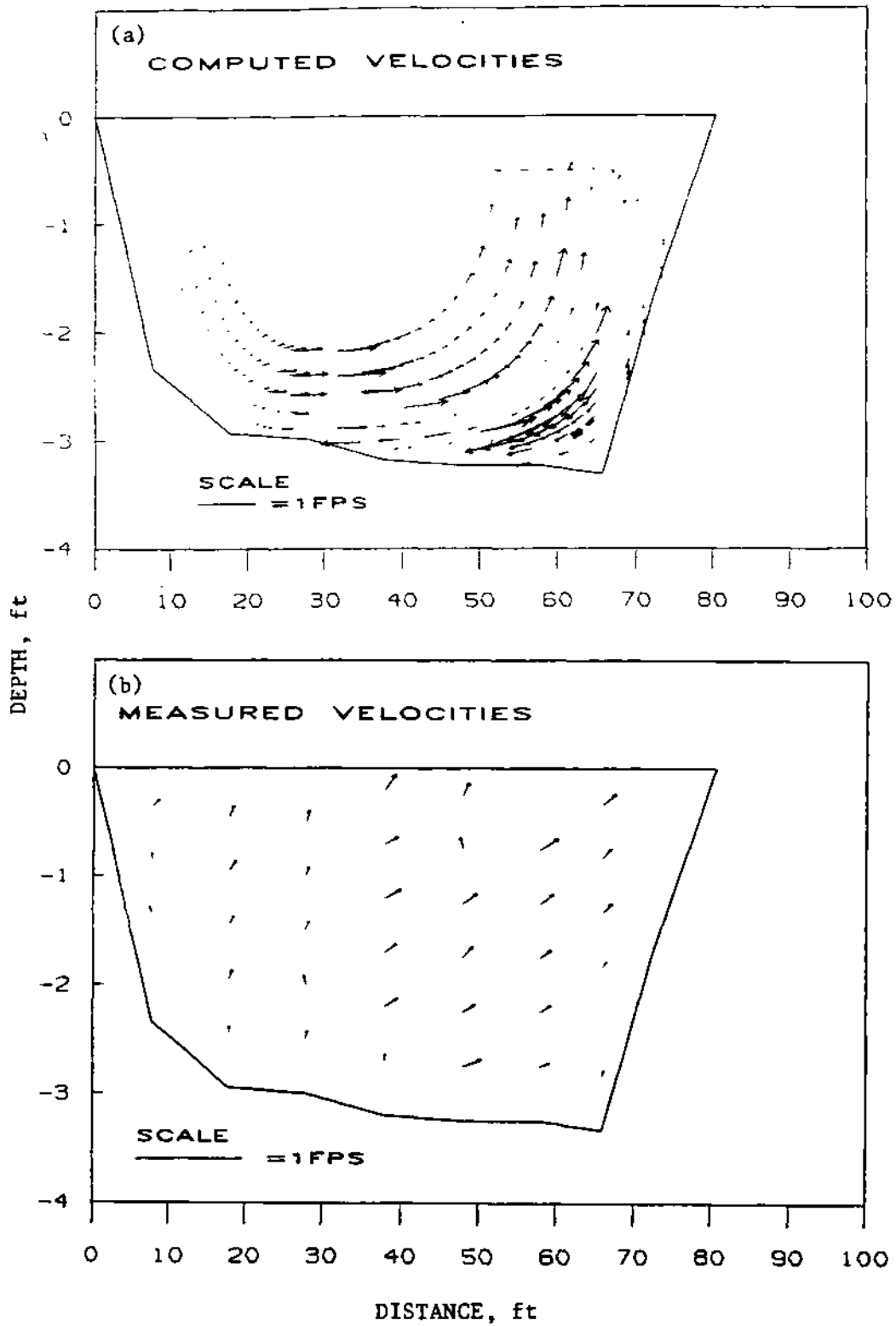
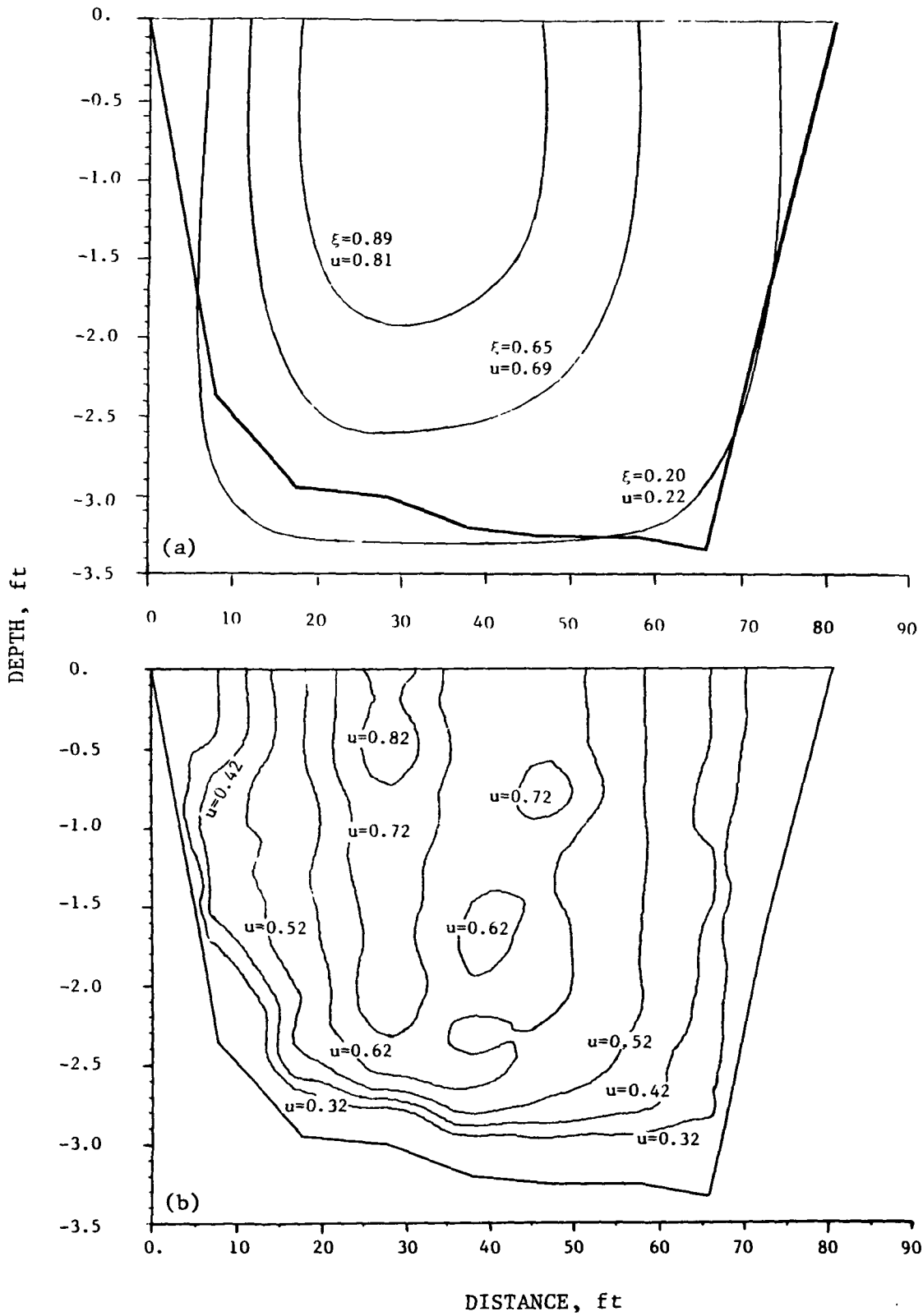Figure 25. Comparison between computed and measured secondary velocities, cross section 5, June 29, 1984

69

Figure 26. Comparison of isovels derived from computed and measured data, cross section 5, June 29, 1984
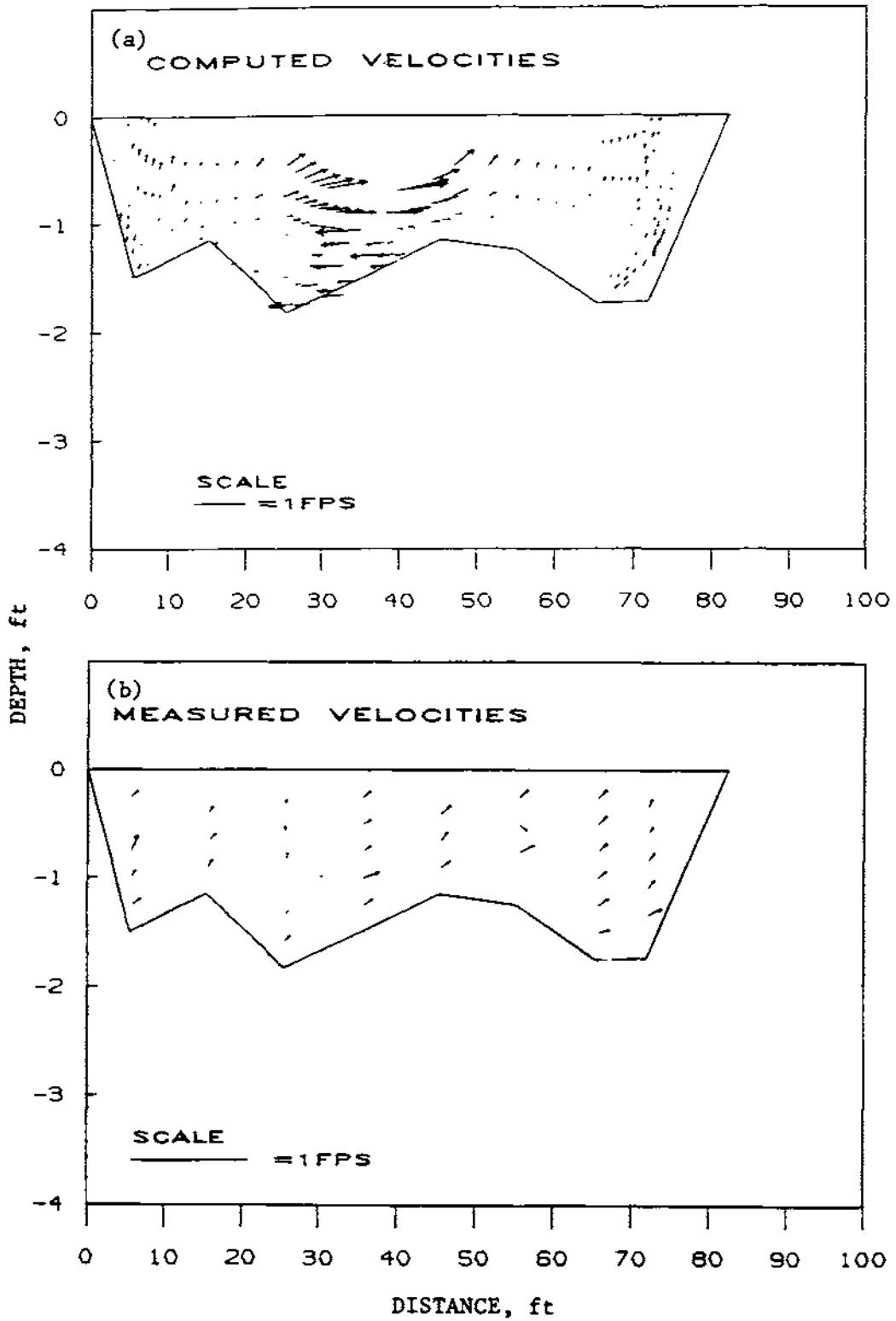
70

Figure 27. Comparison between computed and measured secondary velocities, cross section 3, July 9, 1984
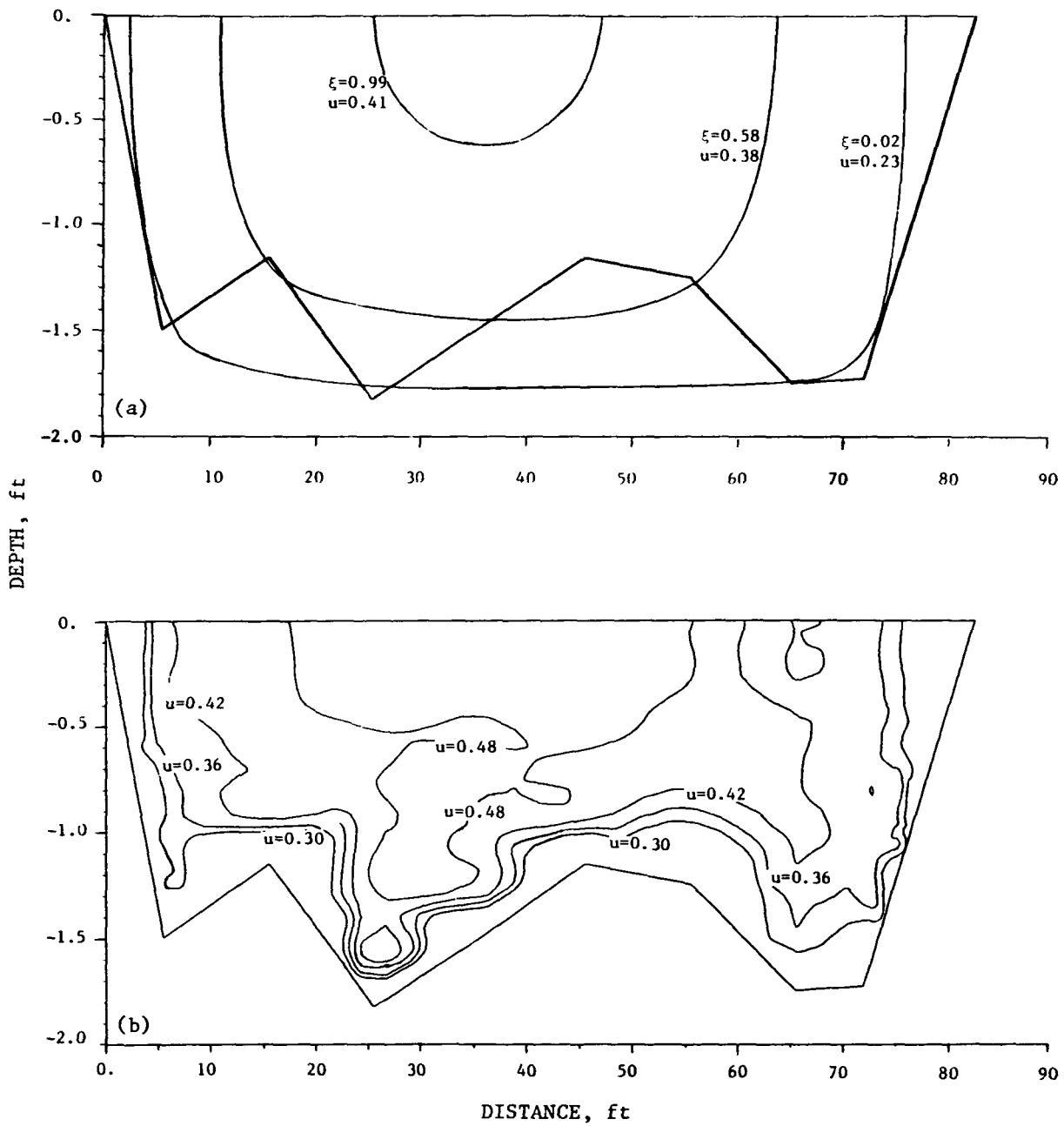
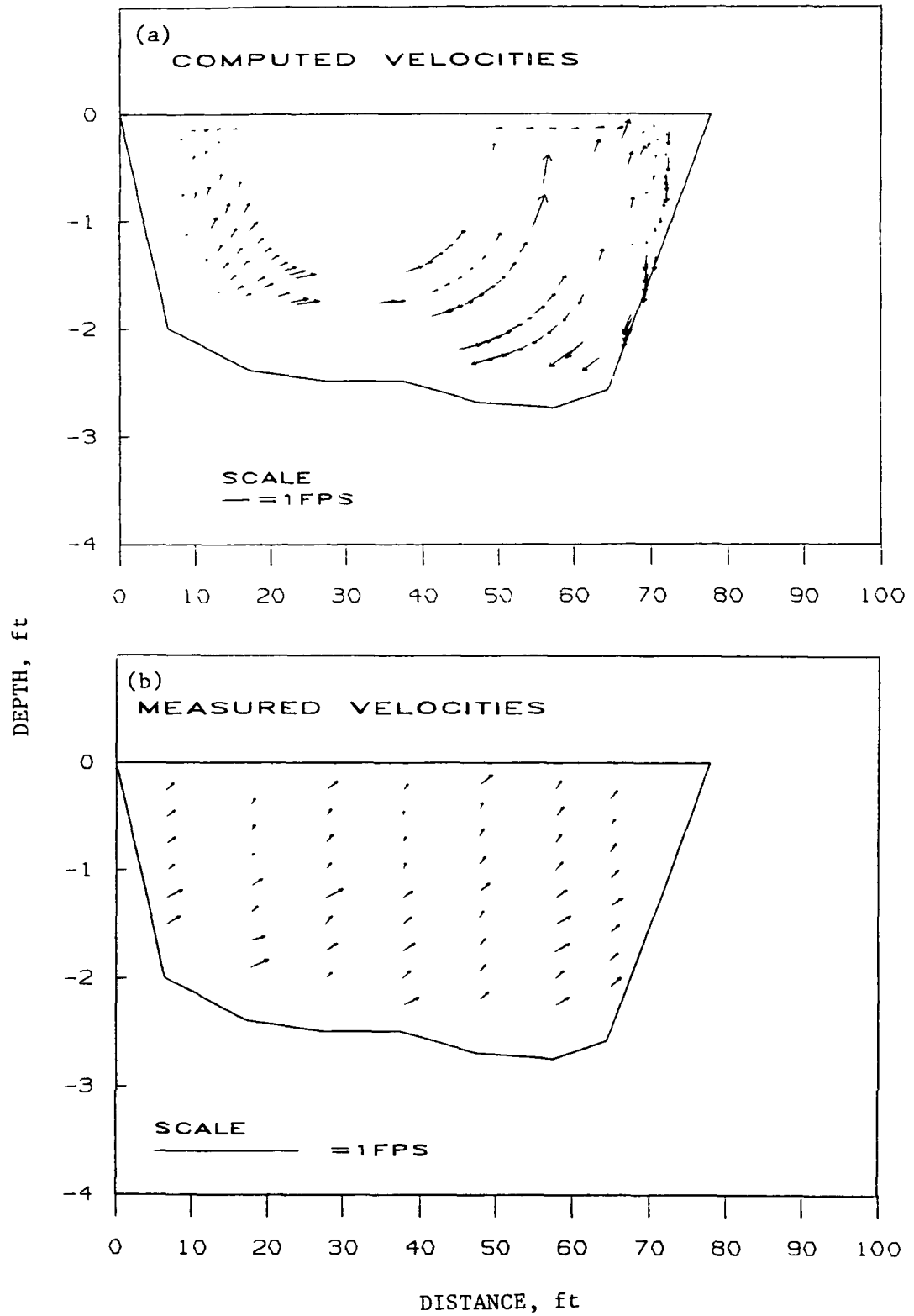Figure 28. Comparison of isovels derived from computed and measured data, cross section 3, July 9, 1984

Figure 29.   Comparison between computed and measured secondary velocities, cross section 4 July 10, 1984
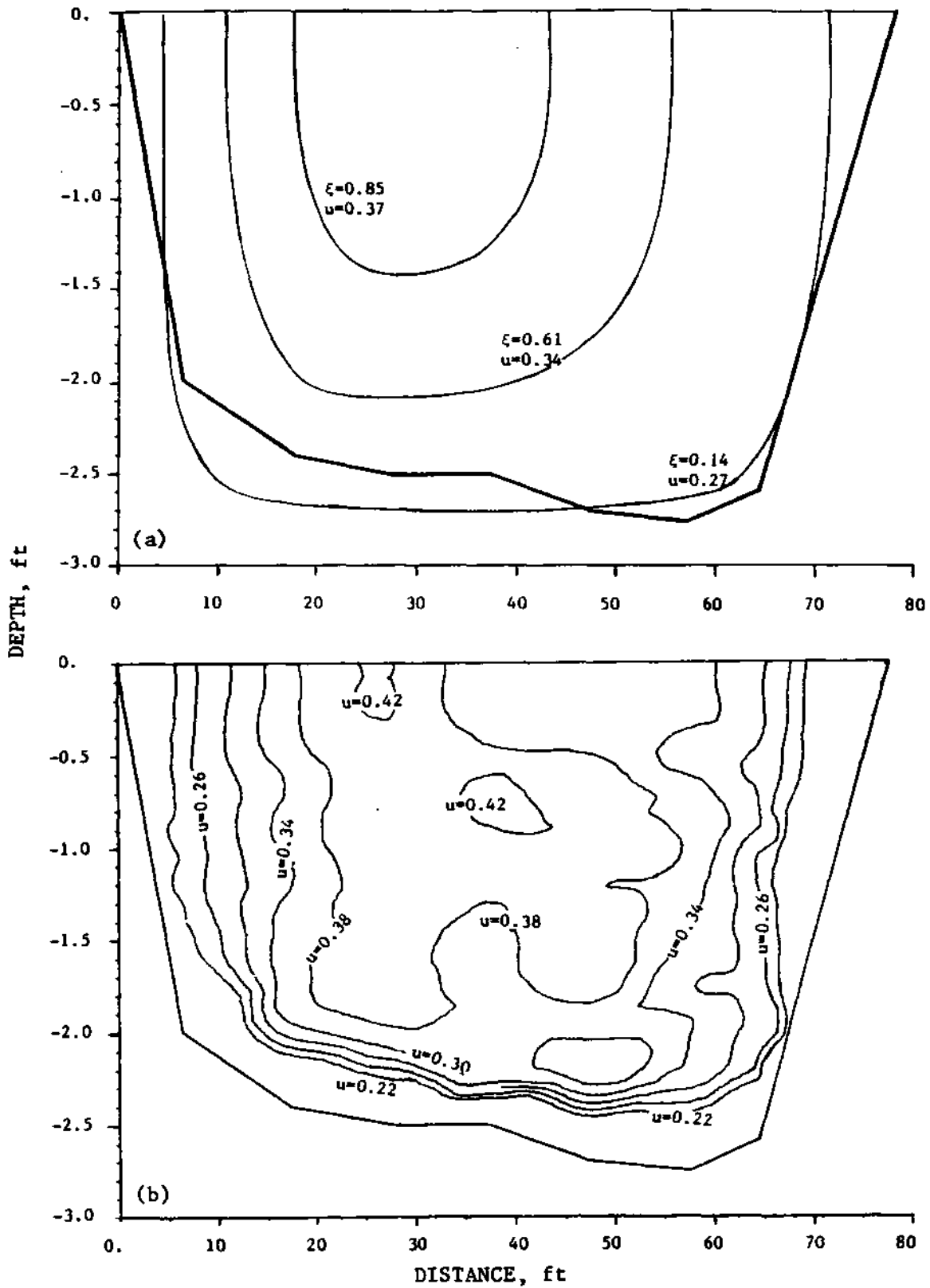
Figure 30. Comparison of isovels derived from computed and measured data, cross section 4, July 10, 1984
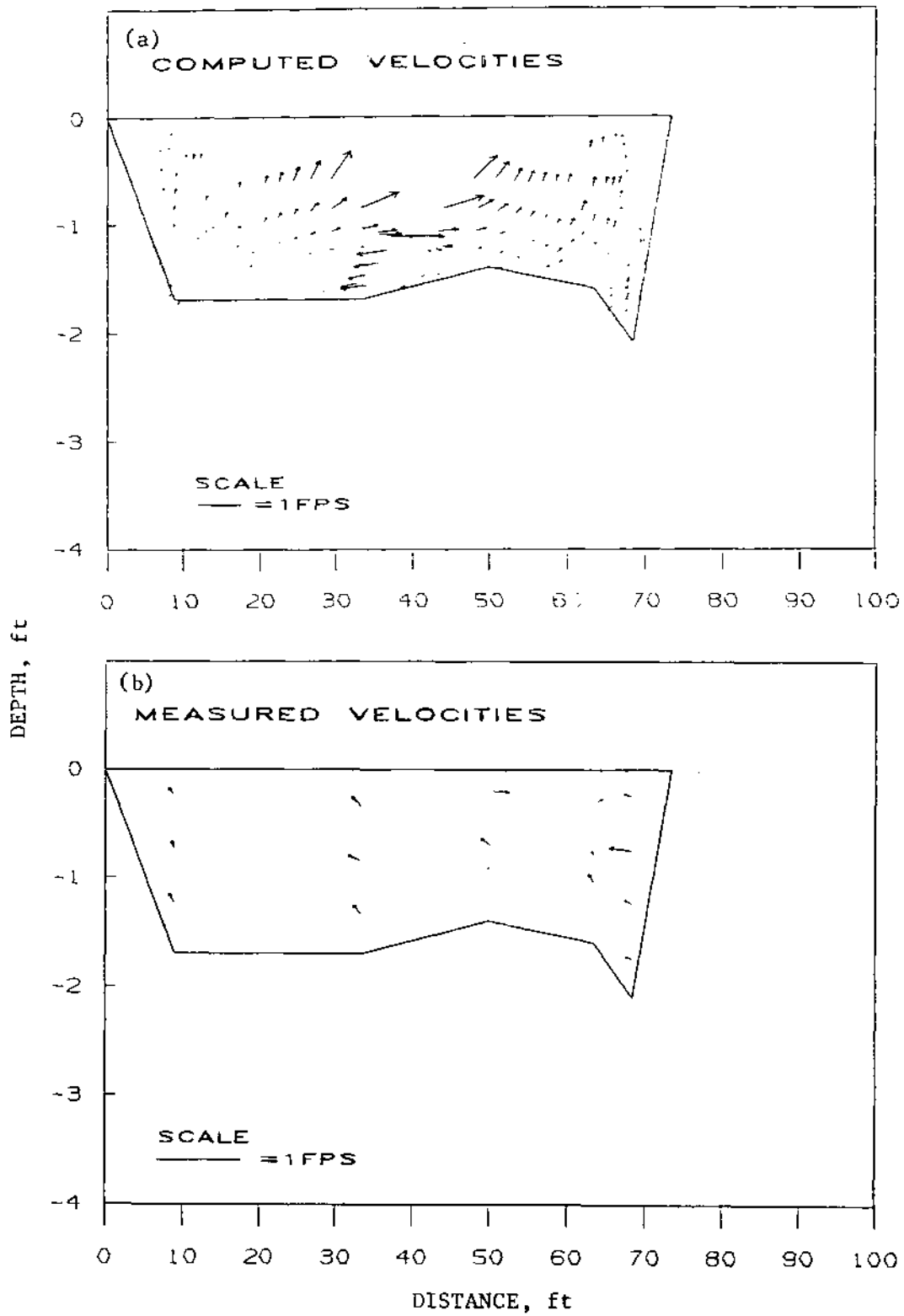
74

Figure 31. Comparison between computed and measured secondary velocities, cross section 5, August 5, 1985
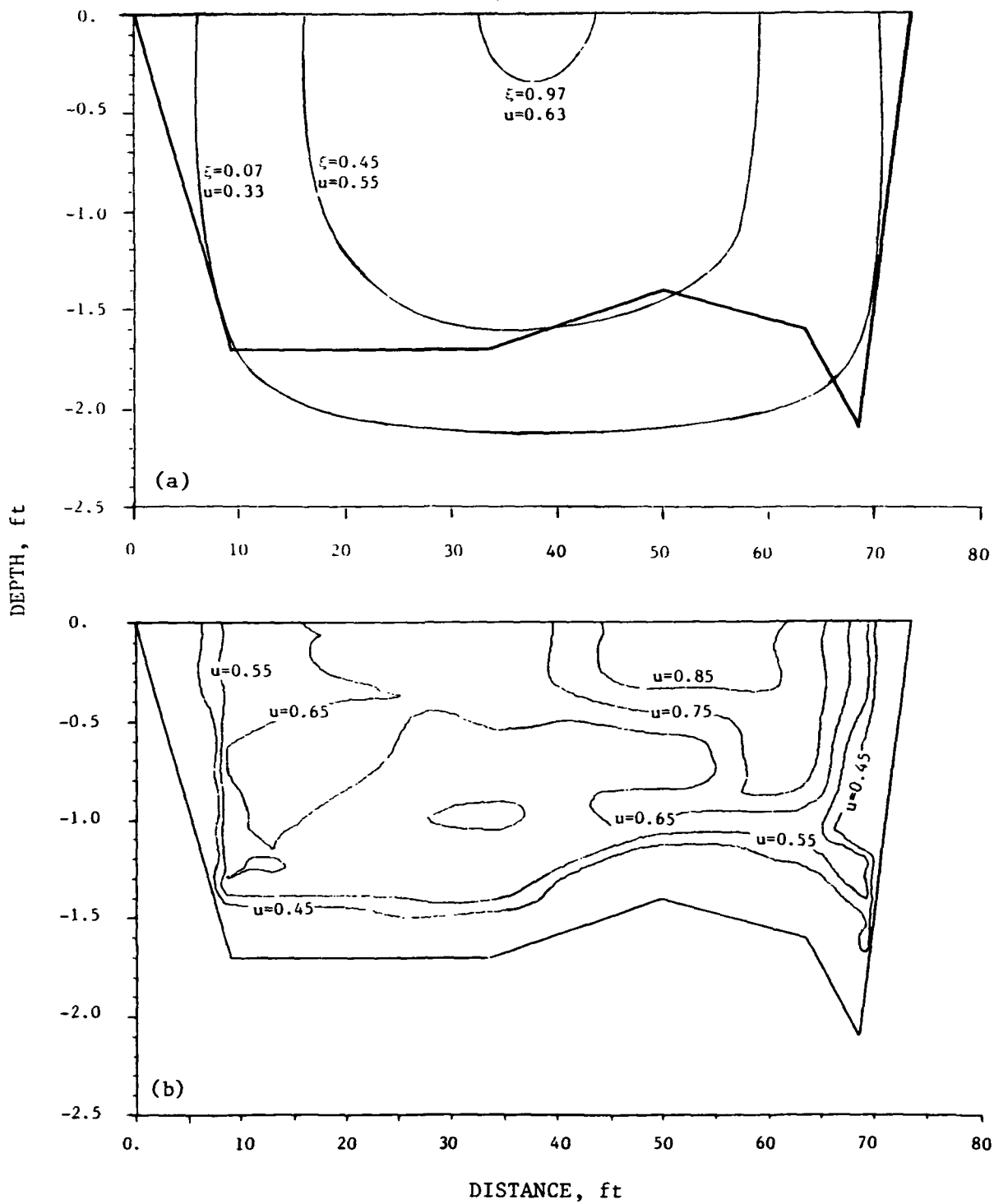
Figure 32. Comparison between isovels derived from computed and measured data, cross section 5, August 5, 1985

Figure 33. Comparison between computed and measured secondary velocities, cross section 6, August 6, 1985

Figure 34.   Comparison of isovels derived from computed and measured data,
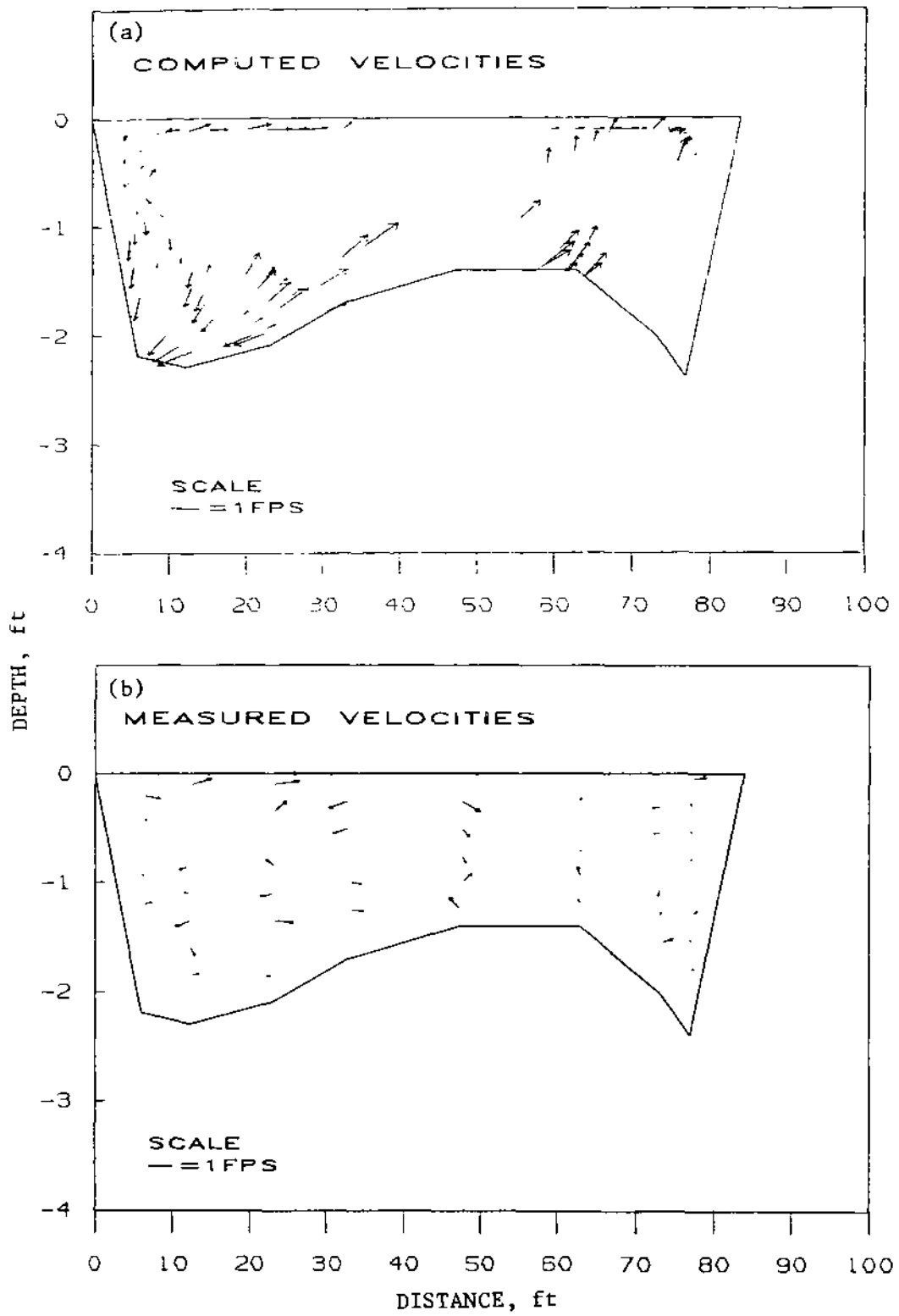cross section 6, August 6, 1985

Figure 35. Comparison between computed and measured secondary velocities,
cross section 8, August 8, 1985

79

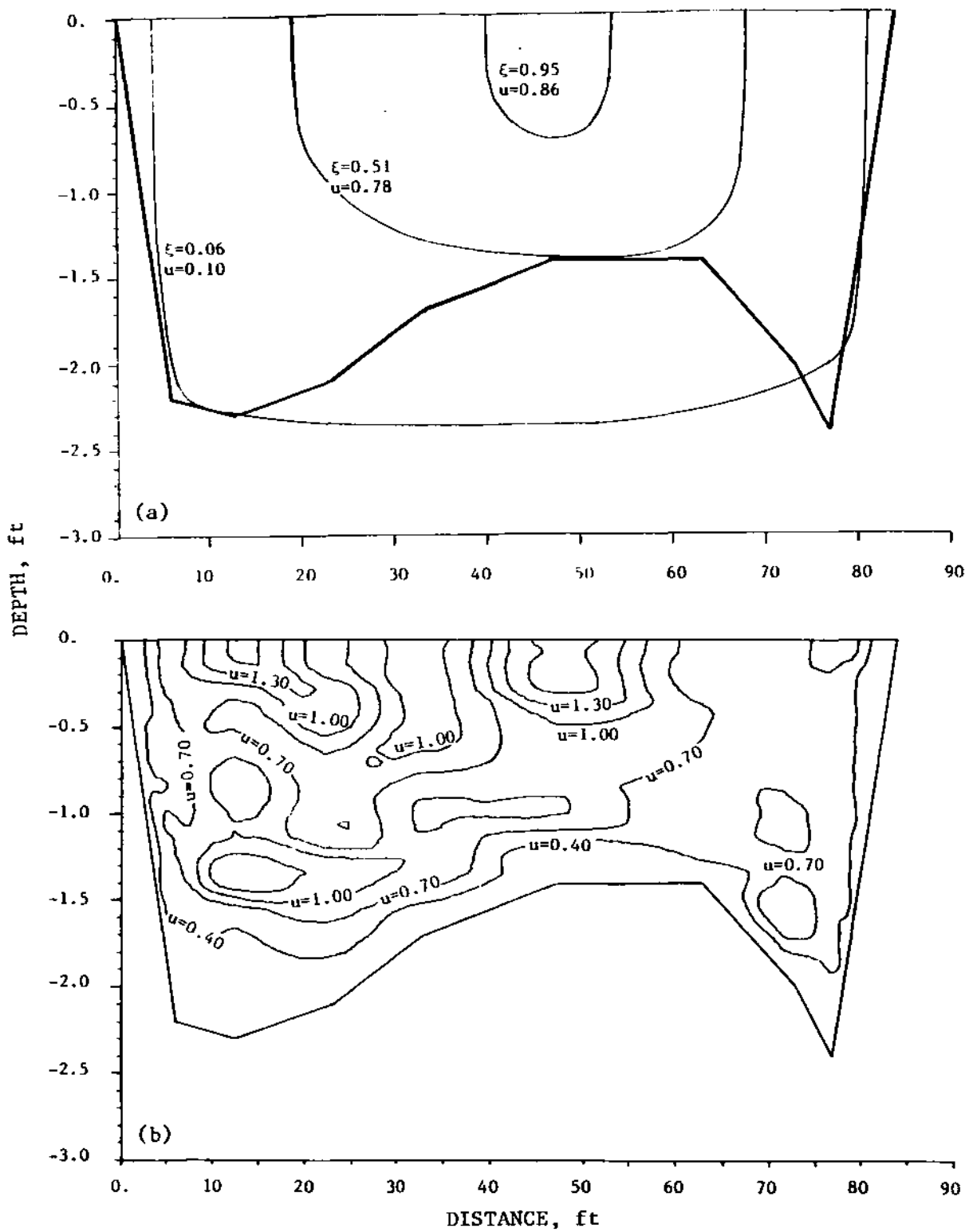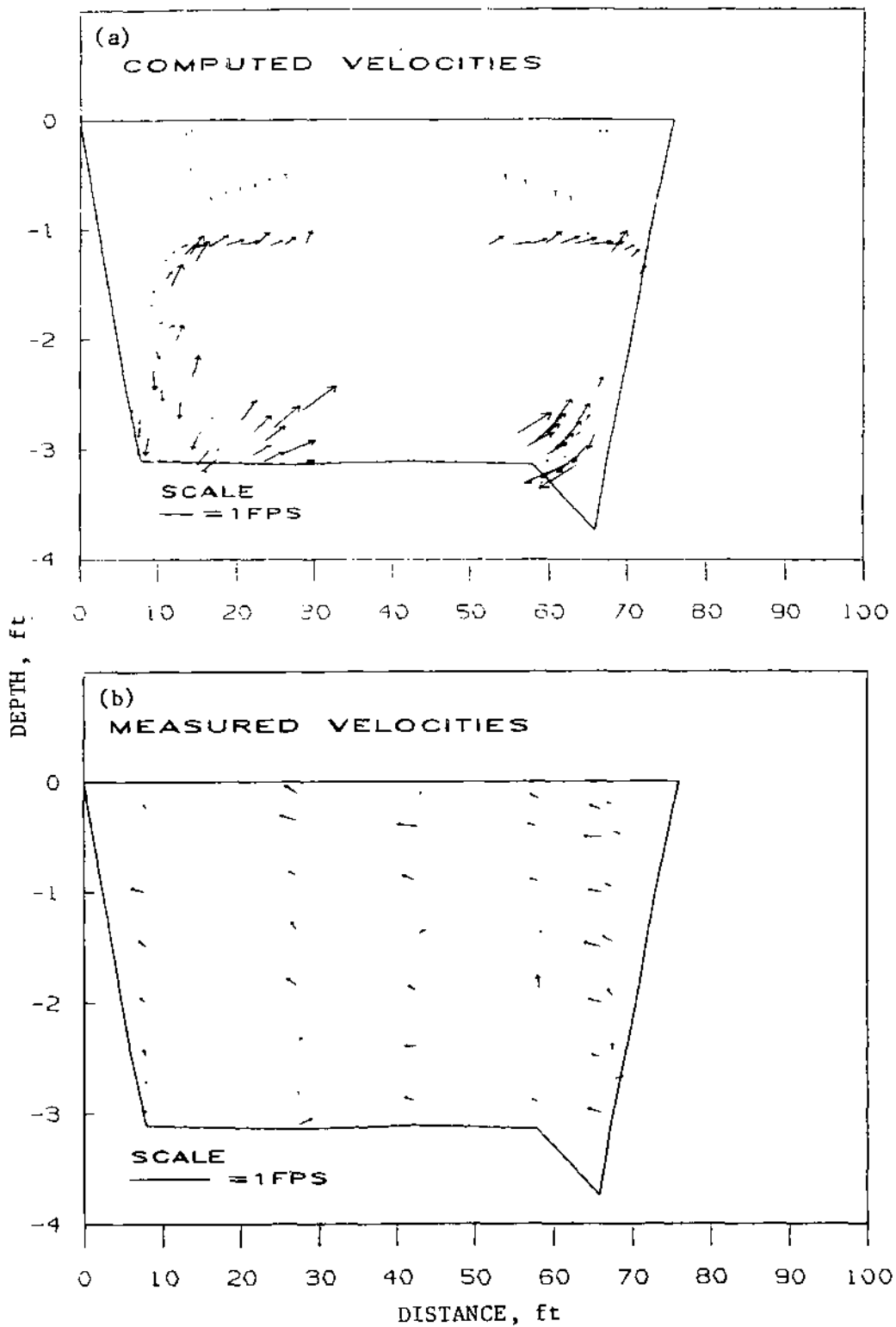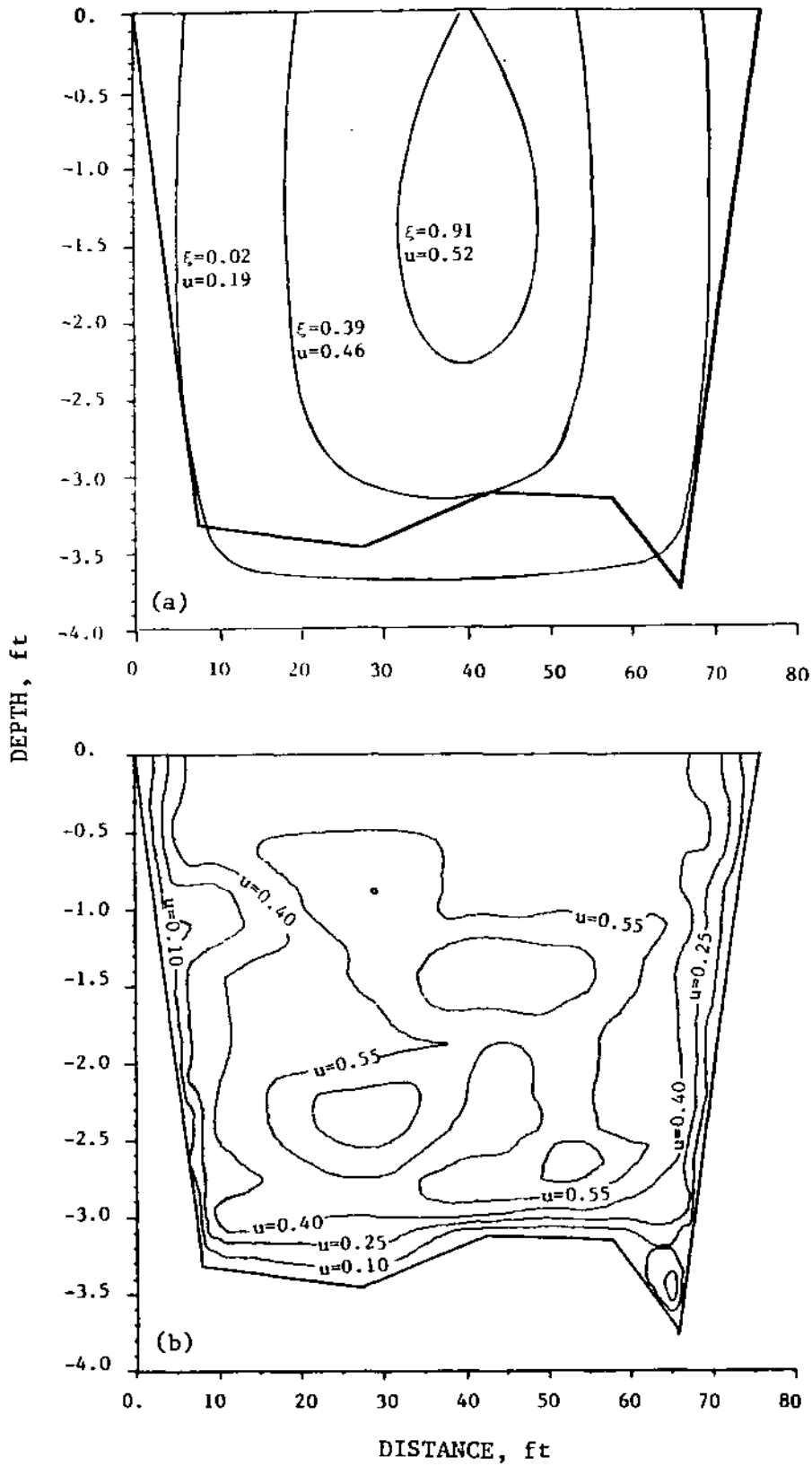Figure 36. Comparison of isovels derived from computed and measured data, cross section 8, August 8, 1985
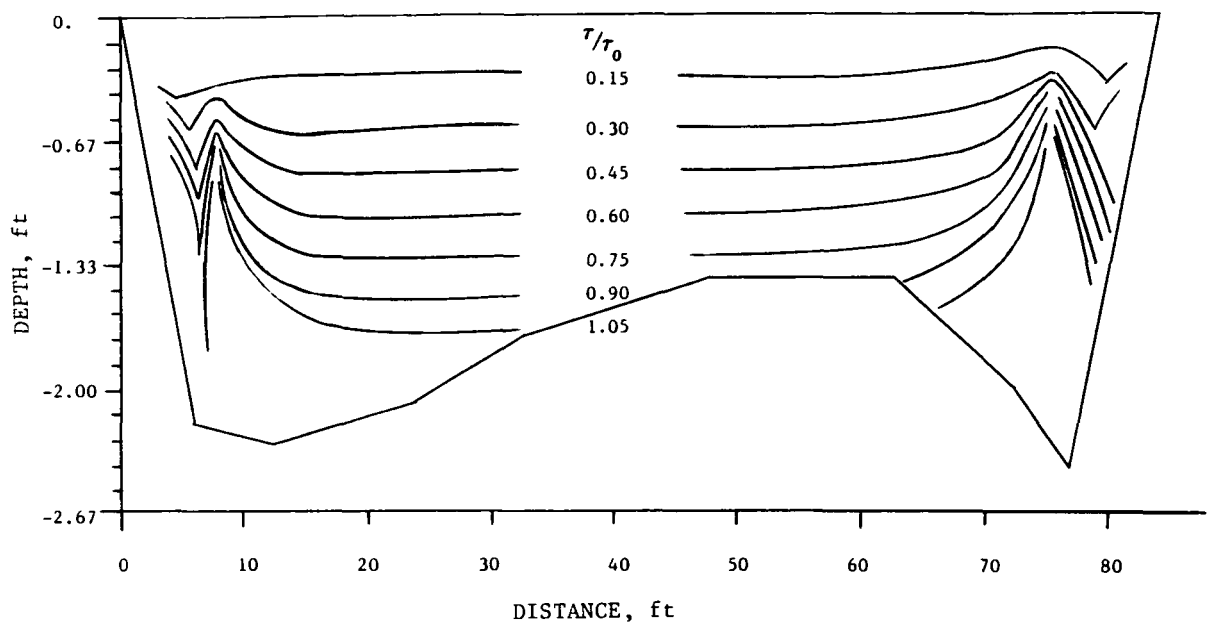
80

Figure 37. Shear stress distribution, cross section 6, June 28, 1985
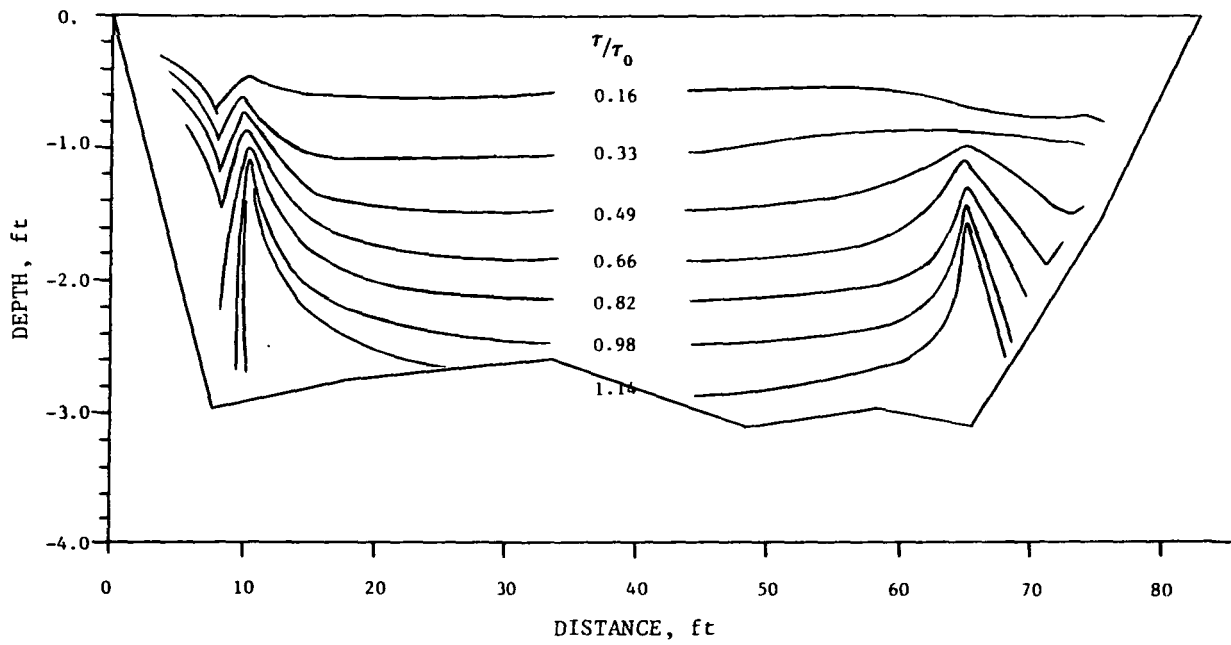
Figure 38. Shear stress distribution, cross section 6, August 6, 1985

SUMMARY AND CONCLUSIONS

Secondary circulation is an important hydraulic phenomenon in natural streams. However, studies in the field have been limited, and in particular actual measurements of secondary circulation have been very few. This is because of the difficulty in measuring very small velocities under natural conditions. The development of mathematical models has also been limited, primarily because of the lack of reliable field data for calibration and verification.

This project is one of the few research projects in the United States that has attempted to measure secondary circulation in natural streams. As a result of this project, a reliable field data collection technique has been developed. The data collection system is computerized to reduce the time required in field data recording and reduction. The system has been used successfully several times to measure secondary circulation data in the Sangamon River near Mahomet, Illinois. All the data collected for the project are included in Appendix B. The data are also analyzed and presented graphically to simplify comparison of data with model results.

At the beginning of this project it was anticipated that an existing model would be available for calibration and verification. However, attempts to obtain existing models were not successful because of the early stages of model development by other researchers. Instead of delaying or dropping the task of calibration and verification of existing models, it was decided to develop a model based on information available in the literature. At that time, the model being developed by Chiu and his associates at the University of Pittsburgh was the best documented model available.

A mathematical model based on Chiu's methods has been developed and was used to compare measured secondary velocities with computed velocities. A complete listing of the computer program for the model is included in Appendix A. The mathematical derivations and the equations used in the model are thoroughly discussed in the report. The model has been used to simulate field conditions for all the cases where field data were collected, and the results are included in the report.

Comparisons of field data and model results show mixed results. In some cases the results are satisfactory while in others they are not. In general, the model is capable of generating similar secondary circulation patterns to those indicated by the field data. However, the magnitudes of the secondary

currents generated by the model are greater than those measured in the field. Comparison of model results with measured values was further hampered by the lack of data points very close to the banks, where the model indicates the existence of consistently downward velocity components. Because of the limitations of the physical setup for collecting field data, secondary circulation data very close to the stream banks could not be collected.

The overall results of the research can be summarized by the following statements:

1) A reliable state-of-the-art secondary circulation data collection system has been developed and used successfully in the field. This will significantly increase the productivity of future research in the area.

2) A mathematical model for secondary circulation has been developed and compared with field measurements. The results of the comparison are not totally satisfactory, and further research is needed to improve the application of the model to flow conditions in natural streams.

REFERENCES

1. American Society for Testing and Materials, 1982 Annual Book of ASTM Standards, Part 31, Water. 1982.

2. Ananian, A.K., "An Approximate Theory of Secondary Flows at the Bend of the River Course," Proceedings, 12th Congress of the IAHR, Volume 1, River Hydraulics, September, 1967, pp. 422-428.

3. Baines, W.D., and Knapp, D.J., "Wind Driven Water Currents," Journal of the Hydraulics Division. ASCE, Volume 91, No. HY2, March, 1965, pp. 205-221.

4. Bathurst, J.C., Thorne, C.R., and Hey, R.D., "Direct Measurements of Secondary Currents in River Bends," Nature. Volume 269, No. 5628, October, 1977, pp. 504-506.

5. Bathurst, J.C., Thorne, C.R., and Hey, R.D., "Secondary Flow and Shear Stress at River Bends," Journal of the Hydraulic Division, ASCE, Volume 105, No. HY10, October, 1979, pp. 1277-1295.

6. Bhowmik, N., "Hydraulics of Flow in the Kaskaskia River, Illinois," Illinois State Water Survey, Report of Investigation 91, 1979, 116p.

7. Bhowmik, Nani G., "Shear Stress Distribution and Secondary Circulation in Straight Open Channels," In Gravel-Bed Rivers, Edited by R.D. Hey, J.C. Bathurst, and C.R. Thorne, John Wiley and Sons. 1982, pp. 31-61.

8. Brundrett, E., and Baines, W.D., "The Production and Diffusion of Vorticity in Duct Flow," Journal of Fluid Mechanics. Volume 19, part 3, 1964, pp. 375-395.

9. Buchanan, T.J., and W.P. Sommers. "Discharge Measurements at Gaging Stations." Book 3, Chapter A8 in Techniques of Water Resource Investigations of the United States Geological Survey. 1969.

10. Chiu, C.L. and McSparran, J.E., "Effect of Secondary Flow on Sediment Transport," Journal of the Hydraulics Division. ASCE, Volume 92, No. HY5, September, 1966, pp. 57-70.

11. Chiu, C.L., "The Role of Secondary Currents in Hydraulics," Proceedings, 12th Congress of the IAHR. Fort Collins, Colorado, 1967, pp. 415-421.

12. Chiu, C.L., Lin, H.C., and Mizumura, K., "Simulation of Hydraulic Processes in Open Channels," Journal of the Hydraulics Division. ASCE, Volume 102, No. HY2, February, 1976, pp. 185-206.

13. Chiu, C.L., Hsiung, D.E., Lin, H.C., "Three Dimensional Open Channel Flow," Journal of the Hydraulics Division. ASCE, Volume 104, No. HY8, August, 1978, pp. 1119-1136.

14. Chiu, C.L., and Hsiung, D.E., "Secondary Flow, Shear Stress and Sediment Transport," Journal of the Hydraulics Division. ASCE, Volume 107, No. HY7, July, 1981, pp. 879-898.

15. Chiu, C.L., and Lin, G.F., "Mathematical Modeling of Three-Dimensional Flow and Shear Distribution," 1983, IAHR.

16. Chiu, C.L., and Lin. G.F.,"Computation of Three-Dimensional Flow and Shear in Open Channels," Journal of the Hydraulics Division. ASCE, Volume 109, No. HY11, November,. 1983, pp. 1424-1440.

17. Chiu, C.L., Nordin, C.F., and Hu, W.D., "A Method for Mathematical Modeling and Computation of Hydraulic Processes in River Bend," Paper Presented at the ASCE Conference, River '83, New Orleans, October 24-26, 1983.

18. Ciray, C, "On Secondary Currents," Proceedings 12th Congress of the IAHR. Fort Collins, Colorado, 1967, pp. 408-414.

19. Cunningham, A., "Recent Hydraulic Experiments," Minutes of Proceedings. Institution of Civil Engineers, London, England, Volume 71, 1882.

20. Demissie, M. , Bhowmik, N., Maxwell, W., Soong, T.W., and Fitzpatrick, W., "Secondary Circulation in Natural Rivers," Progress Report. Illinois State Water Survey, Champaign, IL, October, 1984, 25p.

21. Demissie, M. , Bhowmik, N.G., Maxwell, W.H.C., and T.W. Soong, "Secondary Circulation Data Acquisition System," Proceedings of the Specialty Conference on Hydraulics and Hydrology in the Small Computer Age, Hydraulics Division, ASCE, Volume 2, 1985, pp. 1178-1183.

22. Dietrich, W.E., and Smith, J.D., "Influence of the Point Bar on Flow in Curved Channels," Water Resources Research, Paper 3W1080, Volume 19, No. 4, October, 1983, pp. 1173-1192.

23. Einstein, H.A., and Li, H., "Secondary Currents in Straight Channels," Transactions. American Geophysical Union. Volume 39, No. 6, December, 1958, pp. 1085-1088.

24. Fischer, H.B., "The Mechanics of Dispersion in Natural Streams," Journal of the Hydraulics Division. ASCE, Volume 93, No. HY6, November, 1967, pp. 187-216.

25. Francis, J.B., "On the Cause of the Maximum Velocity of Water Flowing in Open Channels Being Below the Surface," Transactions. ASCE Volume 7, May, 1878.

26. Garde, R.J., and Raju, K.G.R., Mechanics of Sediment Transportation and Alluvial Stream Problems. Wiley Eastern Limited, New Delphi, 1977.

27. Gerard, R., "Secondary Flow in Noncircular Conduits," Journal of the Hydraulics Division. ASCE, Volume 104, No. HY5, May, 1978, pp. 755-773.

28. Gessner, F.B., and Jones, J.B., "On Some Aspects of Fully-Developed Turbulent Flow in Rectangular Channels," <u>Journal of Fluid Mechanics</u>. Volume 23, part 4, 1965, pp. 689-713.

29. Ghosh, S.N., and Roy, N., "Boundary Shear Distribution in Open Channel Flow," <u>Journal of the Hydraulics Division</u>. ASCE, Volume 96, No. HY4, April, 1970, pp. 967-994.

30. Gibson, A.H., "On the Depression of the Filament of Maximum Velocity in a Stream Flowing Through an Open Channel," <u>Proceedings of Royal Society</u>. London, England, Series A, Volume 82, 1909, pp. 149-159.

31. Guy, H.P., and Norman, V.W., "Field Methods for Measurement of Fluvial Sediments," Book 3, Chapter C2, <u>Techniques of Water Resources Investigations of the United States Geological Survey</u>. United States Government Printing Office, Washington, 1976.

32. Helstrom, B., Discussion of "Macroturbulence in Natural Stream Flow," <u>Transactions</u>. American Geophysical Union, Volume 29, No. 2, 1948, pp. 272-273.

33. Hoagland, L.C., "Fully-Developed Turbulent Flow in Straight Rectangular Ducts-Secondary Flow, Its Cause and Effect on the Primary Flow," Doctoral Thesis, Massachusetts Institute of Technology, 1960.

34. Ibragimov, M.H., Petrishchev, V.S., and Sabaley, G.I., "Calculation of Heat Transfer in Turbulent Flow with Allowance for Secondary Flow," <u>International Journal of Heat and Mass Transfer</u>. Volume 14, 1971, pp. 1033-1037.

35. Ikeda, S., "Self-Formed Straight Channels in Sandy Beds," <u>Journal of the Hydraulics Division</u>. ASCE, Volume 107, No. HY4, April, 1981.

36. Kanwisher, J., and Lawson, F., "Electromagnetic Flow Sensors," <u>Limnology and Oceanography</u>. Volume 20, 1975, pp. 174-182.

37. Kennedy, R.J., and Fulton, J.F., "The effect of Secondary Currents upon the Capacity of a Straight Open Channel," ASCE, Hydraulics Conference Paper No. 61-EIC-l, Transactions of the E.I.C., Volume 5, No. 1, 1961, pp. 12-18.

38. Kikkawa, H., Ikeda, S., and Kitagawa, A., "Flow and Bed Topography in Curved Open Channels," <u>Journal of the Hydraulics Division</u>. ASCE, Volume 103, No. HY10, October, 1977, pp. 1173-1189.

39. Lau, Y.L., and Kirshnappan, B.G., "Transverse Dispersion in Rectangular Channels," <u>Journal of the Hydraulics Division</u>. ASCE, Vol. 103, No. HY 10, October 1977, pp. 1173-1189.

40. Launder, B.E., and Ying, W.M., "Secondary Flows in Ducts of Square Cross-Section," <u>Journal of Fluid Mechanics</u>. Volume 54, part 2, 1972, pp. 289-295.

41. Leopold, L.B., and Wolman, M.G., "River Channel Patterns: Braided, Meandering, and Straight," Professional paper 282-B, U.S. Geological Survey, 1957.

42. Liggett, J.A., Miao, L.S., and Chiu, C.L., "Secondary Current in a Corner," Journal of the Hydraulics Division. ASCE, Volume 91, No. HY6, Nov. 1965, pp. 99-117.

43. Muller, A., "Effect of Secondary Flow on Turbulence in an Open Channel Flow," Hydraulic Problems Solved by Stochastic Methods, edited by Hjorth et al., Water Resources Publications, Fort Collins, Colorado, 1977.

44. Naot, D., "Response of Channel Flow to Roughness Heterogeneity," Journal of the Hydraulics Division. ASCE, Volume 110, No. 11, November 1984, pp. 1568-1587.

45. Nouh, M.A., and Townsend, R.D., "Shear-Stress Distribution in Stable Channel Bends," Journal of the Hydraulics Division. ASCE, Volume 105, No. HY10, October 1979, pp. 1233-1245.

46. Odgaard, A.J., "Shear-Induced Secondary Currents in Channel Flows," Journal of Hydraulic Engineering. ASCE, Volume 110, No. 7, July, 1984, pp. 996-1004.

47. Onishi, Y., Jain, S.C., and Kennedy, J.F., "Effects of Meandering in Alluvial Streams," Journal of the Hydraulics Division. ASCE, Volume 106, No. HY7, July, 1976, pp. 899-917.

48. Parratt, L.G., Probability and Experimental Errors in Science. John Wiley and Sons, Inc., New York, 1961.

49. Perkins, H.J., "The Formation of Streamwise Vorticity in Turbulent Flow," Journal of Fluid Mechanics. Volume 44, part 4, 1970, pp. 721-740.

50. Prasad, S.N., "Probability Distribution of Cross Transfer of Momentum Through Turbulent Eddies and Secondary Currents in Channel Flow," Hydraulic Problems Solved by Stochastic Methods, edited by Hjorth et al., Water Resources Publications, Fort Collins, Colorado, 1977.

51. Rice, J.R., "Numerical Methods, Software, and Analysis: IMSL Reference Edition," McGraw-Hill Book Company, New York, 1983, 661 p.

52. Shen, H.W., and Komura, S., "Meandering Tendencies in Straight Alluvial Channels," Journal of the Hydraulics Division. ASCE, Volume 94, No. HY4, July, 1968, pp. 997-1016.

53. Sium, O., "Transverse Flow Distribution in Natural Streams as Influenced by Cross-Sectional Shape," Master's Thesis, University of Iowa at Iowa City, Iowa, 1975.

54. Soliman, M.M., and Tinney, E.R., "Flow Around 180 Bends in Open Rectangular Channels," Journal of the Hydraulics Division. ASCE, Volume 94, No. HY4, July, 1968, pp. 893-908.

55. Stearns, F.P., "On the Current Meter, Together with a Reason Why the Maximum Velocity of Water Flowing in Open Channels Is Below the Surface," Transactions, ASCE, Volume 12, No. 261, August, 1883, pp. 331-338.

56. Thorne, C.R., Rais, S., Zevenbergen, L.W. , Bradley, J.B., and Julien, P.Y., "Measurements of Bend Flow Hydraulics on the Fall River at Low Stage," WRFSL Project Report No. 83-9P, Department of Civil Engineering, Colorado State University, November 1983, 49p.

57. Tracy, H.J., "Turbulent Flow in Three-Dimensional Channel," Journal of the Hydraulics Division. ASCE, Volume 91, No. HY6, November 1965, pp. 9-35.

58. Ward, P.R.B., "Transverse Dispersion in Oscillatory Channel Flow," Journal of the Hydraulics Division. ASCE, Volume 100, No. HY6, June, 1974, pp. 755-772.

59. Wood, De Volson, "On the Flow of Water in Rivers," Transactions. ASCE, Volume 8, July, 1879.